Author Manuscript

Author Manuscript

Author Manuscript

Author Manuscript

HHS Public Access

Author manuscript

*Adv Funct Mater*. Author manuscript; available in PMC 2026 April 08.

Published in final edited form as:

*Adv Funct Mater*. 2025 September 25; 36(11): . doi:10.1002/adfm.202513767.

# Emerging 2D Materials and Their Hybrid Nanostructures for Label-Free Optical Biosensing: Recent Progress and Outlook

**Xinyi Li**,
School of Mechanical and Material Engineering, Washington State University, Pullman, WA 99164, USA

**Yonghao Fu**,
School of Mechanical and Material Engineering, Washington State University, Pullman, WA 99164, USA

**Yuehe Lin**,
School of Mechanical and Material Engineering, Washington State University, Pullman, WA 99164, USA

**Dan Du**
School of Mechanical and Material Engineering, Washington State University, Pullman, WA 99164, USA

Department of Pharmaceutical Sciences, College of Pharmacy and Pharmaceutical Sciences, Spokane, WA 99202, USA

## Abstract

The increasing demand for rapid detection and remote monitoring with high sensitivity and selectivity has driven the development of label-free optical biosensors based on 2D materials (2DMs). Owing to their high surface-to-volume ratio and unique, tunable electrical and optical properties, 2DMs are highly attractive for biosensing applications. Van der Waals heterostructures (vdWHs) that combine different 2DMs allow the creation of hybrid materials with synergistic or novel functionalities. Beyond purely 2D vdWHs, mixed-dimensional hybrid architectures have recently emerged, offering enhanced sensitivity, stability, and reproducibility in label-free optical detection. This review highlights recent advances in surface-enhanced Raman scattering (SERS)- and surface plasmon resonance (SPR)-based biosensing using 2DMs and their hybrid nanostructures, discussing the role of each component and emphasizing their synergistic effects. It also provides an overview of recent progress in multifunctional sensing platforms and the integration of machine learning to improve performance and enable intelligent data analysis. Finally, the current challenges and future opportunities for advancing next-generation label-free optical biosensors are highlighted.

This is an open access article under the terms of the Creative Commons Attribution License, which permits use, distribution and reproduction in any medium, provided the original work is properly cited.

yuehe.lin@wsu.edu, annie.du@wsu.edu.

The ORCID identification number(s) for the author(s) of this article can be found under https://doi.org/10.1002/adfm.202513767

Conflict of Interest
The authors declare no conflict of interest.

Author Manuscript Author Manuscript Author Manuscript Author Manuscript

**Keywords**

2D materials; biosensors; hybrid nanostructures; surface plasmon resonance; surface-enhanced Raman scattering

## 1. Introduction

Nowadays, growing public concern about healthcare and environmental conditions has driven rapid advancements in biosensor technologies, particularly those delivering high sensitivity, fast response, and real-time monitoring capabilities.[1–6] Based on the type of transducer, biosensors are classified into three major categories[7]: electrochemical, physical, and optical (Figure 1). Among them, optical biosensors have become increasingly attractive, owing to their non-invasive nature, reliable performance in harsh environments, and capability for multiplexed analyte detection.[8–10]

Although label-based optical biosensing, which employs fluorescent dyes or other tags on target biomolecules, can achieve high sensitivity down to the single-molecule level,[11,12] it presents notable limitations. Primarily, the presence of labels may disrupt biomolecular function. Furthermore, background fluorescence from unbound labels can introduce signal bias, thereby compromising analytical accuracy, particularly when detecting analytes at ultralow concentrations.[7] In contrast, label-free biosensing neither requires external labels nor relies on their properties, facilitating accurate quantitative analysis of biomolecule detection and interactions. Additionally, label-free approaches are capable of detecting a wide variety of bioanalytes that are difficult to tag or lack known receptors.[7,13,14] Label-free optical biosensors, in particular, offer several advantages over other label-free techniques, including high stability and specificity, multiplexing and real-time monitoring capabilities, and high throughput. These features, combined with their broad applicability across medical diagnostics, environmental monitoring, food safety, and drug development, have driven intensive research efforts into their design and advancement.[14–17]

As biosensor technology progresses, there is an increasing demand for platforms that are not only stable, reliable, and selective but also compact, flexible, and highly sensitive. This is where 2D materials (2DMs) play a key role.[18–25] Their atomically thin nature contributes to the compactness and flexibility of biosensors, while their high surface-to-volume ratio boosts sensing efficiency, enabling ultra-sensitive detection of bioanalytes.[26,27] Moreover, 2DMs exhibit unique electronic and optical properties absent in their bulk counterparts, such as tunable bandgaps, strong light–matter interactions, and strain engineering.[28–30] These features have been extensively explored for label-free biosensing applications. For instance, 2DMs have been used in fabricating field-effect transistor (FET) biosensors, demonstrating their potential in point-of-care diagnostics.[31–33] In particular, 2DMs have shown great promise in advancing label-free optical biosensing platforms, including surface plasmon resonance (SPR)[34–36] and surface-enhanced Raman scattering (SERS) sensors.[37–39]

To further tailor the properties of 2DM-based biosensors, researchers have explored stacking different 2DMs into 2D van der Waals heterostructures (vdWHs), often described as “Lego-like” assemblies (Figure 1). These intentionally designed vdWHs combine the properties

Author Manuscript Author Manuscript Author Manuscript Author Manuscript

of multiple 2DMs, enabling more complex functionalities and greater tunability, thereby surpassing the capabilities of single-material systems.[40–42] This strategy also supports device miniaturization, aligning with the trend toward compact biosensors. Notably, vdWH-based biosensors can offer multimodal detection—providing multiple types of signals in response to the presence of analytes—which allows for cross-validation and improves the sensing accuracy. Moreover, vdWH-based sensors are capable of multiplexed detection of various analytes within a complex biological matrix, significantly improving sensing throughput.

Beyond 2D-2D vdWHs, integrating 2DMs with 0D (e.g., nanoparticles (NPs), quantum dots (QDs)) and 1D (e.g., nanowires (NWs), nanorods (NRs), nanoribbons) nanostructures[43–45] further diversifies biosensor functionality by exploiting confinement across multiple dimensions. Mixed-dimensional hybrid nanostructures offer enhanced performance—including ultra-high sensitivity, real-time monitoring, multiplexed detection, and device miniaturization[46,47]—paving the way toward realizing the “lab-on-a-chip” vision.[48,49]

So far, several reviews have discussed the properties of 2DMs and their label-free optical biosensing applications. However, no existing review comprehensively addresses both 2DMs and their advanced hybrid nanostructures for label-free optical biosensing, emphasizing the unique roles of individual 2DMs along with the synergistic or novel functionalities arising from their nanoarchitectures. Given the growing demand for compact, high-performance, multifunctional biosensors in healthcare and environmental monitoring, it becomes essential to integrate the advantages of various low-dimensional materials. For this purpose, designing mixed-dimensional nanostructures has emerged as a compelling strategy to expand material properties and introduce novel functionalities.

In this review, we summarize the role of 2DMs and their hybrid nanostructures in advancing label-free optical biosensing, emphasizing recent progress from the perspective of their synergistic effects within nanohybrids. We begin with a concise introduction to label-free optical biosensing techniques, including SPR, SERS, surface-enhanced infrared absorption (SEIRA), and photoluminescence (PL) sensing. Next, representative 2DMs—such as graphene, transition metal dichalcogenides (TMDCs), black phosphorus (BP), hexagonal boron nitride (hBN), MXenes, and antimonene—are briefly described, focusing on their optical biosensing-relevant properties. Subsequently, we discuss mixed-dimensional hybrid nanostructures based on 2DMs, their example applications in label-free optical biosensing, and provide a brief overview of their synthesis and fabrication techniques. In particular, we highlight recent advances in emerging 2DMs and their hybrids for SERS- and SPR-based biosensing, as well as the development of multifunctional platforms. Finally, we outline current challenges and future directions, including performance and stability optimization, advanced data analysis using machine learning (ML), and the importance of interdisciplinary research in realizing next-generation biosensors. We anticipate that this review will provide a valuable reference for researchers in optical biosensing and offer timely insights into the design and development of advanced 2DM- and hybrid nanostructure-based sensing platforms.

Author Manuscript Author Manuscript Author Manuscript Author Manuscript

## 2. Representative Label-Free Optical Biosensing Techniques

Label-free optical biosensing is a class of biosensing technologies that rely on changes in optical parameters—such as refractive index (RI), Raman scattering, fluorescence, and absorption—as transduction mechanisms for detecting bioanalytes.[7] Overcoming the drawbacks of fluorescent labels, label-free approaches enable real-time and continuous monitoring of biomolecular interactions while preserving the native function of biomolecules. This enhances the reliability and reproducibility of measurements by minimizing interference from labeling agents and supports the development of miniaturized and multiplexed sensing platforms. Representative examples of label-free optical biosensors include SPR, SERS, SEIRA, and PL biosensors, as illustrated in Figure 2.

### 2.1. SPR Biosensors

SPR biosensors have been widely applied in various fields, including life sciences, food safety, medical diagnostics, and drug delivery.[50] The working principle of SPR biosensors is based on the excitation of surface plasmons at the metal-dielectric interface, typically supported by Au or Ag thin film. This excitation produces an evanescent field that is highly sensitive to RI changes near the surface, enabling the detection of binding events with minimal interference from unbound analytes. Under resonant conditions, the reflected light intensity exhibits a sharp dip, and the corresponding incident angle is referred to as the SPR angle.[35] Binding events at the sensor surface alter the local dielectric function, resulting in a shift in the SPR angle. Recording this measurable shift enables real-time, label-free detection of interactions such as antibody-antigen binding, nucleic acid hybridization, and protein-ligand interactions.

To excite surface plasmons, both energy and in-plane momentum must be matched. For this purpose, coupling elements such as prisms or gratings are often employed. Accordingly, various SPR biosensor configurations have been developed, including the commonly used Kretschmann configuration (Figure 2a), Otto configuration, grating-coupled structures (Figure 2b), and fiber-optic-based setups.

### 2.2. SERS

SERS offers a sensitive and non-destructive approach for label-free optical biosensing (Figure 2c). It is rapid and low-cost compared to traditional analytical techniques.[37] The inherent selectivity required for biosensing is naturally met by Raman scattering, as Raman spectra serve as unique molecular fingerprints. By utilizing metal NPs (e.g., Au NPs, Ag NPs, etc.), the Raman signal can be significantly enhanced when molecules are adsorbed in the vicinity—i.e., at “hot spots” around the NPs—due to the strong localized electromagnetic (EM) fields. This enhancement enables highly sensitive, label-free detection of biomolecules, pathogens, and chemical analytes, making SERS a powerful tool in optical biosensing. Compared with other label-free optical biosensing techniques—for example, PL biosensors—SERS excels in its multiplexed detection capability and high stability.

Recently, SERS substrates based on 2DMs have been developed to overcome the limitations of traditional SERS platforms. In 2DM-based SERS systems, Raman signal amplification

Author Manuscript Author Manuscript Author Manuscript Author Manuscript

is attributed to the chemical mechanism (CM), influenced by the electronic structure of the target analytes and the 2DM interface.[46] In the case of graphene-enhanced Raman scattering (GERS) (Figure 2d), the high electrical conductivity of graphene facilitates both CM and EM enhancement effects, working synergistically to enable highly sensitive and specific detection in Raman spectroscopy.[51]

### 2.3. SEIRA

Similar to SERS, SEIRA is another analytical vibrational spectroscopy technique that leverages localized EM enhancement.[52] Typically, metallic NPs and nanostructure arrays[53] are employed as substrates, increasing the effective IR absorption cross-section of the probing molecules (Figure 2e). Recently, low-dimensional vdW materials have emerged for sensitive IR sensing, including graphene,[54] carbon nanotubes,[55] graphene nanoribbons,[56,57] and hBN nanoresonators.[58–60] While both SERS and SEIRA provide molecular fingerprints and can exhibit high specificity in biosensing, SEIRA probes IR-active (dipole-active) vibration modes, which are inherently more responsive to molecular structure than Raman-active modes.[52,61] Although the intrinsic IR absorption cross-sections are larger than Raman scattering cross-sections, the EM enhancement achievable in SERS is usually significantly larger, leading to stronger overall signal enhancement and single-molecule detection capability.[52,62] However, due to its tighter field confinement, SERS is less effective for probing large biomolecules, as the field enhancement is only sustained within a few nanometers of the substrate surface. In contrast, the enhanced field in SEIRA extends up to ~100 nm, enabling the detection of large biomolecules, including viruses and bacteria.[62] Therefore, the choice between SERS and SEIRA depends on the size and nature of the target analytes. Overall, SEIRA offers label-free, molecular-specific detection with high sensitivity, and is well-suited for real-time analysis of biomolecular interactions, thin films, and surface chemistry.

### 2.4. PL Biosensors

PL biosensors are a type of optical biosensing platform based on changes in the PL properties of the sensing material upon interaction with target bioanalytes (Figure 2f). In this context, the sensing materials are often semiconductors—such as QDs, TMDCs, etc.—that can be excited by light and exhibit PL behavior. The presence of bioanalytes can modulate the PL response—typically through quenching or spectral shifts—via charge transfer mechanisms.[63] Unlike traditional fluorescent biosensors that rely on labeled probes, PL biosensors often enable label-free detection by leveraging the intrinsic optical response of the sensing material itself. Owing to their high sensitivity, tunable emission, and compatibility with miniaturized platforms, PL biosensors are widely explored for the detection of biomolecules, DNA, RNA, metal ions, and environmental pollutants.

## 3. Typical 2DMs for Label-Free Optical Biosensing

2DMs have gained tremendous attention recently due to their extraordinary properties compared to their 3D bulk counterparts.[64] They are particularly favorable for biosensing applications.[20,32,65] For instance, their atomically thin nature enables mechanical flexibility and high strain tolerance, which has advanced the development of wearable and implantable

Author Manuscript Author Manuscript Author Manuscript Author Manuscript

biosensors,[66–68] as well as the miniaturization of biosensing devices.[48] More importantly, their extremely large surface area provides numerous active sites, significantly improving the sensitivity of biosensors. The large surface also allows for surface modification and functionalization, which can be tailored to enhance the selectivity of the biosensor toward different bioanalytes. Additionally, the broad range of electronic properties exhibited by 2DMs—such as tunable bandgaps, confined polaritons, and fluorescence quenching—also plays a critical role in biosensor development. In this section, we introduce several 2DMs commonly used for label-free optical biosensing, highlighting their relevant properties and representative applications (see Table 1).

### 3.1. Graphene

Graphene, the most prominent member of the carbon-based 2DMs family, is composed of a hexagonal lattice of $sp^2$ carbon atoms.[24] It exhibits several remarkable properties, including high tensile strength, excellent thermal conductivity, outstanding intrinsic carrier mobility, and high transparency.[28,42] These attributes have enabled the widespread application of graphene across various fields, such as nanoelectronics, supercapacitors, optoelectronic devices, bioimaging, and biosensors.[66,93]

As a semi-metal with a zero bandgap, graphene possesses unique plasmonic properties that can enhance biosensor performance. It supports IR plasmons with high tunability, strong field confinement, long lifetimes, and low loss—features highly advantageous for label-free optical biosensing. For instance, the local RI at the sensor interface can be significantly modified in the presence of graphene, resulting in larger shifts of the SPR angle and thereby enhancing the sensitivity of SPR biosensors.[69] In SEIRA-based biosensors, graphene enhances IR absorption, leading to improved sensor performance with a lower limit of detection (LOD).[94,95] Notably, graphene plays a key role in the development of GERS, enabling ultrahigh sensitivity in bioanalyte detection. The enhancement in GERS primarily arises from charge transfer between graphene and adsorbed molecules, facilitated by strong $\pi$–$\pi$ interactions.[96]

The concept of using graphene as a SERS substrate was first explored and validated in 2009, as reported by Ling et al.[97] They conducted a series of experiments comparing the Raman signals of deposited molecules—phthalocyanine (Pc), rhodamine 6G (R6G), protoporphyrin IX, and crystal violet (CV)—on $Si/SiO_2$ substrates versus graphene (Figure 3a). The resulting Raman spectra, as shown in Figure 3a, exhibited strong enhancement in the presence of monolayer graphene. Since then, GERS has developed rapidly and has been widely adopted for biosensing applications.[51] Additionally, the GERS effect can be modulated by tuning the Fermi level of graphene—either through electric gating, as demonstrated by adjusting the applied voltage in graphene FETs,[98] or through defect engineering, such as nitrogen doping, as performed by Feng et al.[99] Furthermore, graphene's excellent biocompatibility and ease of surface functionalization further support its integration into a wide range of biosensing platforms for the detection of glucose, DNA/RNA, bacteria, etc.

The successful exfoliation of graphene from graphite in 2004[101] significantly advanced its application. Later, chemical vapor deposition (CVD) techniques were developed,

Author Manuscript Author Manuscript Author Manuscript Author Manuscript

enabling the synthesis of large-area few-layer graphene on Ni foils.[102] Subsequently, the controllable growth of single-crystal monolayer graphene on copper foil has been demonstrated, achieving high uniformity over relatively large areas.[103] More recently, epitaxial graphene (EG) growth on SiC has emerged as another promising approach to produce large-area graphene, with precise control over layer thickness down to a single atomic layer.[104] Unlike CVD-grown graphene, which typically requires transfer to other substrates, EG forms directly on the SiC surface, making it more suitable for device fabrication. Importantly, EG not only retains the key electronic properties of exfoliated graphene[105,106] but also exhibits novel characteristics due to the presence of the SiC substrate—offering potentially valuable insights for biosensing development.

### 3.2. TMDCs

Unlike graphene, which consists of a single layer of carbon atoms, TMDCs have an $MX_2$ structure, i.e., one transition metal layer sandwiched between two chalcogen layers, where the $M$ represents the transition metal (e.g., W, Mo, Nb, etc.) and $X$ represents the chalcogen (e.g., S, Se, etc.). TMDCs exhibit a wide range of bandgaps and band alignments.[107,108] Notably, they demonstrate an indirect-to-direct bandgap transition when their thickness changes from multilayer to single layer.[73]

In biosensing, monolayer TMDCs have garnered increasing interest due to their excellent electrical and optical properties.[74,109] Their semiconducting nature, with a tunable bandgap, has been widely leveraged in the fabrication of FET biosensors.[110–113] Beyond that, the layer-dependent PL properties of TMDCs, their strong fluorescence quenching capabilities, and strain- or doping-induced Raman shifts have advanced their application in label-free optical biosensing.

Among all TMDCs, $MoS_2$ has been extensively studied for the detection of various bioanalytes, including immune components, proteins, DNA, and biochemical compounds.[114] Monolayer $MoS_2$ exhibits varying Förster resonance energy transfer (FRET) quenching efficiencies toward different dye-labeled biomolecules, which has been widely exploited in the design of biosensors for distinguishing certain biomolecules. More interestingly, $MoS_2$ has also demonstrated its potential for label-free detection, based on its PL modulation upon interaction with attached chemical or biological molecules.[72,115,116] For instance, Catalán-Gómez et al.[72] developed a PL biosensor for the breast cancer biomarker miRNA-21 using functionalized monolayer $MoS_2$ flakes (Figure 3b). Upon hybridization—i.e., when the target miRNA-21 bound to the immobilized complementary sequence—the PL of $MoS_2$ exhibited a redshift, demonstrating both the specificity and viability of the designed biosensor.

Besides $MoS_2$, $WS_2$ is another widely explored TMDC for biosensing applications.[35] The most stable configuration of $WS_2$ is its semiconducting 2H phase, which shares similar structural and electronic characteristics with $MoS_2$. Owing to its strong light absorption, integrating $WS_2$ into SPR biosensors can significantly enhance sensitivity. The intrinsically larger spin-orbit coupling of $WS_2$ [117] relative to $MoS_2$ leads to stronger optical absorption at shorter wavelengths, which, under certain configurations, enables $WS_2$-based SPR biosensors to outperform their $MoS_2$ counterparts.[118] Expanding beyond $MoS_2$ and

Author Manuscript Author Manuscript Author Manuscript Author Manuscript

$WS_2$, emerging TMDCs, such as $ReS_2$,[119] $MoTe_2$, and $WTe_2$[120] have also demonstrated potential in label-free optical biosensing. For instance, Kitadai et al.[121] evaluated the SERS activity of various TMDCs for detecting copper phthalocyanine (CuPc) molecules, including $WTe_2$, $WSe_2$, $SnS_2$, $SnSe_2$, $TiSe_2$, $TiS_2$, and $TiTe_2$, and found that several of them—particularly $WSe_2$ and $SnS_2$—exhibited performance comparable to graphene.

### 3.3. MXenes

MXenes are a rapidly emerging class of 2D transition metal carbides, nitrides, or carbonitrides, typically with an $M_{n+1}X_nT_x$ structure, where $M$ represents the transition metal (e.g., Ti, V, Nb, etc.), $X$ represents carbon and/or nitride, and $T_x$ represents the surface functional groups, usually —OH, —O, and —F.[77] The synthesis of MXenes involves selective etching of the $A$-element layer from $MAX$ phases, where the formed type of surface terminations is attributed to the etching environment. These surface groups are essential for the stability, dispersibility, and biosensing functionality of the synthesized MXenes. Additionally, they can also be modified to tailor the electrical, optical, and chemical properties of the material.[76]

The quenching capability of MXenes make them highly attractive for developing fluorescent sensors.[122,123] For example, Xie et al. employed $Ti_3C_2T_x$ MXene nanosheets for real-time detection of $Ag^+$ ions in aqueous solution, achieving a low LOD of 0.035 μM with high selectivity.[123] Notably, 2D MXenes are hydrophilic due to their surface groups and exhibit excellent metallic conductivity, both of which are favorable for label-free optical biosensing.[76, 124–127] Their tunable optical properties, i.e., plasmonic behavior in the near-IR (NIR) to mid-IR (MIR) regime, enable enhanced light–matter interactions and can be exploited in SPR biosensors.[77] For example, Gan et al.[128] developed a $Ti_2C$ MXene-based SPR biosensor for detecting heavy metals with high sensitivity. Their study showed that the presence of an MXene overlayer significantly enhanced SPR sensor performance. Moreover, the abundant functional groups on MXene surfaces enable efficient immobilization of bioanalytes and facilitate strong charge transfer between MXenes and the analytes, making MXenes a promising substrate for SERS detection.[126,127] For instance, as demonstrated in Figure 3c, Li et al.[100] developed a uniform 2D $Ti_3C_2T_x$/Ag NPs SERS substrate exhibiting an enhancement factor (EF) of $3 \times 10^8$. Attributed to synergistic CM and EM mechanisms, this SERS platform enabled R6G detection down to the fm level. Furthermore, MXenes are highly biocompatible and solution-processable, making them suitable for integration into various label-free optical biosensing platforms.[76,124,125]

### 3.4. BP

BP is one of the most stable phosphorus allotropes,[129] compared to white and red phosphorus. It is a layered 2DM with phosphorus atoms arranged in a puckered honeycomb structure. Owing to its unique physicochemical properties—such as high carrier mobility, strong photothermal and photoconductive responses, and a layer-dependent direct bandgap —BP has been explored for a wide range of applications, including batteries,[130] supercapacitors,[131] optoelectronics,[132] and biosensing.[82]

Author Manuscript Author Manuscript Author Manuscript Author Manuscript

BP nanosheets have been utilized in the development of fluorescent biosensors[133,134] due to their strong fluorescence quenching capability. Unlike graphene, BP exhibits high in-plane anisotropy in both its optical and electrical properties, which is advantageous for label-free optical biosensing. This anisotropy enables polarization-sensitive detection, tunable light–matter interactions, and the design of highly selective photonic and optoelectronic biosensors. For instance, Lin et al.[81] studied the anisotropic charge transfer between few-layer BP and CuPc molecules, which induced polarization-dependent Raman signal enhancement, as shown in Figure 3d. These findings shed light on the electronic properties of anisotropic BP 2D sheets and their applications in biosensing. Moreover, BP has broadband optical absorption in the visible to NIR regime,[83] making it favorable for IR-based optical biosensing. Its rich surface chemistry and high biocompatibility further facilitate strong interfacial interactions with biomolecules, enabling label-free detection mechanisms based on photo-induced charge transfer[135–137] and dielectric modulation.[138]

Recent studies have demonstrated the potential of BP nanosheets as a promising substrate for SERS-based biosensors. For instance, Li et al.[86] developed a SERS substrate that integrated BP nanosheets with noble metal NPs (Au and Ag NPs), for the detection of fungicides, demonstrating excellent sensitivity and reproducibility. Liu et al.[84] developed BP-based nanohybrids as multifunctional theranostic platforms for drug delivery, phototherapy, and bioimaging, revealing extraordinary NIR photothermal transduction efficiency and drug delivery capacity, as well as demonstrating good SERS activity under NIR excitation. The minimal spectral interference makes BP nanosheets highly desirable for the SERS detection of biological samples.

However, the practical application of BP is constrained by its instability under ambient conditions, as it degrades upon exposure to air and humidity. To preserve its properties for long-term biosensing, two major strategies are commonly adopted: i) encapsulation, where a protective layer is coated onto BP; or ii) surface modification, i.e., creating a passive layer to prevent oxidation.[134]

### 3.5. hBN

Known as “white graphene,” hBN has a similar honeycomb lattice structure but is composed of alternating boron and nitrogen atoms instead.[37,46] Unlike graphene, hBN is electrically insulating with a large bandgap, making it optically transparent across a broad spectral range from ultraviolet (UV) to the NIR.[25] This makes hBN an ideal substrate and support layer for biosensing applications where minimizing background interference is crucial. Though hBN is not typically used as the direct transducer, its unique optical and surface properties make it indispensable in advancing label-free optical biosensors.[20] Because of its surface smoothness, excellent thermal stability, and chemical inertness, hBN can act as a protective layer or dielectric spacer integrated into label-free optical biosensors, particularly when the transducer material is unstable or prone to oxidation, such as TMDCs. For example, Kim et al.[87] used hBN as an insulating layer to protect metal NPs from photothermal and oxidative damage during SERS detection, thereby improving the overall stability of the system. Additionally, stronger EM fields were generated at the narrow gaps on the hBN

Author Manuscript Author Manuscript Author Manuscript Author Manuscript

surface—referred to as “hot spots” in Figure 3e—which enhanced the Raman scattering signal of R6G when the molecules were in close proximity to these regions.

More recently, scientists have demonstrated label-free optical biosensing using hBN through imaging-based approaches. For instance, Zhang et al.[139] used the selectively activated defect emissions of the hBN surface to achieve label-free single-molecule detection and identification of biomolecules. By using spectrally resolved super-resolution microscopy together with ML, they were able to identify five distinct amino acids. In another work, Sülzle et al.[140] investigated the interactions between DNA and the hBN surface through direct imaging of variations in local optical scattering, where the signal was higher at engineered defects than in pristine regions. These findings highlight hBN as a versatile platform for single-molecule biosensing and pointed out its value and potential in advancing hybrid label-free optical biosensing systems.

### 3.6. Antimonene

Recently, other monoelemental 2DMs (Xenes) beyond graphene and phosphorene, such as arsenene, antimonene, and silicene, have emerged as promising materials for biosensing applications.[92,141] Owing to their unique electronic properties, large surface area, ultrathin nature, and high flexibility, Xenes have been widely explored in advancing FET biosensors,[141] offering ultrahigh sensitivity in detecting proteins, DNA/RNA, and small molecules. Among these Xenes, antimonene has recently demonstrated its promise in developing label-free optical biosensors,[71] such as SPR biosensors for the ultrasensitive detection of miRNA.[88] Antimonene shares the same $sp^2$ honeycomb lattice as graphene but possesses superior electrochemical properties compared to graphene and other 2DMs.[89,90] It has high carrier mobility, a layer-dependent tunable bandgap, and exhibits strong spin-orbit coupling.[91] In particular, its high work function, large adsorption energy, high stability, and hydrophilicity make it highly preferable as a biomolecular recognition layer in constructing SPR biosensors.[71,92] In 2019, Xue et al.[88] reported that antimonene had a substantially stronger interaction with ssDNA than graphene, based on first-principles density functional theory (DFT) calculations. Motivated by this insight, they developed an SPR sensor for miRNA detection (Figure 3f) and achieved an attomolar-level detection limit. Since then, a growing number of studies[142–147] have utilized antimonene in layered SPR biosensors to further improve sensitivity, highlighting its potential in the development of biosensing platforms with high performance.

## 4. Mixed-Dimensional Hybrid Nanostructures for Label-Free Optical Biosensing

In the previous section, we briefly introduced and discussed the properties of different 2DMs and their applications in label-free optical biosensing. With the trend in biosensor design moving toward more controllable, functionally tailored, and high-performance platforms with improved stability, there has been growing interest in designing biosensors by combining 2DMs to create hybrid materials with enhanced properties and functionalities. In this section, we provide an overview of mixed-dimensional hybrid nanostructures composed of 2DMs and other nanomaterials, along with their examples in label-free optical biosensing.

Author Manuscript Author Manuscript Author Manuscript Author Manuscript

### 4.1. Hybrid Nanostructures and Examples in Label-Free Optical Biosensing

To enhance the performance and versatility of label-free optical biosensors, recent efforts have focused on engineering hybrid nanostructures by integrating different 2DMs. The physically combined 2DMs are known as 2D vdWHs,[28,148] where the assembly is attributed to weak vdW forces rather than chemical bonds. The vdWHs can be vertically stacked—such as graphene/$MoS_2$,[63] hBN/graphene,[149] or $WSe_2$/graphene heterostructures[150]—or laterally stitched, such as $WS_2/MoS_2$[151] or $WSe_2/MoSe_2$ heterostructures.[152] In this review, we focus on vertically stacked heterostructures, as schematically illustrated in Figure 4c. Since these vertical vdWHs are composed of 2DMs, they inherit the properties of each individual 2DM and have been extensively explored for biosensing applications. For instance, in label-free optical biosensing, a vertically stacked graphene/$MoS_2$ heterostructure (shown in Figure 4c) was reported[63] in which both the PL response of $MoS_2$ and the GERS signal from graphene were used to detect doxorubicin (DOX), a cancer drug, with high sensitivity and selectivity. Additionally, because the constituent 2DMs possess complementary properties, their vdWHs can exhibit unique or improved electronic, optical, and mechanical characteristics compared to their individual components, enabling novel physical phenomena and advancing various application fields,[29,30] including label-free optical biosensing. Moreover, vdWHs offer additional tunability of their overall electrical and optical properties via chemical doping, electrostatic gating, nanostructure design, and control over stacking configurations (layer arrangement, twist angles, formation of Moiré patterns, etc.).[29] Importantly, vdWHs can mitigate the disadvantages of unstable 2DMs, such as degradation and oxidation under ambient conditions, by using stable 2DMs as protective overlayers. For example, TMDCs are known to degrade upon exposure to air. By transferring a graphene layer on top of $MoS_2$, the overall stability of the biosensor can be significantly improved[63] (Figure 4c).

Inspired by the concept of 2D vdWHs integration, researchers have expanded the design beyond purely 2D to mixed-dimensional hybrid nanostructures—such as 0D–2D, 1D–2D, and 2D–3D systems—which also may not rely solely on vdW interactions. Instead, these structures often integrate multiple material classes using a range of physical or chemical strategies to realize complementary or enhanced biosensing functions. For instance, noble metal NPs, such as Au and Ag, exhibit excellent plasmonic properties and localized surface plasmon resonance (LSPR), which are advantageous for SPR and SERS biosensing. When combined with 2DMs—materials that have large surface areas to support functionalization and effective immobilization of bioanalytes—0D–2D hybrid nanostructures can substantially enhance the overall performance of label-free optical biosensors. Indeed, researchers have actively explored various combinations of metallic and non-metallic NPs, as well as complex compositions, with 2DMs to improve SERS-based biosensors.[46,47] For example, Yu et al.[153] developed an Au NPs/$Ti_3C_2T_x$ hybrid substrate (Figure 4a) for SERS detection of bacteria, achieving high sensitivity, uniformity, and stability.

In SPR biosensors, metallic films are essential for supporting surface plasmon polaritons, which enable label-free detection. However, these films are often prone to oxidation and corrosion. Using 2DMs as protective overlayers on metallic films improves the stability of SPR biosensors. In addition, the large surface area of 2DMs facilitates efficient

Author Manuscript Author Manuscript Author Manuscript Author Manuscript

receptor functionalization, and their high optical absorbance can further enhance SPR sensor performance. Furthermore, the tunability of 2DMs—by adjusting the number of layers, doping levels, and surface functionalization—provides additional flexibility in tailoring SPR sensor designs to meet specific detection requirements. As a result, 2D-3D integration, illustrated in Figure 4d—i.e., hybrid structures of 2DMs with metallic films, or multicomponent architectures comprising alternating 2DMs and metallic layers—has become a widely adopted approach in SPR biosensor development. For example, Hu et al.[155] systematically studied the influence of various 2DMs on Ni/Al bimetallic SPR biosensors, finding that both the real and imaginary components of the 2DMs' RI significantly affected sensor sensitivity. By optimizing material combinations, stacking order, and layer thickness, a maximum angular sensitivity of 542 deg $RIU^{-1}$ was achieved using a BP (1L)/Ni (22 nm)/Al (40 nm) hybrid configuration.

Hybrids of 1D nanostructures and 2DMs represent another promising configuration—integrating NWs, nanoribbons, or nanobelts with 2DMs, as illustrated in Figure 4b—that can benefit both SPR- and SERS-based biosensors. For example, a 1D-2D hybrid structure of hBN nanoribbons/graphene[154] was proposed to enhance SPR performance.

These hybrid nanostructure designs, which extend beyond 2D–2D systems, open new pathways for advancing label-free optical biosensing. However, to fully exploit their potential, a deeper understanding of the underlying light-matter interactions[29,30] and sensing mechanisms is required. Additionally, synthesis methods could significantly influence the morphology, surface chemistry, and uniformity of these materials, thereby affecting their performance in biosensing applications. Depending on the hybrid configuration and materials chosen, appropriate fabrication strategies must be carefully selected to ensure the desired functionality. In the following subsection, we briefly discuss fabrication strategies for 2DMs and their hybrid nanostructures.

### 4.2. Synthesis and Fabrication Techniques

Various methods and techniques have been developed to produce 2DMs and their 2D vdWHs, including mechanical exfoliation[158] (Figure 4e), dry and wet transfer techniques[159] (Figure 4f), liquid-based methods, CVD (Figure 4g), and direct epitaxial growth[157] (Figure 4h). Mechanical exfoliation using Scotch tape was the first reported method for isolating monolayer graphene in 2004,[101] and has since been widely used for exfoliating other 2DMs from their bulk counterparts. This technique involves repeatedly picking up and stamping layered materials with Scotch tape or a polymer stamp, as illustrated the upper panel of Figure 4e, which can yield single-layer flakes over relatively large areas. The resulting 2DMs are fairly clean and smooth, with fewer defects. However, the size, shape, and uniformity of layer numbers are difficult to control. Besides, the time-consuming and manual process makes it unsuitable for scalable production. Recently, metal-assisted mechanical exfoliation has been introduced (as shown in the lower panel of Figure 4e), where a metal film is directly evaporated onto the bulk crystal surface.[160,161] It was reported that the thickness and type of metal film can affect the number of layers exfoliated.[161] However, to expose the 2DM surface for 2D vdWH assembly, the metal layer

Author Manuscript Author Manuscript Author Manuscript Author Manuscript

must be removed by chemical etching, which often introduces extra contamination or doping to the exfoliated 2D flakes.[161]

Liquid-based methods, such as hydrothermal and solvothermal synthesis, as well as liquid-phase exfoliation, offer cost-effective and scalable routes for producing 2D nanosheets. For example, ultrasonic-assisted liquid-phase exfoliation has been successfully applied to synthesize BP nanosheets[84,136,137] and $Ti_3C_2T_x$ Mxenes.[153, 162–164] The 2D sheets synthesized by these methods often have functionalized surface groups. However, the crystallinity and interface sharpness are often not as high-quality as those produced by CVD or other methods.

CVD is one of the most widely used techniques for the controlled, wafer-scale synthesis of high-quality, crystalline 2DMs. For example, CVD has been used to grow monolayer graphene on copper,[165] $MoS_2$ on $Si/SiO_2$,[63] and hBN on sapphire.[166] To fabricate 2D vdWHs from these CVD-grown 2DMs, transfer techniques—either wet or dry—are often required. Wet transfer methods (as illustrated in the lower two panels of Figure 4f) typically involve either chemical etching of the growth substrate or bubbling from electrochemistry to lift the as-grown 2DMs off the substrate. In both cases, a support layer, e.g., spin-coated polymethyl methacrylate (PMMA) or drop-cast polycarbonate, is used to protect the 2DM during the transfer process. While wet transfer can yield large-area, uniform monolayers, it can introduce hard-to-remove chemical residues and, consequently, affect the optical and electrical properties of the resulting vdWHs. Additionally, post-treatments are often necessary for wet transfer methods, such as heating the substrate with transferred 2DMs for better adhesion, removal of the polymer support layer, and annealing to relax the 2DMs and reduce wrinkles. For dry transfer, on the other hand, a polydimethylsiloxane (PDMS) stamp is used to directly peel off the 2DMs and transfer them to a new substrate without any post-treatment process (as shown in the upper panel of Figure 4f).

For applications requiring precise control over the interface and stacking order, direct growth of one 2DM over another grown or transferred 2DM is a straightforward approach to fabricate vdWHs. For example, researchers have used controlled CVD to directly grow $MoS_2$[156] and $WSe_2$[150] on top of graphene. In other works, CVD-based epitaxial growth was successfully achieved for $MoS_2$[167] and $WSe_2$[168] on mechanically exfoliated hBN. Epitaxial growth between TMDC crystals was also explored, such as growing $MoTe_2$ monolayer on $MoS_2$ substrate.[169] Need to mention that, vdW epitaxy can be repeated multiple times to fabricate complex multicomponent heterostructures. For example, Lin et al.[170] used trilayer EG as a substrate to directly grow $WSe_2$ by a combination of oxide powder vaporization and metal-organic CVD (MOCVD) process. Subsequently, a second layer of $MoS_2$ was grown on top of the initially grown heterostructure by vaporization of $MoO_3$ and sulfur, forming $MoS_2/WSe_2$/EG vertical heterostructures.

2D–3D hybrid nanostructures can be fabricated using all of the aforementioned methods. For 0D–2D systems, i.e., NPs/2DM hybrids, the synthesis methods are slightly different. A commonly used approach is chemical reduction, where metal precursors and nanosheets are mixed and reduced in situ using suitable agents, as demonstrated in the synthesis of Au NPs/MXene[153,171] hybrid structures. In other studies, scientists have also used self-

Author Manuscript Author Manuscript Author Manuscript Author Manuscript

assembly between nanosheets and metal NPs,[100,162,172] driven by electrostatic adsorption. This process often involves ultrasonication or stirring to ensure even dispersion of the NPs and to prevent aggregation. To directly deposit NPs onto 2DMs on a substrate, physical vapor deposition (PVD) methods—such as sputtering and electron beam evaporation—are commonly used. For example, Mei et al.[173] used magnetron sputtering and electron beam evaporation to deposit Ag and Au layers, respectively, in the fabrication of Au/graphene/Ag/ZnO hybrid nanostructures. Lu et al.[174] used magnetron sputtering to deposit an Ag layer onto a 3D polystyrene (PS) substrate for fabricating graphene oxide (GO)/Ag/3D PS hybrid nanostructures.

The fabrication of 1D–2D hybrids often requires additional patterning techniques, such as electron-beam lithography or reactive ion etching, beyond the fabrication of 2D vdWHs. For example, graphene nanoribbons have been fabricated on the $Si/SiO_2$ substrate using reactive ion etching.[57] In another study, patterned graphene nanoribbons were created on the $CaF_2/SiO_2/Si$ substrate using electron-beam lithography.[175]

## 5. Recent Advances in 2DMs and Their Hybrid Nanostructures for Label-Free Optical Biosensing

2DMs and their mixed-dimensional hybrid nanostructures have emerged as promising platforms for the development of label-free optical biosensors. In this section, we provide an overview of recent advances in their design and application for SERS- and SPR-based biosensing. Furthermore, we highlight the development of multifunctional sensing platforms that enable multiplexed and multimodal detection, along with the incorporation of ML techniques to enhance signal interpretation and overall sensor performance.

### 5.1. Recent Advances in SERS-Based Biosensing

Conventional SERS substrates are predominantly based on noble metal NPs, i.e., Au NPs, Ag NPs, etc. However, because of their proneness to aggregation, poor stability, limited reproducibility, and the high cost of noble metal precursors, scientists have explored alternative materials beyond pure metallic NPs as SERS substrates. 2DMs, owing to their unique and tunable optical and electrical properties, large surface-to-volume ratios, and high biocompatibility, have attracted tremendous attention for the development of promising SERS substrates. In this subsection, we discuss recent innovations in leveraging novel 2DMs and their mixed-dimensional hybrid nanostructures to advance SERS-based biosensing toward higher sensitivity and practical feasibility.

**5.1.1. Pure 2DMs:** To date, several 2DMs have demonstrated strong potential as SERS substrates. Graphene, the most widely studied 2DM, has been extensively employed in GERS and biosensing applications.[51] TMDCs, such as $MoS_2$ and $WS_2$, have also demonstrated their capability in enhancing Raman signals. More recently, other TMDCs[176–180] have emerged as promising SERS-active materials. For example, Ekoya et al.[176] demonstrated the SERS detection of dye molecules—R6G and Nile blue A (NBA)—using 2H-$TaS_2$ as the substrate, where LODs of $3.01 \times 10^{-18}$ M and $4.05 \times 10^{-21}$ M were achieved for R6G and NBA, respectively. The maximum EF for R6G reached $1.3 \times 10^{14}$, owing

Author Manuscript Author Manuscript Author Manuscript Author Manuscript

to the strong interactions between the dye molecules and the 2H-$TaS_2$ substrate. Li et al.[177] utilized 2D $HfTe_2$ nanosheets as a SERS substrate for R6G detection, where an EF of $2.32 \times 10^6$ was achieved. Notably, this SERS platform was further explored to detect uric acid, a gout disease-associated biomarker, where a LOD of 0.1 mmol $L^{-1}$ was obtained, illustrating its potential for nano-diagnostics. Since early diagnosis is essential for timely interventions, it is of great interest to detect disease biomarkers. In another study, few-layer semi-metallic $MoTe_2$ was used as a SERS substrate for detecting $\beta$-sitosterol,[178] a lipid disease biomarker, achieving a LOD of 1 nM. The Raman signal enhancement was attributed to the charge-transfer process upon the formation of surface-analyte complex. Compared with noble-metal SERS substrates, the $MoTe_2$ film exhibited higher homogeneity and reproducibility, as well as reusability.

Beyond graphene and TMDCs, MXenes have also emerged as compelling SERS substrates. Among them, $Ti_3C_2$ [78,163,181,182] and $Ti_2N$[183] are the most widely used. More recently, a broader range of MXenes[184–187] has shown strong potential for SERS-based biosensing. For instance, 2D $V_2C$ and $V_4C_3$[185] achieved R6G detection with a LOD of $10^{-7}$ M, where a layer-dependent EF was observed. The SERS performance was further enhanced by a 2D downsizing strategy and molecular enrichment, reaching a LOD of $5 \times 10^{-9}$ M. In another study, He et al.[186] synthesized TiVC through a single-step chemical etching process and evaluated its SERS performance, achieving a femtomolar-level LOD for R6G with an EF of $10^{12}$. Similarly, Lan et al.[188] assessed the SERS performance of $Ta_4C_3$ and $Nb_4C_3$ for R6G and CV detection. Owing to the photo-induced charge transfer between MXene and adsorbed molecules, an EF of ~$10^5$ and a LOD of $10^{-7}$ M were achieved. These studies pave the way for using MXenes as promising SERS substrates; however, more research needs to be carried out for practical biosensing applications. Impressively, Peng et al.[187] theoretically designed and experimentally studied the excellent SERS performance of $Nb_2C$ and $Ta_2C$, with the latter showing remarkable capability in detecting the SARS-CoV-2 S protein (Figure 5a). An exceptionally low LOD of $5 \times 10^{-9}$ M was reported, indicating the feasibility of real-time monitoring and early detection of novel coronavirus, and highlighting MXenes as a strong candidate for practical SERS applications.

hBN has also been investigated as the SERS substrate. Both exfoliated[75] and CVD-grown[192] hBN have shown enhanced Raman signals of probe molecules, with the enhancement attributed primarily to dipole-dipole interactions and remaining unaffected by the number of hBN layers. However, due to its relatively low EF, hBN is unlikely to be used in practical applications without additional design or engineering. Similarly, BP sheets also exhibit limited enhancement. Even with special engineering, such as creating nano-void arrays on BP sheets,[193] which consequently enhanced the local electric field for SERS detection, the EF of R6G remains significantly lower than those achieved with other 2DM-based SERS substrates. Table 2 summarizes recently emerged 2DMs employed as SERS substrates.

**5.1.2. Hybrid Nanostructures Used as SERS Substrates:** Different from SERS substrates composed of plasmonic NPs, where enhancement is dominated by the EM mechanism, most 2DM-based SERS relies on the CM. While 2DM-based SERS substrates offer distinct advantages over noble metal NP-based counterparts, such as high homogeneity

Author Manuscript Author Manuscript Author Manuscript Author Manuscript

and reproducibility, their EFs and sensitivities remain comparatively lower. To overcome these limitations, the design of 0D-2D hybrid nanostructures—integrating metallic NPs with 2DMs—has emerged as a promising strategy to achieve significantly enhanced SERS performance through synergistic CM and EM effects, while simultaneously improving stability, reproducibility, selectivity, and biocompatibility.

The weak EF of hBN has led to its integration with metal NPs for SERS-based biosensing.[87,192,195,196] Similarly, recent studies have also demonstrated the SERS capability of metal NPs/BP hybrid nanostructures[84,86,135,197] and their potential for highly sensitive biomarker detection. For instance, Kundu et al.[197] fabricated Ag NPs/BP hybrids as the SERS substrate for the sensitive detection of sepsis biomarkers. The Raman spectra of the biomarkers were sharp and significantly enhanced in the presence of Ag NPs/BP flakes, with no background interference from BP itself. The EF reached the order of $10^{14}$, and the LODs for both prognostic and diagnostic biomarkers were as low as 1000 fm and 100 fm, respectively. Moreover, this high-performance SERS platform revealed fingerprint peaks of sepsis biomarkers at low frequencies, paving the way for future development of multiplexed detection of these biomarkers in more complex biological matrices. In another work, Lin et al.[135] developed Ag NPs/BP hybrid nanosheets that exhibited remarkable SERS performance and single-molecule detection capability, as illustrated in Figure 5b. Owing to the synergistic resonance enhancement of molecular resonance, photo-induced charge transfer, and the EM effect, this SERS substrate achieved a low LOD of $10^{-20}$ mol $L^{-1}$ for R6G. Utilizing a new polarization-mapping method combined with ML, the Ag NPs/BP hybrid nanosheets enabled detection and recognition of different tumor exosomes at the single-molecule level, demonstrating their potential for biomonitoring and early cancer detection. Beyond the single function of SERS sensing, Ma et al.[198] fabricated a hybrid nanostructure of Au NPs and Ag NPs on BP nanosheets for both detection and degradation of hazardous materials. The abundant active “hot spots” induced by the Au-Ag NPs, along with the charge transfer between BP and probing molecules, led to a low LOD of $4.5 \times 10^{-10}$ M for 4-Mercaptobenzoic acid (4-MBA). For practical application, this SERS substrate was further incorporated into flexible SERS chips for in situ monitoring of thiram, where a LOD of $2.6 \times 10^{-6}$ mg $mL^{-1}$ was achieved. Additionally, owing to the formation of a metal–semiconductor heterojunction, this SERS chip possesses photocatalytic self-cleaning properties, enabling repeatable and reliable assays.

Hybrid structures of metal NPs and MXenes[100, 153, 162, 171, 172, 199–202] have also demonstrated high SERS performance and, especially, their potential in practical biosensing applications related to food safety[172,202,203] and human health.[100,153,162,200,201] For instance, Au NPs/TiC nanosheets were developed and employed for the SERS detection of chlorpromazine,[199] achieving a wide linear range ($10^{-1}$–$10^{-10}$ M) and an ultralow LOD of $3.92 \times 10^{-11}$ M. In another example, Ag NPs/$Ta_4C_3$ hybrids were fabricated and explored as SERS substrates for the sensitive detection of pesticide ziram,[202] achieving a LOD of $10^{-6}$ M. Liu et al.[162] fabricated Ag NPs/$Ti_3C_2$ hybrid nanosheets for the sensitive detection of 4-MBA molecules, exhibiting excellent SERS performance, long-term stability, and good uniformity. MXene-based nanohybrids have also been employed to develop SERS chips that combine superior sensing capability with additional practical features. For example, a wearable SERS sensor based on Au NPs/TiVC hybrids was engineered for physiological

Author Manuscript Author Manuscript Author Manuscript Author Manuscript

monitoring.[201] In addition to the sensitive detection of nicotine, methotrexate, nikethamide, and 6-acetylmorphine in sweat, this sensor also exhibited good mechanical durability and long-term stability. In another example, Au NPs/$Ti_3C_2$ hybrids, synthesized via electrostatic self-assembly, were not only capable of sensitive SERS detection of *E. coli* and *B. subtilis*,[153] but also exhibited antibacterial and photothermal sterilization effects. Chen et al.[200] fabricated a flexible SERS chip by integrating Ag NPs/$Ti_3C_2T_x$ hybrids with PMMA for SARS-CoV-2 detection. The synergistic effects from Ag NPs and MXene led to high SERS performance, whereas PMMA integration provided the sensor chip with both mechanical flexibility and self-rectification functionality. In another study, Au nanostars/$Ta_4C_3$[204] hybrids were used as SERS substrates and exhibited a LOD of $10^{-9}$ M for detecting 4-aminothiophenol (PATP). By combining with filter paper, the fabricated paper-based SERS substrate was able to detect thiram residues after directly wiping the apple surface. Notably, Xue et al.[189] developed a SERS substrate based on Ag nanocubes (NCs)/$Ti_3C_2T_x$ MXene hybrid nanostructures (Figure 5c) for therapeutic drug monitoring. From the Raman spectra shown in Figure 5c, the maximum enhancement was achieved when integrating $Ti_3C_2T_x$ with Ag NCs, compared to using Ag NCs or $Ti_3C_2T_x$ alone as the SERS substrate. This superior performance was attributed to dual EM-CM enhancement—specifically, the dual effect of EM "hotspots" formed in the nanoscale gaps between clustered Ag NCs, and effective photo-induced charge transfer between the 2D $Ti_3C_2T_x$ matrix and target molecules.

In addition to MXenes, $MoS_2$ nanosheets—the most common TMDC—have been combined with Au NPs into hybrid structures for SERS-based biosensing.[205,206] With the EM effect of Au NPs and special surface modifications, such a biosensor was able to detect 2,4,6-trinitrotoluene (TNT) explosives[205] with a LOD of $2 \times 10^{-7}$ M and high selectivity. Dou et al.[206] also demonstrated the SERS performance of Au NPs/$MoS_2$ for the rapid and sensitive detection of trace malachite green (MG) in flowing water, with a LOD of $1 \times 10^{-8}$ mol $L^{-1}$ and high selectivity. While metal NPs/TMDC hybrid structures have shown promise for SERS biosensing, the fabrication process of metallic nanostructures may cause damage to the TMDC, potentially compromising sensor performance. To address this, Zhang et al.[207] developed a general approach for fabricating such high-performance hybrid platforms. The as-prepared SERS substrates—Au NPs/$ReSe_2$, Au NPs/$MoS_2$, and Au NPs/$PdSe_2$—exhibited LODs of $10^{-10}$ M, $10^{-10}$ M, and $10^{-12}$ M for R6G, respectively.

0D-2D hybrids between metal NPs and graphene or its derivatives—such as GO and reduced GO (rGO)—have also been widely explored as SERS substrates. Example integrations include: Au NPs/graphene,[208] Ag NPs/graphene,[209–211] Au NPs/GO,[212,213] Ag NPs/rGO;[214] as well as hybrids with non-spherical NPs, such as Au nanostars/rGO,[215] Ag NCs/graphene,[216] and triangular Ag nanoplates/GO.[217] These hybrid systems have demonstrated practical and sensitive SERS detection across a broad range of analytes, including pesticide residues,[218,219] Alzheimer's disease (AD) biomarkers,[212] persistent organic pollutants (POPs),[216] bacteria,[217] and biomolecules associated with early-stage cancer.[220] For instance, Zhao et al.[221] fabricated an ultrasensitive SERS substrate by integrating both Au nanostars and Au@Ag NPs onto GO nanosheets. This platform exhibited analyte enrichment capability and leveraged a multidimensional plasmonic coupling effect induced by the Au@Ag NPs, achieving an ultralow LOD of $10^{-11}$ M for

Author Manuscript Author Manuscript Author Manuscript Author Manuscript

bilirubin (BR) detection. In another study, Atta et al.[219] developed a GO-coated Au@Ag nanostar-based SERS sensor for pesticide detection, demonstrating ultrahigh sensitivity with LODs of 10, 50, 100, and 100 pM for ziram, phorate, triazophos, and azinphos-methyl, respectively. These findings highlight the strong potential of such hybrid platforms for multiplexed and ultrasensitive biosensing in complex samples. Table 3 summarizes recently reported hybrid structures of noble metal NPs with 2DMs for SERS sensing.

Beyond metal NPs, 2DMs have also been integrated with more complex[164,190,191,222,223] or specially engineered[224–228] nanostructures to advance SERS-based biosensing. For example, Qiu et al. designed a heterostructure composed of graphene microflowers (Gr MFs) and wrinkled 2H-phase $MoS_2$[190] for plasmon-free SERS detection (Figure 5d). The Gr MFs/wrinkled $MoS_2$ hybrids exhibited a LOD of $5 \times 10^{-11}$ M for rhodamine B (RhB), with an EF of $2.96 \times 10^7$. This excellent SERS performance was attributed to the molecular enrichment provided by abundant active SERS regions in Gr MFs, along with synergistic effects from enhanced charge transfer and multiple light-scattering events. Similarly, in another study, $MoS_2$@Ag nanoflowers (NFs)/rGO[229] hybrid nanostructures were fabricated, exhibiting excellent SERS performance and multiplexed capability. Benefiting from the synergistic effects of numerous “hot spots” introduced by $MoS_2$@Ag NFs, as well as the large molecular enrichment and CM effect of rGO, this SERS substrate achieved ultralow LODs of $4.7 \times 10^{-9}$, $5.6 \times 10^{-9}$, and $7.7 \times 10^{-8}$ M for detecting melamine, VA, and BPA in milk, respectively. Notably, this sensing platform also possesses photocatalytic capability, enabling recyclable detection through in situ degradation of these mixed additives in milk. Ghopry et al.[222] developed a novel vdWH composed of TMDC ($MoS_2$ and $WS_2$) nanodomes (NDs) and monolayer graphene, exhibiting excellent SERS performance comparable to that of metal NPs/graphene hybrids. Both CM and EM effects were enhanced, resulting from the increased electric dipole moment and dipole-dipole interactions at the vdW interface, as well as the LSPR near the TMDC NDs. Subsequently, the same group developed an Au NPs/$WS_2$ NDs/graphene heterostructure[191] for SERS-based biosensing (Figure 5e), achieving an order of magnitude higher sensitivity than the previous TMDC NDs/graphene system, owing to the superimposed LSPR effects from both $WS_2$ NDs and Au NPs. This SERS substrate can be fabricated via layer-by-layer growth, indicating its potential for scalable and low-cost biosensor production. Later on, they fabricated intermixed $WS_2$ and $MoS_2$ nanodisks on graphene for sensitive SERS detection.[230] Owing to the superposition of the LSPR effects, this sensing platform outperformed the SERS substrate based on a single type of TMDC on graphene. Zhao et al.[164] fabricated a hybrid SERS substrate by integrating core-shell Au@$Cu_2O$ nanotriangles with $Ti_3C_2T_x$ MXene ultrathin nanosheets. The system exhibited excellent SERS performance arising from the synergistic EM enhancement at the Au tips and across the entire nanotriangles, along with multiple charge-transfer pathways within the hybrid structures. Bian et al.[231] fabricated a MOF@Ag/MXene hybrid structure on PDMS for the sensitive SERS detection of *E. coli* (Figure 6a). The overall high performance was attributed to the combined effects of CM enhancement, analyte enrichment, and EM amplification contributed by each component. In another work, Liu et al.[232] developed a sensitive and flexible SERS sensor based on ZnO QDs/$Ti_3C_2$ MXene hybrids, as illustrated in Figure 6b. It achieved a LOD of $1 \times 10^{-7}$ M for the detection of 4-mercaptopyridine (4-MPY) due to the combination of several effects:

Author Manuscript Author Manuscript Author Manuscript Author Manuscript

multiple charge transfer paths, improved charge-transfer efficiency facilitated by oxygen vacancies in ZnO QDs, and the presence of a Schottky barrier between $Ti_3C_2$ and ZnO QDs. Additionally, this biosensor demonstrated self-cleaning capability via photocatalysis and exceptional reusability in methylene blue (MB) detection, suggesting its strong potential for in situ molecular detection in food safety and environmental monitoring. Impressively, Li et al.[223] fabricated $Fe_3O_4$@Au NPs/GO hybrid structures for rapid SERS detection and in situ monitoring of harmful polycyclic aromatic hydrocarbons (PAHs) in water, achieving a LOD of 3.8 μg $L^{-1}$ for Benzo[a]pyrene (BaP) and μg $L^{-1}$-level detection for other PAHs. The combination of excellent magnetic enrichment facilitated by $Fe_3O_4$, the strong adsorption capability of GO, and the pronounced LSPR effect of Au NPs enabled both sensitive SERS detection and photocatalytic removal of BaP, making it a promising approach for environmental monitoring and remediation.

Specially engineered nanostructures have also been actively explored for integration with 2DMs to expand their sensing capabilities. For example, Liang et al.[224] fabricated Au nanopyramids/graphene hybrids as a label-free SERS platform. Combining it with principal component analysis (PCA) enabled precise differentiation and profiling of cell lines and cellular states. In another work, graphene-coated Au nanopyramids were designed, theoretically studied, and experimentally applied for label-free SERS sensing of AD biomarkers, offering rapid, quantitative, and high-sensitivity detection.[225] More sophisticated nanostructures—such as Au NPs/graphene/Cu cone cavities[226] and flexible graphene/Au NPs/rectangular pyramid PMMA hybrids[227]—were also fabricated as innovative SERS substrates for sensitive analyte detection. Extending beyond graphene, Miao et al.[228] developed $Ti_3C_2$ MXene-coated Au/Ag bimetallic nanocuboids as SERS substrates for the multiplexed detection of CV, MG, and MB in natural pond water, achieving high sensitivity and accuracy. Table 4 provides a summary of recently reported 0D-2D hybrids with complex or specially engineered architectures for SERS sensing.

1D nanostructures, such as NRs[233–236] and NWs,[237] have also been utilized in hybrid structures for SERS applications. For example, hBN/Ag NRs[234] hybrid nanostructures were fabricated as recyclable substrates for label-free SERS detection of BR. Without sample pretreatment, this sensor achieved a LOD of $2.5 \times 10^{-8}$ M for detecting BR in blood, owing to the strong affinity and high stability of hBN combined with the EM enhancement provided by Ag NRs. In another work, ultrathin $Ti_3C_2$ MXene nanosheets were decorated onto Ag NRs[235] for sensitive on-site SERS detection of 3,3′,4,4′-tetrachlorobiphenyl (PCB-77) and 4-chlorobiphenyl (PCB-3), reaching LODs of $2.43 \times 10^{-10}$ and $2.14 \times 10^{-9}$ M, respectively. The effective protection of Ag NRs from oxidation by the MXene overlayer, along with the synergistic EM and CM enhancements within the MXene/Ag NRs hybrids, enabled multiplexed detection of PCBs in real soil samples with high sensitivity, stability, and reproducibility. MXene/ZnO NRs[236] hybrid nanostructures were developed with potential for environmental pollutant monitoring (Figure 7a), in which the enhanced analyte affinity and strong charge transfer at the interface facilitated ultrasensitive SERS detection of R6G, achieving a LOD of $10^{-11}$ M. Additionally, this semiconductor nanoarray/2D MXene integration also demonstrated its potential for miRNA detection. More recently, 1D vdW NWs have also gained increasing interest in fabricating noble-metal-free SERS substrates with high sensitivity. For instance, Lv et al. synthesized 1D-2D $WO_{3-x}$

Author Manuscript Author Manuscript Author Manuscript Author Manuscript

NW/$WSe_2$ heterostructures,[237] as demonstrated in Figure 7b, which exhibited attomolar-level sensitivity for MB detection, with a LOD of $5 \times 10^{-18}$ M. The exceptionally high EF of $5.0 \times 10^{11}$ was attributed to ultrafast charge transfer induced by the NWs and strong interlayer coupling in the hybrid system. Table 5 summarizes recently reported 1D-2D hybrid nanostructures for SERS applications.

In 2014, Ling et al.[75] investigated the Raman enhancement effects on different 2DMs. Since then, researchers have been exploring new 2DMs or stacking 2DMs together to create vdWHs for fabricating noble-metal-free SERS substrates with enhanced performance.[240] Particularly, graphene/$MoS_2$ vdWHs are among the most widely studied[241] and have demonstrated significant potential in SERS-based biosensing applications. More recently, Wei et al.[242] used first-principles DFT calculations to systematically investigate the wavelength-dependent SERS response of different 2DMs and of vdWHs with varying numbers of layers, where $MoS_2$ and graphene exhibited strong and broadband enhancement effects. Experimentally, graphene/$MoS_2$ vdWHs have been fabricated and utilized as label-free optical biosensors for detecting DOX,[63] demonstrating good stability, sensitivity, and selectivity. More importantly, multidimensional imaging revealed the mechanisms controlling the biosensing performance, i.e., the doping level of $MoS_2$ and graphene, the charge transfer between them, and the sources of non-uniform doping.[63] More attractively, the SERS performance can be tuned by manipulating the doping state of exfoliated $MoS_2$ monolayers, with n-doped $MoS_2$/dopant hybrids demonstrating enhanced SERS signals for R6G detection.[243] On the other hand, epitaxial graphene with the Fermi level modulated by intercalated 2D metals, i.e., atomically thin, air-stable metal layers fabricated by confinement heteroepitaxy (CHet),[244] also exhibited improved GERS detection with higher sensitivity and selectivity.[245] Meanwhile, the interlayer distance between $MoS_2$ and graphene also influences the SERS performance,[246] i.e., shorter distance enhances the dipole-dipole interactions and charge transfer, thereby increasing SERS efficiency. These insights offer valuable guidance for engineering 2D vdWHs through rational design of stacking configurations—such as stacking order and twist angles[247]—and tuning doping levels to maximize SERS performance. Although varying the number of layers in the heterostructure could optimize the SERS performance,[240] calculations have shown that the topmost contact layer exerts the most significant influence within multilayer vdWH systems.[242]

Rationally designed multicomponent hybrid nanostructures with mixed dimensions have emerged to achieve synergistic enhancements in SERS performance. Since the undesired fluorescence background in SERS, originating from either analytes or substrates, can interfere with Raman signals, integrating materials that effectively quench fluorescence can significantly improve SERS performance. For example, in the design of hBN/graphene/Ag NPs hybrid structures for SERS detection,[248] Cai et al. used graphene to suppress the fluorescence background from probe molecules. The SERS substrates can be regenerated by heating, while the hBN overlayer protects both graphene and Ag NPs from oxidation during this process. The multicomponent structures can also facilitate collective contributions from different mechanisms, further enhancing SERS performance. For instance, Lu et al.[174] developed GO/Ag/3D PS nanospheres as SERS substrates for sensitive and multiplexed detection of melamine and dicyandiamide in dairy products. Jiang et al.[249] fabricated

Author Manuscript Author Manuscript Author Manuscript Author Manuscript

Ag nanostars-multiwall carbon nanotube (MWCNT)/GO hybrids for nanoplastic detection. Owing to the EM enhancement of Ag nanostars, along with the CM and enrichment effects of MWCNT/GO, this SERS platform achieved a LOD of $5 \times 10^{-5}$ mg $mL^{-1}$ for detecting 50 nm PS nanoplastics. Wang et al.[238] constructed metal-dielectric-metal nanostructures composed of Au NPs/GO/Ag NWs as SERS biosensors for identifying and detecting PAHs, as illustrated in Figure 7c. By leveraging the localized enhanced EM field generated between Au NPs and Ag NWs, along with the effective trapping of PAHs by GO through $\pi$–$\pi$ interactions, this platform achieved LODs of $10^{-8}$ M for pyrene, anthracene, and phenanthrene, and $10^{-7}$ M for BaP, respectively, demonstrating excellent selectivity, sensitivity, and multiplexing capability. Similarly, Mei et al.[173] developed Au/graphene/Ag/ZnO hybrid nanostructures that leveraged multidimensional plasmonic coupling for enhanced SERS performance. The graphene middle layer not only facilitated excellent analyte enrichment but also served as a protective barrier against Ag oxidation, which improved the overall stability and reproducibility of the system. In another work, Zhang et al.[250] also exploited multidimensional plasmonic coupling of precious metals and fabricated a flexible Ag NPs/graphene/Cu hybrid SERS substrate with high performance. Notably, Sun et al.[239] designed Ag NPs/graphene/$WTe_2$ hybrid nanostructures on a Si/$SiO_2$ substrate (Figure 7d). By leveraging the energy-level alignment between $WTe_2$ and graphene, the charge transfer process was promoted, resulting in a significantly enhanced CM effect in SERS. This system exhibited substantially higher SERS performance than Ag NPs/$WTe_2$ or Ag NPs/graphene, with the LOD reduced by three orders of magnitude for R6G, providing insights into the rational design of highly sensitive SERS platforms with stronger CM contribution. MXenes have also been integrated into multicomponent nanostructures. For instance, Liu et al.[251] developed Au NPs/$MoS_2$/MXene hybrids for miRNA detection, achieving a linear range of 10 aM–1 nM and a LOD of 6.61 aM, indicating the strong potential of multicomponent nanohybrids for ultra-sensitive SERS sensing. Table 6 summarizes recently reported multicomponent nanohybrids with mixed dimensions for SERS applications.

### 5.2. Recent Advances in SPR Biosensing

SPR biosensors offer significant advantages for real-time monitoring of molecular interactions and analyte binding without the need for labeling. Since the working principle of SPR biosensors relies on the excitation of surface plasmons, metallic thin films (such as Au and Ag), which possess prominent plasmonic properties in the visible regime, are crucial components in the sensor design. Au thin films are particularly favorable due to their chemical inertness and robustness in supporting surface plasmons. However, Au does not adsorb bioanalytes efficiently, limiting the sensitivity of conventional SPR biosensors. Ag thin films, while exhibiting stronger plasmonic behavior than Au and enhancing the sensitivity, i.e., with SPR peaks of greater intensity and narrower width, are prone to oxidation and corrosion,[252] which affects the stability of SPR biosensors. To overcome these limitations, other metals have been explored, with Cu emerging as a compelling alternative due to its similar plasmonic behavior to Au but with higher electrical conductivity.[253,254] The Cu-based SPR biosensor exhibited a narrower SPR peak width and a lower minimum reflectance value compared to that of the Au-based sensor (Figure 8a).[255] Additionally, Cu is more cost-effective and feasible for scalable fabrication.

Author Manuscript Author Manuscript Author Manuscript Author Manuscript

Beyond finding substitute metals, researchers have also explored multilayer designs to improve sensor performance. As illustrated in Figure 8a, each layer serves its specific function in the Kretschmann configuration, such as an affinity layer for binding events, an encapsulation layer above the sensing layer for protection, and an interface layer between the prism and the sensing film for better adhesion. The choice of different materials for these layers significantly impacts the overall sensor performance, which has been systematically evaluated.[255]

When integrating 2DMs with SPR biosensors, the plasmonic properties and thereby the sensor performance can be further tuned. The large surface area of 2DMs supports numerous active sites, ensuring efficient bioanalyte adsorption. Covering metallic thin films with 2DMs can also prevent oxidation and corrosion, thus improving the durability of SPR biosensors. Additionally, the surface of 2DMs can be functionalized with different molecules or complementary target analytes, providing selective and sensitive detection for various applications. In particular, 2DMs facilitate strong light–matter interactions, which could promote the coupling between incident light and surface plasmons. Moreover, the tunability of the electrical and optical properties of 2DMs allows further tailoring of the SPR properties to suit specific purposes. By stacking 2DMs together into multilayer systems, more possibilities arise for enhancing the light-matter interaction, particularly by increasing the optical absorption of the system and thereby improving the performance of SPR biosensors. In this subsection, we review recent advances in SPR biosensors that benefit from 2DMs and their hybrid structures, discussing the roles of individual 2DMs as well as their synergistic effects in enhancing sensor performance.

**5.2.1. SPR Biosensors Based on Kretschmann Configuration:** Graphene has been widely used to enhance the performance of SPR biosensors. Due to $\pi$-$\pi$ interactions, its strong surface affinity enables efficient binding of bioanalytes, thereby improving the detection capability. In addition, its high carrier mobility and strong optical absorption can enhance the responsiveness of SPR biosensors to the surface binding events, consequently increasing sensitivity and enabling real-time monitoring. Moreover, the optical properties of graphene can be tuned by electrical gating,[262] strain engineering, or doping, offering greater flexibility in optimizing sensor performance. For instance, Chung et al.[263] reported an SPR biosensor with improved sensing performance by depositing graphene on an Ag thin film and uncovered the mechanism underlying this enhancement. By measuring the work function of graphene/Au with varying numbers of graphene layers and doping levels, they deduced that the sensitivity enhancement was attributed to the surface dipole induced by the charge transfer between graphene and Au. Notably, they observed less sensitivity enhancement with three layers of graphene than with monolayer or bilayer graphene, which was explained by the damping of surface plasmons. This phenomenon was also observed in another study, where Panda et al.[264] investigated the performance of a graphene/Au-based SPR biosensor for glucose and gas detection. A nearly twofold increase in the electric field intensity was observed in the optimized structure with monolayer graphene on 55 nm Au, compared to a conventional Au-based SPR biosensor without graphene. However, as the number of graphene layers increased, the SPR curves became broader and shallower, due to the damping of surface plasmons by graphene. Given that more

Author Manuscript Author Manuscript Author Manuscript Author Manuscript

graphene layers could potentially improve the optical absorption, these collective findings suggest that one should carefully consider the competing effects and balance the number of graphene layers to achieve optimal sensor performance. In other works, graphene was also reported to serve as a protective layer for Ag thin films,[69,265] improving both the sensitivity and stability of SPR biosensors. More recently, Jena et al.[266] proposed an SPR biosensor with graphene/AlN/Ag/$TiO_2$/BK7 prism structure. By optimizing the thickness of each constituent layer through simulation, they achieved sensitivities of 138.46 deg $RIU^{-1}$, 163.63 deg $RIU^{-1}$, and 182.85 deg $RIU^{-1}$ for detecting infected plasma, platelets, and hemoglobin, respectively, indicating the potential of SPR biosensors for rapid and high-sensitivity detection of pathogens. In another work, graphene was used in a proposed SPR biosensor for detecting the SARS-CoV-2 virus.[267] Upon optimization, a maximum sensitivity of 433.63 deg $RIU^{-1}$ was achieved using monolayer $BaTiO_3$ and bilayer graphene within the thiol-tethered ssDNA/graphene/$BaTiO_3$/Ag/$TiO_2$/$CaF_2$ prism structure.

Beyond 2D graphene, fabricating a periodic array of 1D graphene nanoribbons can more effectively couple incident light to surface plasmons. Hwang[256] computationally designed an SPR biosensor based on gate-controlled graphene nanoribbons, as illustrated in Figure 8b. Notably, owing to the localized enhanced field at the nanoribbon edges, the binding of target analytes significantly modulates the SPR frequency, thereby enabling sensitive and metal-free SPR detection. Unlike conventional SPR configurations, this device generates the SPR curve by sweeping the graphene chemical potential while maintaining a fixed incident angle. For analytes with a RI of 1.33, the calculated sensitivity reached 36 401.1 mV $RIU^{-1}$. In another work, Barrios[268] investigated the optical response and sensitivity of a graphene nanoribbon/Au-based SPR biosensor integrated with a microfluidic flow cell. Nanoribbons with a high height-to-width aspect ratio were found to be optimal for minimizing the LOD.

As an analog to graphene but with superior physical and chemical properties, antimonene has recently emerged and attracted great interest in enhancing the performance of SPR biosensors.[71] In addition to high hydrophilicity and large surface area, the high adsorption energy and large work function make antimonene preferable as an affinity layer compared to other 2DMs. For example, an Au NRs/antimonene-based SPR biosensor[88] achieved label-free, molecular-level quantification of miRNA with a LOD of 10 aM. In another study, Singh et al.[142] proposed an SPR biosensor with antimonene/Au/BK7 prism structure for miRNA detection. It exhibited a sensitivity of 181.9 deg $RIU^{-1}$, outperforming both graphene/Au-based (147.95 deg $RIU^{-1}$) and conventional Au-based SPR biosensors (144.45 deg $RIU^{-1}$). Notably, three layers of antimonene led to a less pronounced improvement in sensitivity, similar to the observed phenomenon with graphene layers, which was attributed to the electron energy loss. However, since the imaginary part of its dielectric constant is small, antimonene exhibits much less energy loss compared to graphene. These antimonene-based SPR biosensors are not only promising for real-time detection of hybridization events, but also demonstrate strong potential for practical applications in early cancer diagnosis. Beyond miRNA detection, antimonene-based SPR biosensors have also been proposed for detecting other analytes[146,147] with high sensitivity. For instance, Singh et al.[147] designed an antimonene/$BaTiO_3$/Ag/$BaF_2$ prism SPR biosensor for hemoglobin detection, achieving a sensitivity of 303.83 deg $RIU^{-1}$, with antimonene serving as a highly efficient biomolecular recognition layer.

Author Manuscript Author Manuscript Author Manuscript Author Manuscript

Besides graphene, TMDCs have also been utilized to enhance SPR biosensors due to their higher optical absorption. Kumar et al.[257] conducted a comparative study of $WS_2$-, $MoS_2$-, and graphene-covered $BaTiO_3$/Ag/ZnO/BK7 prism SPR sensors (Figure 8c). Among them, $WS_2$ exhibited the highest sensitivity (180 deg $RIU^{-1}$), outperforming $MoS_2$ (174 deg $RIU^{-1}$) and graphene (157 deg $RIU^{-1}$). Although the graphene/$BaTiO_3$/Ag/ZnO/BK7 prism biosensor showed an SPR peak with a narrower full width at half maximum (FWHM), along with higher quality factor and detection accuracy, the highest optimized sensitivity (235 deg $RIU^{-1}$) was achieved with the $WS_2$ (bilayer)/$BaTiO_3$/Ag/ZnO/BK7 prism configuration. In another work, Ouyang et al.[269] studied the enhancement effect of various TMDCs ($MoS_2$, $MoSe_2$, $WS_2$, and $WSe_2$) integrated with a Si thin film in conventional Au-based SPR biosensors, where these additional dielectric layers served as effective light-absorbing media. The topmost TMDC layer was in direct contact with target bioanalytes, acting as an affinity layer. Additionally, the induced charge transfer from the TMDC to Au enhanced the overall SPR performance. The highest sensitivity was achieved using the $WS_2$ (monolayer)/Si (7 nm)/Au (35 nm) configuration. More recently, Daher et al.[270] theoretically investigated an Ag-based SPR biosensor coated with $WSe_2$/Si for detecting urea in blood, achieving a maximum sensitivity of 373.49 deg $RIU^{-1}$ after optimization. Various TMDC layers, such as $WS_2$[271] and $WSe_2$,[272] have also been employed as highly effective biomolecular recognition layers, further enhancing SPR sensor performance. Dey et al.[273] designed a $WSe_2$/Al/Ag SPR biosensor with improved performance. They attributed the enhanced sensitivity to the increased optical absorption arising from the large number of excited electrons at the metal/$WSe_2$ interface, as indicated by the electric field intensity peak at the $WSe_2$/analyte interface.

MXenes also play an important role in enhancing SPR performance. They support surface plasmon polaritons and can amplify the plasmonic resonance when integrated with metal thin films. Notably, the plasmonic properties of MXenes can be tuned by modifying their surface functional groups.[80] Besides, the charge transfer between MXenes and metal thin films can further modulate the electronic and optical properties at the interface, contributing to the development of highly sensitive and tunable SPR biosensors. Additionally, the MXene layer coated on top of Ag film can act as a protective barrier against oxidation.[274–276] Moreover, MXenes can serve as effective biomolecular recognition layers in SPR biosensors, enhancing the sensing capabilities.[79,277] Gan et al.[128] developed a 2D $Ti_2C$ MXene-based SPR biosensor, the performance of which strongly depended on the thickness of $Ti_2C$ nanosheets. The optimized design showed a 79% improvement in sensitivity compared to an SPR sensor without the $Ti_2C$ overlayer. This biosensor also demonstrated its ability to detect heavy metal ions, achieving LODs of 79.2, 56.5, and 92.8 ng $L^{-1}$ for $Pb^{2+}$, $Cr^{2+}$, and $Hg^{2+}$ ions, respectively.

BP, with good hydrophilicity and a large surface-to-volume ratio, can not only act as an affinity layer for bioanalytes, but its layer-dependent bandgap also enables strong and tunable optical absorption, thus enhancing the electric field intensity at the interface when integrated with metal thin films.[278–281] For example, in a BP/Ag-based SPR biosensor,[278] the presence of the BP layer facilitated strong light-matter interaction, leading to improved sensor performance. Bouandas et al.[279] proposed an SPR biosensor with BP/Ni/$SiO_2$/Cu/BK7 prism structure, in which the superior properties of BP significantly enhanced

Author Manuscript Author Manuscript Author Manuscript Author Manuscript

the sensitivity. In another study, Karki et al.[281] compared the performance of SPR biosensors incorporating different metal thin films (Au, Ag, Cu) in the BP/metal/$BaTiO_3$/metal/BK7 prism structure, and observed a significantly increased electric field intensity at both the BP/Cu and sensing medium/BP interfaces. However, despite these promising results, the major drawback limiting the practical application of BP in SPR biosensors is its instability in both air and water.

Covering BP with other 2DMs can prevent its oxidation, which improves the overall stability of SPR biosensors. Additionally, such hybrid structures may further enhance sensitivity.[143,144,259,282] For instance, Akib et al.[283] systematically compared different 2DM combinations within an Ag-based SPR biosensor designed for SARS-CoV-2 detection. Among these, graphene/BP exhibited the highest sensitivity of 390 deg $RIU^{-1}$, along with the best detection accuracy. Similarly, in a later study, they presented the most effective configuration integrating graphene/BP with a Cu-based SPR biosensor for real-time monitoring of the SARS-CoV-2 Omicron variant (Figure 8d),[258] where an enhanced sensitivity of 410 deg $RIU^{-1}$ was obtained. The achieved performance improvements in these graphene/BP-integrated SPR biosensors are attributed to: i) the high optical absorption of BP; ii) the enhanced electric field resulting from charge transfer between the graphene/BP heterostructure and the metal thin film; and iii) the strong adsorption of bioanalytes on graphene via $\pi$–$\pi$ interactions. In another study, Yuan et al.[282] designed an Au-based SPR biosensor with a few layers of BP covered by monolayer graphene. While increasing the number of BP layers improves optical absorption, excess layers can lead to optical loss and plasmon damping. Therefore, the optimal sensing performance was achieved by carefully balancing the Au film thickness and the number of BP layers. Notably, considering that anisotropic BP acts as an optical polarizer, the sensitivity was further improved through optimization of the rotation angle of the proposed SPR sensor.

Besides graphene, the outstanding stability of antimonene also makes it a desirable protective layer in SPR biosensors.[143,144,259] For example, an antimonene/BP-based SPR biosensor was proposed for detecting DNA hybridization.[143] This design not only facilitated strong charge transfer between antimonene/BP and the Al thin film, thereby enhancing SPR sensitivity, but the antimonene overlayer also effectively protected BP from degradation, thus improving the stability of the proposed biosensor. In another study, Singh et al.[259] presented a high-performance Ni/Cu-based SPR biosensor that integrated an antimonene/BP heterostructure, as illustrated in Figure 8e. In addition to the strong charge transfer between antimonene/BP and the bimetallic Ni/Cu thin films, as the number of BP layers increased, higher carrier mobility was obtained due to the reduced effective mass, resulting in significantly enhanced sensitivity. Moreover, by leveraging the anisotropic optical properties of BP, the sensitivity of the designed sensor was further optimized through rotation-angle tuning. Consequently, an ultrahigh sensitivity of 446.90 deg $RIU^{-1}$ was achieved using five BP layers covered by monolayer antimonene, outperforming all other 2DM-based SPR biosensors at that time. The monolayer antimonene not only allowed effective binding of bioanalytes but also acted as a passivation layer protecting BP against oxidation.

Author Manuscript Author Manuscript Author Manuscript Author Manuscript

Graphene/TMDC is another widely used heterostructure in SPR biosensors. The use of graphene alone for signal enhancement is limited due to its relatively low optical absorption compared to TMDCs,[284,285] while the inherent instability of TMDCs also constrains the performance of SPR biosensors. To address these issues, researchers have explored graphene/TMDC heterostructures to enhance overall sensor performance[284] and minimize device size.[285] For instance, Rouf et al.[286,287] proposed a graphene/$MoSe_2$/Ag/Ti/BK7 prism SPR biosensor for detecting various bioanalytes, including DNA hybridization events. A maximum sensitivity of 215.5 deg $RIU^{-1}$ was reported, which is 2.42 times higher than that of graphene/Au-based SPR biosensors. In another work, Kumar et al.[288] conducted a comparative study of the SPR performance based on three different designs, i.e., graphene, graphene/MXene, and graphene/$MoS_2$, on Ag/Ti/BK7 prism structure, for the detection of carcinoembryonic antigen (CEA) biomarkers. They found that the integration of graphene/$MoS_2$ provided the greatest enhancement in overall sensor performance.

Heterostructures composed of MXenes and other 2DMs have also been reported to enhance SPR performance. For example, the designed $Ti_3C_2T_x$/graphene-based SPR sensor[289] demonstrated its highest sensitivity of 241.20 deg $RIU^{-1}$ when using three layers of MXene. In another study, an antimonene/$Ti_3C_2T_x$ hybrid structure[290] was employed in an Au-based SPR biosensor, where a sensitivity of 224.26 deg $RIU^{-1}$ was achieved, owing to the high conductivity of MXene and the superior properties of antimonene. Kumar et al.[291] proposed an SPR biosensor using a $Ti_3C_2T_x$/BP hybrid structure on bimetallic Ni/Cu thin films, achieving a maximum sensitivity of 304.47 deg $RIU^{-1}$. In another work, they designed a similar SPR biosensor[260] using an Ag thin film instead, with an additional Si layer inserted between the $Ti_3C_2T_x$/BP heterostructure and the Ag film (Figure 8f). This design exhibited a significantly improved sensitivity of 127.58% over that of a conventional Au-based SPR sensor, owing to: i) the high metallic conductivity, biocompatibility, hydrophilicity, and strong surface affinity of functionalized $Ti_3C_2T_x$;[260,291] ii) the high charge carrier mobility and carrier confinement,[260] as well as the layer-dependent direct and tunable bandgap of BP;[291] and iii) the integration of a high-RI Si layer.[260] The heterostructure of MXene/BP could provide higher charge carrier mobility, and these layered materials also facilitate strong light-matter interactions, which consequently increase the overall sensitivity of SPR biosensors.

By constructing heterostructures of 2DMs, additional coupling effects can be introduced into the system, further enhancing sensitivity. For instance, Kumar et al.[261] proposed a Fano resonance-based SPR biosensor with hBN/LiF/Ag/SF11 prism structure (Figure 8g), achieving a phase sensitivity of 1000 deg $RIU^{-1}$ and a wavelength sensitivity of 900 nm $RIU^{-1}$. The Fano resonance was produced by the coupling between surface plasmon polaritons and the photonic waveguide modes supported by 2D hBN.[261] This Fano resonance introduces a sharp and steep feature, allowing for much more sensitive detection compared to standard SPR systems. In another work, Wang et al.[292] designed a tunable Fano resonance-enhanced SPR biosensor based on MXene/$MoS_2$ heterostructure. An optical waveguide layer was introduced to support planar waveguide modes. These modes coupled with the SPR, which was enhanced by the MXene/$MoS_2$ heterostructure. This effective coupling substantially improved the responsiveness of the biosensor to bioanalytes and enhanced the overall sensitivity.[292]

Author Manuscript Author Manuscript Author Manuscript Author Manuscript

Integrating multilayer heterostructures of 2DMs into SPR biosensors not only allows for further tuning of the system but also enables detection across a broader range of RIs, accommodating diverse biological samples.[293,294] For instance, an SPR biosensor with blue phosphorus-$MoS_2$/Au/$PtSe_2$/$CaF_2$ prism structure[293] was capable of detecting across a broad RI range from 1.33 to 1.36; another sensor with $WS_2$/$HfSe_2$/BP/Ag/BAK1 prism[294] configuration could detect across an extended RI range from 1.33 to 1.39. Ghodrati et al.[295] proposed a multilayer SPR biosensor composed of $Ti_3C_2T_x$/$MoO_3$/$MoS_2$/Ag/BK7 prism aimed at detecting glucose in aqueous solutions with varying RIs. Table 7 summarizes recent 2DM- and their hybrid nanostructure-based SPR biosensors with the Kretschmann configuration.

The use of multilayer 2DM structures also enables the miniaturization of SPR biosensors for practical applications. In particular, optical fiber-based SPR biosensors are favored due to their compact size and flexibility for in situ and remote sensing. Additionally, optical fibers can withstand complex and harsh environments. From an application perspective, fiber-optic SPR biosensors have demonstrated versatility in both environmental monitoring and medical diagnostics. In the next subsection, we provide an overview of recent advances in fiber-optic SPR biosensors utilizing 2DMs and their hybrid nanostructures.

**5.2.2. Optical Fiber-Based SPR Biosensors:** Fiber-optic SPR biosensors are well known for their advantages in miniaturization, flexibility, and the ability to remotely monitor bioanalytes. However, due to the limited sensing area, their sensitivity is generally lower compared to prism-coupled SPR biosensors. To address this limitation, researchers have explored the integration of 2DM hybrids to enhance sensor performance. For example, Rahman et al.[296] proposed a highly sensitive optical fiber-based SPR biosensor integrating graphene/$MoS_2$ hybrid structure with Ag for the detection of DNA hybridization. Numerical modeling showed that the designed sensor achieved a high sensitivity of 105.71 deg $RIU^{-1}$ and a detection accuracy of 1.626. In another work, Rahman et al.[297] theoretically studied the performance of a fiber-optic SPR biosensor integrating 2DM/BP with Ag, where maximum improvement was achieved using 10 layers of BP covered with 3 layers of graphene. Recently, Vikas et al.[145] designed a tapered fiber-optic SPR biosensor composed of antimonene/graphene/Au for the detection of cancerous cells. Owing to the effective charge transfer from antimonene/graphene to Au, and the strong optical absorption of antimonene/graphene, the sensitivity was significantly enhanced. Through numerical simulations, a sensitivity of 7.3465, 10.9250, 11.8914, and 15.2414 μm $RIU^{-1}$ was obtained for sensing skin, cervical, blood, and adrenal gland cancer, respectively, indicating the potential application of this biosensor in early-stage cancer diagnosis. More recently, Ma et al.[298] developed a fiber-optic SPR biosensor integrating graphene/$MoS_2$ with Au/Cr thin films (Figure 9a) for the sensitive detection of glucose. This heterostructure-modified biosensor exhibited a 9.11-fold increase in sensitivity compared to the Au-based optical fiber SPR sensor, achieving a sensitivity of up to 12 593.06 nm $RIU^{-1}$ for glucose concentrations ranging from 0–500 mg $dL^{-1}$, along with excellent selectivity. These results highlight the strong potential of this optical fiber-based SPR sensor for continuous glucose monitoring.

Hybrid structures of 2DMs and NPs have also been demonstrated to enhance fiber-optic biosensors based on LSPR, and have been widely investigated by researchers. Li et al.[300]

Author Manuscript Author Manuscript Author Manuscript Author Manuscript

reported a double S-tapered optical fiber-based LSPR biosensor using Au NPs coated with either $Nb_2CT_x$ MXene or GO for comparison. The detection sensitivities of tyramine were 17 and 34 pm $\mu M^{-1}$ across a concentration range of 0–300 μM, respectively, with the superior performance of $Nb_2CT_x$ MXene/Au NPs attributed to the abundant functional groups on the $Nb_2CT_x$ surface. Subsequently, the same group developed a W-shaped fiber-optic LSPR biosensor based on $Nb_2CT_x$/Au NPs[301] for the detection of tyramine, achieving a LOD of 6.96 μM. The sensor also exhibited high specificity, good stability, repeatability, and reusability. Impressively, Li et al.[299] functionalized the optical fibers with $Ti_3C_2$ MXene/Au NRs for the ultrasensitive detection of renal cancer proteins and cells (Figure 9b). This biosensor achieved an ultralow LOD of 13.8 zM in pure buffer solution and 0.19 aM in 30% serum solution. Additionally, it successfully identified live renal cancer cells in culture media with a LOD of 180 cells $mL^{-1}$ and high specificity. These findings highlight the potential of this sensing platform for early-stage cancer biomarker detection. More recently, Zhang et al.[302] demonstrated the clinical potential of a designed optical fiber-based LSPR biosensor for the rapid and accurate detection of neurotransmitters. Based on $Ti_3C_2$ MXene/Au NRs, it achieved a high sensitivity for acetylcholine with a LOD of 4.42 μM. Table 8 summarizes recent 2DM hybrid nanostructure-integrated fiber-optic SPR biosensors.

### 5.3. Toward Multifunctional Platforms: Multiplexing, Multimodal, and ML

The rational design of mixed-dimensional hybrid nanostructures based on 2DMs and novel nanomaterials not only provides an approach for improving the performance of biosensors, such as the synergistic enhancements for SERS, but also enables the development of biosensing platforms with complex functions, including multiplex and multimodal detection.

Simultaneous detection of multiple analytes within one single test is more efficient and offers higher throughput to provide a comprehensive understanding of the tested system, which is essential in medical diagnostics and environmental monitoring. However, multiplexing often demands higher performance of the biosensor in sensitivity, selectivity, and reliability. Thus, scientists have explored different strategies in developing multiplexed biosensing platforms, one of which is the employment of mixed-dimensional hybrid nanostructures based on 2DMs. For instance, a SERS substrate consisting of Au/Ag bimetallic nanocuboids coated with $Ti_3C_2$ nanosheets[228] enabled the highly sensitive and reproducible identification of multiple fish drug residues in pond water. The GO-coated Ag-Au nanostars[219] were used as a solution-based SERS biosensing platform for the ultrasensitive and multiplex detection of pesticides, exhibiting high stability and reproducibility. The MXene/Ag NRs substrate[235] was developed to perform multiplex biosensing of PCBs in real soil samples with high sensitivity, reliability, and good recovery percentages, indicating its great potential in simultaneous SERS detection of multiple pollutants at the point of need. The developed GO/Ag/3D PS nanospheres hybrid SERS substrate[174] has demonstrated multiplexed capability in the detection of melamine and dicyandiamide in dairy products. Ag NPs/GO/Ag NWs[238] hybrids were explored as SERS-based biosensors for identifying and multiplexed detection of PAHs. These hybrid nanostructures are very powerful in sensitive and selective detection of target analytes in complex sample matrices, without compromising their reliability and stability. In another

Author Manuscript Author Manuscript Author Manuscript Author Manuscript

work, a robust SERS sensor was fabricated using MXene/GO fibers[303] for the rapid, multiplexed, and label-free detection of pesticide residues. Besides SERS, SPR biosensors can also be developed for multiplex detection. When integrated with microfluidics, the SPR-based platforms not only offer real-time detection but also enable multiplexed biosensing with high throughput.[304–306]

In addition to multiplexing, scientists have also developed biosensing platforms capable of multimodal detection. For instance, the graphene/$MoS_2$ heterostructure was used for multimodal detection of DOX.[63] The PL of $MoS_2$ was modulated by the existence of DOX, and with the help of GERS, the Raman signal of DOX was significantly enhanced. This PL-GERS combination enabled more accurate and reliable detection. In another work, an SPR-SERS plasmonic sensor was developed based on graphene/Au NPs hybrid nanostructures,[307] for the sensitive and dual-modal detection of pesticide residues in soil. This multifunctional sensing platform provided more options for detecting and verifying data, improving both the reliability and repeatability of the detection. Furthermore, optical biosensors can also be integrated with electrochemical detection to form a dual-modal sensing platform. For instance, Kim et al.[308] fabricated a multifunctional biosensor based on GO/$MoS_2$ hybrid nanocomposites capable of detecting Middle East respiratory syndrome coronavirus (MERS-CoV). This biosensor supports both electrochemical and SERS sensing, providing highly sensitive and selective detection of MERS-CoV. Very impressively, utilizing $Ni_3V_2O_8$ nanospheres/rGO/Au hybrid nanostructures, Singh et al.[309] developed a microfluidic device, as illustrated in Figure 10a, for the rapid and dual-modal (electrochemical and SPR) detection (Figure 10b) of cardiac myoglobin (cMb) and cardiac troponin I (cTnI), with pg $mL^{-1}$-level LODs. This sensing platform enables real-time monitoring of the dynamic antibody-antigen interactions, and facilitates self-validation through dual modes, which reduces false readouts. The combination of electrochemical and SPR biosensing complements the advantages of both techniques, providing a multifunctional sensing platform with both high sensitivity and superior tracking of molecular interactions. This innovative sensing platform demonstrated its potential for cardiovascular disease management and monitoring other clinically important biomolecules. In another work, Zhu et al.[203] developed a bifunctional nanosensing platform based on $Ti_2C$ MXene/Au-Ag nanoshuttles hybrid structures. The dual-modal detection, combining electrochemical response and SERS, facilitated accurate determination of carbendazim (CBZ) residues in tea and rice, with improved reliability through cross-validation of the two methods. Additionally, ML models were developed to perform intelligent analysis of both electrochemical and SERS data.

ML is very powerful in building algorithms that allow computers to learn patterns from a large dataset without being explicitly programmed for each specific task. Particularly, ML algorithms are useful in analyzing complex or huge datasets[310] and uncovering the underlying relationships that may not be immediately captured or apparent to human analysts. Recently, researchers have been integrating ML algorithms with optical biosensors to further advance the field. Specifically, ML has been employed for frequency shift analysis of SERS to process large datasets, identify patterns, and recognize subtle spectral changes.[311] For instance, by integrating PCA with a pattern-optimized SERS substrate, Wu et al.[225] achieved breakthroughs in label-free structural analysis, quantification, and species

Author Manuscript Author Manuscript Author Manuscript Author Manuscript

identification of three key AD biomarkers. ML algorithms can also be used for designing highly sensitive SPR biosensors[312] and quantifying the measured biological interactions.[313] Scientists also used ML to extract useful information from experimental data, such as rapid determination of binding affinity,[314] identification of cross-reactive species, and separation of the response signals.[315]

## 6. Conclusion and Outlook

In this review, we discussed the emerging role of 2DMs and their mixed-dimensional hybrid nanostructures in advancing label-free optical biosensing. Specifically, we highlighted the unique properties of representative 2DMs, including graphene, TMDCs, MXenes, BP, and hBN, as well as their biosensing applications. We then extended our discussion beyond 2DMs to their mixed-dimensional hybrid nanostructures for label-free optical biosensing, along with the introduction of commonly used synthesis and fabrication strategies. Recent progress in SERS and SPR-based biosensors employing 2DMs and their hybrid architectures was also assessed, with a focus on leveraging synergistic properties for enhanced biosensor performance. Multifunctional platforms based on these hybrid materials were reviewed, including multiplexing, multimodal detection, and the integration of ML for performance optimization, advanced spectral analysis, and data interpretation.

Despite the promising progress, several challenges remain that limit the practical application of 2DMs and their hybrid nanostructures in biosensing. One major issue is the instability and potential toxicity of certain 2DMs. Several strategies can be applied to overcome this limitation, such as surface passivation, encapsulation, or modification of material composition. Through doping, alloying, or developing functional derivatives of the material, improved environmental stability and reduced toxicity can be achieved.

Scalability and reproducibility of hybrid structures also remain challenging. For instance, the performance of SERS substrates with complex integration of mixed-dimensional materials is often difficult to reproduce. In addition, to date, many SPR biosensors with multilayer or complicated structures are still primarily proposed or studied through theoretical modeling or numerical simulations, as these methods are more time-efficient and cost-effective. In practical applications, the majority of commercial SPR biosensors are functionalized relying on Au thin films rather than multilayer structures. Therefore, overcoming the challenges of integration complexity and bridging the gap between theoretical and experimental performance are crucial for the development of biosensors and their translation into real-world applications.

To tackle these issues, researchers are exploring large-area, controllable fabrication techniques that are more robust and capable of producing wafer-scale 2DM heterostructures with high uniformity. Standardized fabrication protocols and reproducible workflows are also essential to ensure consistent quality and performance across biosensors. Additionally, characterization techniques such as Raman mapping, AFM, and XPS should be actively employed to analyze and verify the structural and optical properties of these systems.

Author Manuscript Author Manuscript Author Manuscript Author Manuscript

Furthermore, a deeper understanding of the underlying physics within multicomponent hybrid nanostructures is essential. Scattering-type scanning near-field optical microscopy (sSNOM), an AFM-based technique, has proven to be highly effective in revealing light–matter interactions and coupling phenomena at the nanoscale. Complementing such advanced techniques with additional characterization methods can provide a more comprehensive understanding of the properties of the studied hybrid nanostructures.

Looking ahead, the future of label-free optical biosensing lies in sensor miniaturization and interdisciplinary integration across physics, materials science, chemistry, optical engineering, and biomedical engineering. The unique properties of 2DMs and their hybrid nanostructures are well-suited to enabling miniaturized and flexible platforms, paving the way toward the “lab-on-a-chip” vision. By leveraging both the flexibility and unique optical properties of 2DMs, wearable label-free optical biosensors could enable non-invasive detection and remote monitoring with high sensitivity and specificity. Integrating ML with biosensing technologies could further enhance system performance, enable rapid and sophisticated analysis of large or multidimensional datasets, and support real-time data interpretation. Interdisciplinary efforts will continue to drive the development of next-generation intelligent biosensors—capable of non-invasive, real-time, remote monitoring for healthcare diagnostics and beyond.

## Acknowledgements

This work was supported by the Centers for Disease Control and Prevention/National Institute for Occupational Safety and Health (CDC/NIOSH) Grant No. 1 R01OH012579-01-00. Its contents are solely the responsibility of the authors and do not necessarily represent the official views of CDC.

## Biographies

**Xinyi Li** received her Ph.D. degree (2024) in Engineering Science from The Pennsylvania State University, with research focused on using near-field imaging and other characterization techniques to study the nanoscale properties of 2D materials and their van der Waals heterostructures. She obtained her B.S. in Applied Physics from the University of Science and Technology of China and M.S. in Physics from Lehigh University. Currently, Dr. Li is a postdoctoral researcher in the School of Mechanical and Materials Engineering at Washington State University, working on developing portable biosensors based on advanced nanomaterials and smartphone integration for health monitoring and biomedical diagnostics.

Author Manuscript Author Manuscript Author Manuscript Author Manuscript

**Yonghao Fu** is a Ph.D. candidate in Materials Science and Engineering at Washington State University. His research focuses on nanomaterials, additive manufacturing, and biosensor technologies, with emphasis on flexible electrochemical sensors, wearable devices, and advanced drug delivery systems. He investigates the integration of 3D printing with nanostructured materials to develop multifunctional platforms for health monitoring and environmental diagnostics. His work also explores nanocarrier systems designed to improve therapeutic delivery and treatment outcomes.

**Yuehe Lin** is a Professor at Washington State University whose research focuses on nanotechnology, particularly the synthesis of functional nanomaterials for biomedical, energy, and environmental applications. He has authored over 600 peer-reviewed publications with ~100,000 citations (h-index 162) and has been recognized as a Highly Cited Researcher (20142024). Dr. Lin holds 20 patents, with half licensed for industrial commercialization. He is a Fellow of the National Academy of Inventors, AAAS, AIMBE, the Royal Society of Chemistry, and the Electrochemical Society, as well as an elected member of the Washington State Academy of Sciences.

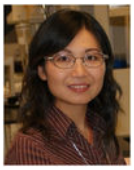

**Dan Du** is a Research Professor at Washington State University with expertise in biochemistry and nanosensors. Her research focuses on nano-biotechnology, particularly the synthesis of functional nanomaterials and the development of small-scale devices for biomedical diagnostics, drug delivery, and health monitoring. She has authored more than 350 peer-reviewed publications with over 42 000 citations and has been recognized as a Highly Cited Researcher (20202024)

## References

[1]. Kim ER, Joe C, Mitchell RJ, Gu MB, Trends Biotechnol. 2023, 41, 374. [PubMed: 36567185]
[2]. Hemdan M, Ali MA, Doghish AS, Mageed SSA, Elazab IM, Khalil MM, Mabrouk M, Das DB, Amin AS, Sensors 2024, 24, 5143. [PubMed: 39204840]
[3]. Shahid A, Nazir F, Khan MJ, Sabahat S, Naeem A, Front Bioeng Biotechnol 2023, 11.

Author Manuscript Author Manuscript Author Manuscript Author Manuscript

[4]. Jiao L, Xu W, Wu Y, Yan H, Gu W, Du D, Lin Y, Zhu C, Chem. Soc. Rev 2021, 50, 750. [PubMed: 33306069]

[5]. Ruan X, Wang Y, Cheng N, Niu X, Chang Y, Li L, Du D, Lin Y, Adv. Mater. Technol 2020, 5, 2000171.

[6]. Lyu Z, Ding S, Fang L, Li X, Li T, Xu M, Pan X, Zhu W, Zhou Y, Du D, Lin Y, Anal. Chem 2023, 95, 4521. [PubMed: 36843270]

[7]. Samuel VR, Rao KJ, Biosens. Bioelectron. X 2022, 11, 100216.

[8]. Singh AK, Mittal S, Das M, Saharia A, Tiwari M, Alexandria Eng. J 2023, 67, 673.

[9]. Pirzada M, Altintas Z, Micromachines 2020, 11, 356. [PubMed: 32235546]

[10]. Mostufa S, Rezaei B, Ciannella S, Yari P, Gómez-Pastora J, He R, Wu K, ACS Omega 2024, 9, 24181. [PubMed: 38882113]

[11]. Moerner WE, Proc. Natl. Acad. Sci. USA 2007, 104, 12596. [PubMed: 17664434]

[12]. Dey S, Dolci M, Zijlstra P, ACS Phys. Chem. Au 2023, 3, 143. [PubMed: 36968450]

[13]. Sang S, Wang Y, Feng Q, Wei Y, Ji J, Zhang W, Crit. Rev. Biotechnol 2015, 1.

[14]. Nava G, Zanchetta G, Giavazzi F, Buscaglia M, Nanophotonics 2022, 11, 4159. [PubMed: 39634532]

[15]. Khansili N, Rattu G, Krishna PM, Sens. Actuators B Chem 2018, 265, 35.

[16]. Rasheed S, Kanwal T, Ahmad N, Fatima B, Najam-ul-Haq M, Hussain D, TrAC, Trends Anal. Chem 2024, 173, 117640.

[17]. Soler M, Lechuga LM, ChemistryEurope 2025, 3, 202400106.

[18]. Lei Z, Guo B, Adv. Sci 2022, 9, 2102924.

[19]. Kizhepat S, Rasal AS, Chang J-Y, Wu H-F, Nanomaterials 13, 2023 1520. [PubMed: 37177065]

[20]. Verma A, Yadav BC, Sustainable Mater. Technol 2024, 40, 00900.

[21]. Hassan JZ, Raza A, Din Babar ZU, Qumar U, Kaner NT, Cassinese A, J. Mater. Chem. A Mater 2023, 11, 6016.

[22]. Chia HL, Mayorga-Martinez CC, Pumera M, Adv. Funct. Mater 2021, 31, 2102555.

[23]. Yang G, Zhu C, Du D, Zhu J, Lin Y, Nanoscale 2015, 7, 14217. [PubMed: 26234249]

[24]. Zhu C, Du D, Lin Y, 2D Mater. 2015, 2, 032004.

[25]. Luo Y, Li Z, Zhu C, Cai X, Qu L, Du D, Lin Y, Trends Biotechnol. 2018, 36, 1145. [PubMed: 29954613]

[26]. Wang Y, Li Z, Hu D, Lin C-T, Li J, Lin Y, J. Am. Chem. Soc 2010, 132, 9274. [PubMed: 20565095]

[27]. Ruan X, Liu D, Niu X, Wang Y, Simpson CD, Cheng N, Du D, Lin Y, Anal. Chem 2019, 91, 13847. [PubMed: 31575114]

[28]. Novoselov KS, Mishchenko A, Carvalho A, Castro Neto AH, Science 2016, 353.

[29]. Basov DN, Fogler MM, García De Abajo FJ, Science 1979, 354.

[30]. Guo X, Lyu W, Chen T, Luo Y, Wu C, Yang B, Sun Z, de Abajo FJG, Yang X, Dai Q, Adv. Mater 2023, 35, 2201856.

[31]. Dai C, Liu Y, Wei D, Chem. Rev 2022, 122, 10319. [PubMed: 35412802]

[32]. Nisar S, Dastgeer G, Shazad ZM, Zulfiqar MW, Rasheed A, Iqbal MZ, Hussain K, Rabani I, Kim D, Irfan A, Chaudhry AR, Adv. Sci 2024, 11, 2401386.

[33]. Li J, Wijaya LNA, Jang DW, Hu Y, You J, Cai Y, Gao Z, Mi Y, Luo Z, Small 2025, 21, 2408961.

[34]. Duan Q, Liu Y, Chang S, Chen H, Chen J, Sensors 2021, 21, 5262. [PubMed: 34450704]

[35]. Philip A, Kumar AR, TrAC, Trends Anal. Chem 2024, 171, 117497.

[36]. Bansal A, Srivastava SK, Sens. Actuators A Phys 2024, 369, 115159.

[37]. Jebakumari K, Murugasenapathi N, Palanisamy T, Biosensors 2023, 13, 102. [PubMed: 36671937]

[38]. Yin Z, Xu K, Jiang S, Luo D, Chen R, Xu C, Shum P, Liu YJ, Mater. Today Phys 2021, 18, 100378.

[39]. Pinto de Sousa B, Fateixa S, Trindade T, Chem. Eur. J 2024, 30, 202303658.

[40]. Ma Q, Ren G, Mitchell A, Ou JZ, Nanophotonics 2020, 9, 2191.

Author Manuscript Author Manuscript Author Manuscript Author Manuscript

[41]. Oh S-H, Altug H, Jin X, Low T, Koester SJ, Ivanov AP, Edel JB, Avouris P, Strano MS, Nat. Commun 12, 2021 3824. [PubMed: 34158483]

[42]. Sakthivel R, Keerthi M, Chung R-J, He J-H, Prog. Mater. Sci 2023, 132, 101024.

[43]. Liu Y, Huang Y, Duan X, Nature 2019, 567, 323. [PubMed: 30894723]

[44]. Wang P, Jia C, Huang Y, Duan X, Matter 2021, 4, 552.

[45]. Pham PV, Bodepudi SC, Shehzad K, Liu Y, Xu Y, Yu B, Duan X, Chem. Rev 2022, 122, 6514. [PubMed: 35133801]

[46]. Guselnikova O, Lim H, Kim H, Kim SH, Gorbunova A, Eguchi M, Postnikov P, Nakanishi T, Asahi T, Na J, Yamauchi Y, Small 2022, 18, 2107182.

[47]. Li B, Liu S, Huang L, Jin M, Wang J, Coord. Chem. Rev 2023, 494, 215349.

[48]. Li S, Chen Z, Yang F, Yue W, Microchem. J 2023, 194, 109247.

[49]. Lopez GA, Estevez M-C, Soler M, Lechuga LM, Nanophotonics 2017, 6, 123.

[50]. Yesudasu V, Pradhan HS, Pandya RJ, Heliyon 2021, 7, 06321.

[51]. Wu W, Ranasinghe JC, Chatterjee A, Huang S, Mater. Chem. Phys 2024, 318, 129281.

[52]. Wang H-L, You E-M, Panneerselvam R, Ding S-Y, Tian Z-Q, Light Sci. Appl 2021, 10, 161. [PubMed: 34349103]

[53]. Dizaji AN, Ozek NS, Yilmaz A, Aysin F, Yilmaz M, Colloids Surf. B Biointerfaces 2021, 206, 111939. [PubMed: 34186307]

[54]. Yager T, Chikvaidze G, Wang Q, Fu Y, Nanomaterials 2023, 13, 2113. [PubMed: 37513124]

[55]. Wang R, Xu W, Chen D, Zhou R, Wang Q, Gao W, Kono J, Xie L, Ying Y, ACS Appl. Mater. Interfaces 2020, 12, 40629. [PubMed: 32805801]

[56]. Wu C, Guo X, Duan Y, Lyu W, Hu H, Hu D, Chen K, Sun Z, Gao T, Yang X, Dai Q, Adv. Mater 2022, 34, 2110525.

[57]. Bareza N J.r., Gopalan KK, Alani R, Paulillo B, Pruneri V, ACS Photonics 2020, 7, 879.

[58]. Autore M, Li P, Dolado I, Alfaro-Mozaz FJ, Esteban R, Atxabal A, Casanova F, Hueso LE, Alonso-González P, Aizpurua J, Nikitin AY, Vélez S, Hillenbrand R, Light Sci. Appl 2017, 7, 17172.

[59]. Bareza N J.r., Paulillo B, Slipchenko TM, Autore M, Dolado I, Liu S, Edgar JH, Vélez S, Martín-Moreno L, Hillenbrand R, Pruneri V, ACS Photonics 2022, 9, 34.

[60]. Wang J, Li X, Ding Y, Zhang L, Zhao H, Hu Y, Du W, Wang T, Rapid Res. Lett 2024, 18, 2400163.

[61]. Kozuch J, Ataka K, Heberle J, Nat. Rev. Methods Primers 2023, 3, 70.

[62]. Altug H, Oh S-H, Maier SA, Homola J, Nat. Nanotechnol 2022, 17, 5. [PubMed: 35046571]

[63]. Ignatova T, Pourianejad S, Li X, Schmidt K, Aryeetey F, Aravamudhan S, Rotkin SV, ACS Nano 2022, 16, 2598. [PubMed: 35061372]

[64]. Lin Y-C, Torsi R, Younas R, Hinkle CL, Rigosi AF, Hill HM, Zhang K, Huang S, Shuck CE, Chen C, Lin Y-H, Maldonado-Lopez D, Mendoza-Cortes JL, Ferrier J, Kar S, Nayir N, Rajabpour S, van Duin ACT, Liu X, Jariwala D, Jiang J, Shi J, Mortelmans W, Jaramillo R, Lopes JMJ, Engel-Herbert R, Trofe A, Ignatova T, Lee SH, Mao Z, et al., ACS Nano 2023, 17, 9694. [PubMed: 37219929]

[65]. Bolotsky A, Butler D, Dong C, Gerace K, Glavin NR, Muratore C, Robinson JA, Ebrahimi A, ACS Nano 2019, 13, 9781. [PubMed: 31430131]

[66]. Akter M, Anik HR, Tushar SI, Tania IS, Chowdhury M.d.K. H., Hasan S. M.d.M., Bristy BF, Adv. Sensor Res 2024, 3, 2300120.

[67]. Pang Y, Yang Z, Yang Y, Ren T, Small 2020, 16, 1901124.

[68]. Chen S, Xu S, Fan X, Xiao X, Duan Z, Zhao X, Chen G, Zhou Y, Chen J, Mater. Sci. Eng.: R: Rep 2025, 164, 100971. [PubMed: 41890625]

[69]. Tene T, Bellucci S, Arias Arias F, Carrera Almendariz LS, Flores Huilcapi AG, Vacacela Gomez C, Sensors 2024, 24, 4670. [PubMed: 39066066]

[70]. Tanaka T, Yano T, Kato R, Nanophotonics 2022, 11, 2541. [PubMed: 39635668]

[71]. Yuan Y, Peng X, Weng X, He J, Liao C, Wang Y, Liu L, Zeng S, Song J, Qu J, Biosens. Bioelectron 2023, 241, 115672. [PubMed: 37716156]

Author Manuscript Author Manuscript Author Manuscript Author Manuscript

[72]. Catalán-Gómez S, Briones M, Cortijo-Campos S, García-Mendiola T, de Andrés A, Garg S, Kung P, Lorenzo E, Pau JL, Redondo-Cubero A, Sci. Rep 2020, 10, 16039. [PubMed: 32994454]

[73]. Gutiérrez HR, Perea-López N, Elías AL, Berkdemir A, Wang B, Lv R, López-Urías F, Crespi VH, Terrones H, Terrones M, Nano Lett. 2013, 13, 3447. [PubMed: 23194096]

[74]. Sun H, Li D, Yue X, Hong R, Yang W, Liu C, Xu H, Lu J, Dong L, Wang G, Li D, Front. Bioeng. Biotechnol 2022, 10, 941135. [PubMed: 35769098]

[75]. Ling X, Fang W, Lee Y-H, Araujo PT, Zhang X, Rodriguez-Nieva JF, Lin Y, Zhang J, Kong J, Dresselhaus MS, Nano Lett. 2014, 14, 3033. [PubMed: 24780008]

[76]. Amara U, Hussain I, Ahmad M, Mahmood K, Zhang K, Small 2023, 19, 2205249.

[77]. Bhardwaj SK, Singh H, Khatri M, Kim K-H, Bhardwaj N, Biosens. Bioelectron 2022, 202, 113995. [PubMed: 35065477]

[78]. Limbu TB, Chitara B, Garcia Cervantes MY, Zhou Y, Huang S, Tang Y, Yan F, J. Phys. Chem. C 2020, 124, 17772.

[79]. Srivastava A, Prajapati YK, J. Mater. Sci.: Mater. Electron 2022, 33, 8519.

[80]. Hasanah L, Mutia R, Wulandari C, Mulyanti B, Sahari SK, Pawinanto RE, Hamzah AA, Results Opt. 2023, 12, 100438.

[81]. Lin J, Liang L, Ling X, Zhang S, Mao N, Zhang N, Sumpter BG, Meunier V, Tong L, Zhang J, J. Am. Chem. Soc 2015, 137, 15511. [PubMed: 26583533]

[82]. An D, Zhang X, Bi Z, Shan W, Zhang H, Xia S, Qiu M, Adv. Funct. Mater 2021, 31, 2106484.

[83]. Chen X, Ponraj JS, Fan D, Zhang H, Nanoscale 2020, 12, 3513. [PubMed: 31904052]

[84]. Liu Z, Chen H, Jia Y, Zhang W, Zhao H, Fan W, Zhang W, Zhong H, Ni Y, Guo Z, Nanoscale 2018, 10, 18795. [PubMed: 30277241]

[85]. Liu Y, Zou J, Chen S, Zhong B, Wang Y, Wang H, Huang X, Spectrochim. Acta A Mol. Biomol. Spectrosc 2022, 271, 120861. [PubMed: 35051798]

[86]. Li P, Chen W, Liu D, Huang H, Dan K, Hu X, Yu S, Chu PK, Yu X-F, Nanotechnology 2019, 30, 275604. [PubMed: 30909172]

[87]. Kim G, Kim M, Hyun C, Hong S, Ma KY, Shin HS, Lim H, ACS Nano 2016, 10, 11156. [PubMed: 28024355]

[88]. Xue T, Liang W, Li Y, Sun Y, Xiang Y, Zhang Y, Dai Z, Duo Y, Wu L, Qi K, Shivananju BN, Zhang L, Cui X, Zhang H, Bao Q, Nat. Commun 2019, 10, 28. [PubMed: 30604756]

[89]. Pizzi G, Gibertini M, Dib E, Marzari N, Iannaccone G, Fiori G, Nat. Commun 2016, 7, 12585. [PubMed: 27557562]

[90]. Gibaja C, Rodriguez-San-Miguel D, Ares P, Gómez-Herrero J, Varela M, Gillen R, Maultzsch J, Hauke F, Hirsch A, Abellán G, Zamora F, Angew. Chem., Int. Ed 2016, 55, 14345.

[91]. Pumera M, Sofer Z, Adv. Mater 2017, 29, 1605299.

[92]. Dongre S S, S R, Hunsur Ravikumar C, C L, Balakrishna RG, Adv. Mater. Interfaces 2022, 9, 2200442.

[93]. Sun M, Zhang C, Lu S, Mahmood S, Wang J, Sun C, Pang J, Han L, Liu H, Adv. Funct. Mater 2024, 34, 2405471.

[94]. Rodrigo D, Limaj O, Janner D, Etezadi D, García de Abajo FJ, Pruneri V, Altug H, Science 2015, 349, 165. [PubMed: 26160941]

[95]. Liu X, Zhang D, Wu Y-C, Yang M, Wang Q, Coileáin CÓ, Xu H, Yang C, Abid M, Abid M, Liu H, Chun BS, Shi Q, Wu H-C, Carbon N Y 2017, 122, 404.

[96]. Kang L, Chu J, Zhao H, Xu P, Sun M, J. Mater. Chem. C Mater 2015, 3, 9024.

[97]. Ling X, Xie L, Fang Y, Xu H, Zhang H, Kong J, Dresselhaus MS, Zhang J, Liu Z, Nano Lett. 2010, 10, 553. [PubMed: 20039694]

[98]. Xu H, Xie L, Zhang H, Zhang J, ACS Nano 2011, 5, 5338. [PubMed: 21678950]

[99]. Feng S, dos Santos MC, Carvalho BR, Lv R, Li Q, Fujisawa K, Elías AL, Lei Y, Perea-López N, Endo M, Pan M, Pimenta MA, Terrones M, Sci. Adv 2016, 2.

[100]. Li L, Zhang T, Zhang L, Wang G, Huang X, Li W, Wang L, Li Y, Li J, Lu R, Anal. Chim. Acta 2024, 1331, 343330. [PubMed: 39532415]

Author Manuscript Author Manuscript Author Manuscript Author Manuscript

[101]. Novoselov KS, Geim AK, Morozov SV, Jiang D, Zhang Y, Dubonos SV, Grigorieva IV, Firsov AA, Science 2004, 306, 666. [PubMed: 15499015]

[102]. Yu Q, Lian J, Siriponglert S, Li H, Chen YP, Pei S-S, Appl. Phys. Lett 2008, 93, 113103.

[103]. Li X, Magnuson CW, Venugopal A, Tromp RM, Hannon JB, Vogel EM, Colombo L, Ruoff RS, J. Am. Chem. Soc 2011, 133, 2816. [PubMed: 21309560]

[104]. Robinson J, Weng X, Trumbull K, Cavalero R, Wetherington M, Frantz E, LaBella M, Hughes Z, Fanton M, Snyder D, ACS Nano 2010, 4, 153. [PubMed: 20000439]

[105]. Wu X, Hu Y, Ruan M, Madiomanana NK, Hankinson J, Sprinkle M, Berger C, de Heer WA, Appl. Phys. Lett 2009, 95, 223108.

[106]. Berger C, Song Z, Li X, Wu X, Brown N, Naud C, Mayou D, Li T, Hass J, Marchenkov AN, Conrad EH, First PN, de Heer WA, E. Confinement, C., P. E. Graphene, Science 2006, 312, 1191. [PubMed: 16614173]

[107]. Manzeli S, Ovchinnikov D, Pasquier D, Yazyev OV, Kis A, Nat. Rev. Mater 2017, 2, 17033.

[108]. Mueller T, Malic E, npj 2D Mater. Appl 2018, 2, 29.

[109]. Lam CYK, Zhang Q, Yin B, Huang Y, Wang H, Yang M, Wong SHD, J. Compos. Sci 2021, 5, 190.

[110]. Nisar S, Basha B, Dastgeer G, Shahzad ZM, Kim H, Rabani I, Rasheed A, Al-Buriahi MS, Irfan A, Eom J, Kim D, Adv. Sci 2023, 10, 2303654.

[111]. Nisar S, Shahzadi M, Shahzad ZM, Kim D, Dastgeer G, Irfan A, ACS Appl. Electron. Mater 2023, 5, 5714.

[112]. Nisar S, Dastgeer G, Zafar MS, Zulfiqar MW, Amina M, Rabani I, Iqbal MZ, Opt. Mater 2025, 158, 116489.

[113]. Nisar S, Dastgeer G, Shahzadi M, Shahzad ZM, Elahi E, Irfan A, Eom J, Kim H, Kim D, Mater. Today Nano 2023, 24, 100405.

[114]. Zhu X, Ding R, Wang Z, Wang Y, Guo X, Song Z, Wang Z, Dong M, Nanotechnology 2019, 30, 502004. [PubMed: 31505472]

[115]. Aryeetey F, Pourianejad S, Ayanbajo O, Nowlin K, Ignatova T, Aravamudhan S, RSC Adv. 2021, 11, 20893. [PubMed: 35479368]

[116]. Loan PTK, Zhang W, Lin C, Wei K, Li L, Chen C, Adv. Mater 2014, 26, 4838. [PubMed: 24841824]

[117]. Cong C, Shang J, Wang Y, Yu T, Adv. Opt. Mater 2018, 6.

[118]. AlaguVibisha G, Nayak JK, Maheswari P, Priyadharsini N, Nisha A, Jaroszewicz Z, Rajesh KB, Jha R, Opt. Commun 2020, 463, 125337.

[119]. Wang N, Li Y, Wang L, Xie C, ACS Appl. Mater. Interfaces 2025, 17, 16892. [PubMed: 40051225]

[120]. Tao L, Chen K, Chen Z, Cong C, Qiu C, Chen J, Wang X, Chen H, Yu T, Xie W, Deng S, Xu J-B, J. Am. Chem. Soc 2018, 140, 8696. [PubMed: 29927248]

[121]. Kitadai H, Wang X, Mao N, Huang S, Ling X, J. Phys. Chem. Lett 2019, 10, 3043. [PubMed: 31117687]

[122]. Kumar V, Chopada R, Singh A, Kumar N, Misra M, Kim K-H, Adv. Colloid Interface Sci 2024, 332, 103264. [PubMed: 39116585]

[123]. Xie H, Liu X, Yu H, Selim MS, Chen X, Hao Z, ACS Appl. Nano Mater 2022, 5, 16933.

[124]. Ali A, Majhi SM, Siddig LA, Deshmukh AH, Wen H, Qamhieh NN, Greish YE, Mahmoud ST, Biosensors 2024, 14, 497. [PubMed: 39451710]

[125]. Huang W, Hu L, Tang Y, Xie Z, Zhang H, Adv. Funct. Mater 2020, 30, 2005223.

[126]. Liu Z-W, Wang G, Li Y-F, Yu Y, Front. Chem 2024, 12, 1378985. [PubMed: 38545468]

[127]. Gao Z, Lai W, ChemPhysChem 2025, 26, 202400604.

[128]. Gan S, Ruan B, Xiang Y, Dai X, IEEE Sens. J 2021, 21, 347.

[129]. Luo M, Fan T, Zhou Y, Zhang H, Mei L, Adv. Funct. Mater 2019, 29, 1808306.

[130]. Zhu J, Xiao G, Zuo X, Nanomicro Lett. 2020, 12, 120. [PubMed: 34138144]

[131]. Patra A, Rout CS, Langmuir 2024, 40, 18781. [PubMed: 39194011]

Author Manuscript Author Manuscript Author Manuscript Author Manuscript

[132]. Higashitarumizu N, Wang S, Wang S, Kim H, Bullock J, Javey A, Nano Lett. 2024, 24, 13107. [PubMed: 39404072]

[133]. Huang C, Hu S, Zhang X, Cui H, Wu L, Yang N, Zhou W, Chu PK, Yu X-F, Biosens. Bioelectron 2020, 165, 112384. [PubMed: 32729509]

[134]. Hu Z, Li Y, Hussain E, Huang X, Zhang Y, Niu N, Shahzad SA, Yu C, Talanta 2019, 197, 270. [PubMed: 30771934]

[135]. Lin C, Liang S, Peng Y, Long L, Li Y, Huang Z, Long NV, Luo X, Liu J, Li Z, Yang Y, Nanomicro Lett. 2022, 14, 75. [PubMed: 35290533]

[136]. Ma J, Xue D, Xu T, Wei G, Gu C, Zhang Y, Jiang T, Colloids Surf. B Biointerfaces 2023, 227, 113338. [PubMed: 37167693]

[137]. Xue D, Tang J, Zhang J, Liu H, Gu C, Zhou X, Jiang T, Shi L, Appl. Surf. Sci 2024, 661, 160001.

[138]. Nangare S, Patil P, Crit. Rev. Anal. Chem 2021, 53, 1. [PubMed: 34053388]

[139]. Zhang M, Lozano CI, van Veen S, Albertazzi L, arXiv 2024, 10.48550/arXiv.2409.18702.

[140]. Sülzle J, Yang W, Shimoda Y, Ronceray N, Mayner E, Manley S, Radenovic A, ACS Photonics 2024, 11, 737. [PubMed: 38405387]

[141]. Wang H, Wang C, Zhang Y, Wang Z, Zhu Y, Wang Y, Hong X, Zhang H, Fan N, Qiu M, Adv. Sci 2025, 12, 2500752.

[142]. Singh MK, Pal S, Prajapati YK, Saini JP, Mater. Today Proc 2020, 28, 1776.

[143]. Singh MK, Pal S, Verma A, Prajapati YK, Saini JP, J. Nanophotonics 2020, 14, 046015.

[144]. Verma A, Sharma AK, Prajapati YK, Opt. Mater 2021, 119, 111355.

[145]. Vikas PS, ACS Omega 2023, 8, 4627. [PubMed: 36777565]

[146]. Zaman MU, Pal A, Uniyal A, Alqhtani NR, Sharma M, Farzan MSA, Karki B, Kumar R, J. Mater. Sci.: Mater. Electron 2024, 35, 1831.

[147]. Singh MK, Pal S, Verma A, Das R, Prajapati YK, Appl. Phys. A 2021, 127, 832.

[148]. Castellanos-Gomez A, Duan X, Fei Z, Gutierrez HR, Huang Y, Huang X, Quereda J, Qian Q, Sutter E, Sutter P, Nat. Rev. Methods Primers 2022, 2, 58.

[149]. Yankowitz M, Ma Q, Jarillo-Herrero P, LeRoy BJ, Nat. Rev. Phys 2019, 1, 112.

[150]. Huet B, Bachu S, Alem N, Snyder DW, Redwing JM, Carbon N Y 2023, 202, 150.

[151]. Zhu J, Li W, Huang R, Ma L, Sun H, Choi J-H, Zhang L, Cui Y, Zou G, J. Am. Chem. Soc 2020, 142, 16276. [PubMed: 32847357]

[152]. Liu X, Wu Q, Dai M, Xu Q, Zhang X, Cai Z, Ostrikov KK, Gu X, Nan H, Xiao S, ACS Appl. Electron. Mater 2023, 5, 5494.

[153]. Yu Z, Jiang L, Liu R, Zhao W, Yang Z, Zhang J, Jin S, Chem. Eng. J 2021, 426, 131914.

[154]. Liu C, Li H, Xu H, Zhao M, Xiong C, Li M, Ruan B, Zhang B, Wu K, New J Phys. 2020, 22, 073049.

[155]. Hu M, Li M, Li M-Y, Wen X, Deng S, Liu S, Lu H, Sensors 2023, 23, 1714. [PubMed: 36772761]

[156]. Shi J, Liu M, Wen J, Ren X, Zhou X, Ji Q, Ma D, Zhang Y, Jin C, Chen H, Deng S, Xu N, Liu Z, Zhang Y, Adv. Mater 2015, 27, 7086. [PubMed: 26445312]

[157]. Zhang Z, Yang X, Liu K, Wang R, Adv. Sci 2022, 9, 2105201.

[158]. Huang Y, Pan Y-H, Yang R, Bao L-H, Meng L, Luo H-L, Cai Y-Q, Liu G-D, Zhao W-J, Zhou Z, Wu L-M, Zhu Z-L, Huang M, Liu L-W, Liu L, Cheng P, Wu K-H, Tian S-B, Gu C-Z, Shi Y-G, Guo Y-F, Cheng ZG, Hu J-P, Zhao L, Yang G-H, Sutter E, Sutter P, Wang Y-L, Ji W, Zhou X-J, et al., Nat. Commun 2020, 11, 2453. [PubMed: 32415180]

[159]. Cheliotis I, Zergioti I, 2D Mater. 2024, 11, 022004.

[160]. Desai SB, Madhvapathy SR, Amani M, Kiriya D, Hettick M, Tosun M, Zhou Y, Dubey M, Ager JW, Chrzan D, Javey A, Adv. Mater 2016, 28, 4053. [PubMed: 27007751]

[161]. Moon J-Y, Kim M, Kim S-I, Xu S, Choi J-H, Whang D, Watanabe K, Taniguchi T, Park DS, Seo J, Cho SH, Son S-K, Lee J-H, Sci. Adv 2020, 6.

[162]. Liu R, Jiang L, Yu Z, Jing X, Liang X, Wang D, Yang B, Lu C, Zhou W, Jin S, Sens. Actuators B Chem 2021, 333, 129581.

Author Manuscript Author Manuscript Author Manuscript Author Manuscript

[163]. Peng Y, Cai P, Yang L, Liu Y, Zhu L, Zhang Q, Liu J, Huang Z, Yang Y, ACS Omega 2020, 5, 26486. [PubMed: 33110976]

[164]. Zhao Y-X, Zheng Z-X, Zhang L-S, Feng J-R, Ma L, Ding S-J, Phys. Chem. Chem. Phys 2023, 25, 15209. [PubMed: 37232126]

[165]. Huet B, Raskin J-P, Chem. Mater 2017, 29, 3431.

[166]. Bansal A, Hilse M, Huet B, Wang K, Kozhakhmetov A, Kim JH, Bachu S, Alem N, Collazo R, Robinson JA, Engel-Herbert R, Redwing JM, ACS Appl. Mater. Interfaces 2021, 13, 54516. [PubMed: 34748305]

[167]. Yan A, Velasco J, Kahn S, Watanabe K, Taniguchi T, Wang F, Crommie MF, Zettl A, Nano Lett. 2015, 15, 6324. [PubMed: 26317240]

[168]. Zhang X, Zhang F, Wang Y, Schulman DS, Zhang T, Bansal A, Alem N, Das S, Crespi VH, Terrones M, Redwing JM, ACS Nano 2019, 13, 3341. [PubMed: 30758945]

[169]. Diaz HC, Chaghi R, Ma Y, Batzill M, 2D Mater. 2015, 2, 044010.

[170]. Lin Y-C, Ghosh RK, Addou R, Lu N, Eichfeld SM, Zhu H, Li M-Y, Peng X, Kim MJ, Li L-J, Wallace RM, Datta S, Robinson JA, Nat. Commun 2015, 6, 7311. [PubMed: 26088295]

[171]. Rajput P, Devi P, Graphene 2D Mater. 2022, 7, 107.

[172]. Chen J, Cao X, Liu W, Liu J, Qi L, Wei M, Zou X, Foods 2024, 13, 3064. [PubMed: 39410099]

[173]. Mei L, Wang Z, Niu Y, Deng W, Shao Y, Opt. Express 2023, 31, 29768. [PubMed: 37710770]

[174]. Lu L, Xu L, Zhang Y, Jiang T, Appl. Surf. Sci 2022, 603, 154419.

[175]. Hu H, Yang X, Zhai F, Hu D, Liu R, Liu K, Sun Z, Dai Q, Nat. Commun 2016, 7, 12334. [PubMed: 27460765]

[176]. Ekoya BGM, Shan Y, Cai Y, Okombi NI, Yue X, Xu M, Cong C, Hu L, Qiu Z-J, Liu R, ACS Appl. Nano Mater 2022, 5, 8913.

[177]. Li Y, Chen H, Guo Y, Wang K, Zhang Y, Lan P, Guo J, Zhang W, Zhong H, Guo Z, Zhuang Z, Liu Z, Photonics Res. 2021, 9, 1039.

[178]. Fraser JP, Postnikov P, Miliutina E, Kolska Z, Valiev R, Švorčík V, Lyutakov O, Ganin AY, Guselnikova O, ACS Appl. Mater. Interfaces 2020, 12, 47774. [PubMed: 32985181]

[179]. Adhikari B, Limbu TB, Vinodgopal K, Yan F, Nanotechnology 2021, 32, 335701.

[180]. Rani D, Patel S, Austeria P M, Babu PV, Sampath S, J. Phys. Chem. C 2023, 127, 3131.

[181]. Sarycheva A, Makaryan T, Maleski K, Satheeshkumar E, Melikyan A, Minassian H, Yoshimura M, Gogotsi Y, J. Phys. Chem. C 2017, 121, 19983.

[182]. Chen K, Yan X, Li J, Jiao T, Cai C, Zou G, Wang R, Wang M, Zhang L, Peng Q, Nanomaterials 2019, 9, 284. [PubMed: 30781665]

[183]. Soundiraraju B, George BK, ACS Nano 2017, 11, 8892. [PubMed: 28846394]

[184]. Shevchuk K, Sarycheva A, Gogotsi Y, MRS Bull. 2022, 47, 545.

[185]. Lan L, Fan X, Yu S, Gao J, Zhao C, Hao Q, Qiu T, ACS Appl. Mater. Interfaces 2022, 14, 40427. [PubMed: 35998890]

[186]. He Z, Rong T, Li Y, Ma J, Li Q, Wu F, Wang Y, Wang F, ACS Nano 2022, 16, 4072. [PubMed: 35179019]

[187]. Peng Y, Lin C, Long L, Masaki T, Tang M, Yang L, Liu J, Huang Z, Li Z, Luo X, Lombardi JR, Yang Y, Nanomicro Lett. 2021, 13, 52. [PubMed: 33425476]

[188]. Lan L, Ni Z, Zhao C, Gao J, Tang X, Qu Z, Zheng L, Fan X, Qiu T, Langmuir 2024, 40, 20945. [PubMed: 39320080]

[189]. Xue D, Dai X, Zhao J, Zhang J, Liu H, Liu K, Xu T, Gu C, Zhou X, Jiang T, Biosens. Bioelectron 2024, 245, 115844. [PubMed: 38000309]

[190]. Qiu H, Wang M, Zhang L, Cao M, Ji Y, Kou S, Dou J, Sun X, Yang Z, Sens. Actuators B Chem 2020, 320, 128445.

[191]. Ghopry SA, Alamri M, Goul R, Cook B, Sadeghi SM, Gutha RR, Sakidja R, Wu JZ, ACS Appl. Nano Mater 2020, 3, 2354.

[192]. Basu N, Satya Bharathi MS, Sharma M, Yadav K, Parmar AS, Soma VR, Lahiri J, Nanomaterials 2021, 11, 622. [PubMed: 33801504]

[193]. Kundu A, Rani R, Hazra KS, Nanoscale 2019, 11, 16245. [PubMed: 31453997]

Author Manuscript Author Manuscript Author Manuscript Author Manuscript

[194]. Ye Y, Yi W, Liu W, Zhou Y, Bai H, Li J, Xi G, Sci. China Mater 2020, 63, 794.
[195]. Yang S, Zhang Z, Zhao J, Yu Z, Jiang H, Mater. Lett 2014, 131, 78.
[196]. Cai Q, Li LH, Yu Y, Liu Y, Huang S, Chen Y, Watanabe K, Taniguchi T, Phys. Chem. Chem. Phys 2015, 17, 7761. [PubMed: 25714659]
[197]. Kundu A, Rani R, Ahmad A, Kumar A, Raturi M, Gupta T, Khan R, Hazra KS, Sensors Diagn. 2022, 1, 449.
[198]. Ma J, Xu L, Zhang Y, Dong L, Gu C, Wei G, Jiang T, J. Colloid Interface Sci 2022, 626, 787. [PubMed: 35820214]
[199]. Barveen NR, Wang T-J, Chang Y-H, Microchim. Acta 2022, 189, 16.
[200]. Chen J, Zhang X, Wang C, Wang S, Gu C, Zeng S, Jiang J, Jiang T, Wu K, Sens. Actuators B Chem 2025, 422, 136610.
[201]. Liu X, Li T, Lee T-C, Sun Y, Liu Y, Shang L, Han Y, Deng W, Yuan Z, Dang A, ACS Sens. 2024, 9, 483. [PubMed: 38206578]
[202]. Hua K, Li L, Liang P, Biosensors 2025, 15, 426. [PubMed: 40710076]
[203]. Zhu X, Liu P, Xue T, Ge Y, Ai S, Sheng Y, Wu R, Xu L, Tang K, Wen Y, Ceram. Int 2021, 47, 173.
[204]. Wang T, Zhu C, Dong P, Langmuir 2024, 40, 22015. [PubMed: 39382521]
[205]. Wu J, Lu Y, Wu Z, Li S, Zhang Q, Chen Z, Jiang J, Lin S, Zhu L, Li C, Liu Q, Sens. Actuators B Chem 2018, 261, 279.\
[206]. Dou X, Zhao L, Li X, Qin L, Han S, Kang S-Z, Appl. Surf. Sci 2020, 509, 145331.
[207]. Zhang X, Lei Z, Pan Z, Hu J, Tao L, Zheng Z, Feng X, Xue J, Tao L, Zhao Y, J. Alloys Compd 2023, 938, 168468.
[208]. Ayhan ME, Microelectron. Eng 2021, 241, 111546.
[209]. Kaushik V, Kagdada HL, Singh DK, Pathak S, Appl. Surf. Sci 2022, 574, 151724.
[210]. Bhatia H, Dhakate SR, Subhedar KM, Diam. Relat. Mater 2024, 150, 111734.
[211]. Tao G, Li J, Zhang X, Appl. Surf. Sci 2025, 682, 161754.
[212]. Wang L, Chen H, Ma S, Chang M, Zhang X, Vib. Spectrosc 2023, 129, 103614.
[213]. Chen Y-F, Lee Y-C, Lin W-W, Lu M-C, Yang Y-C, Chiu C-W, ACS Omega 2024, 9, 1894. [PubMed: 38222643]
[214]. Jia Y, Zhang K, RSC Adv 2025, 15, 8764. [PubMed: 40124914]
[215]. Zhang L, Wang X, Chen C, Wang R, Qiao X, Waterhouse GIN, Xu Z, Food Chem. 2023, 421, 136171. [PubMed: 37094406]
[216]. Wang X, Chen H, Han Z, Wei P, Amin MU, Zhu C, Microchem. J 2025, 208, 112325.
[217]. Chen Y-F, Chang W-R, Wang J-H, Kuo C-FJ, Cheng C-C, Chiu C-W, ACS Appl. Nano Mater 2023, 6, 13604.
[218]. Zhao Z, Cao M, Wei D, Li X, Wang M, Zhai W, Analyst 2024, 149, 1151. [PubMed: 38259149]
[219]. Atta S, Sharaf T, Vo-Dinh T, ACS Appl. Nano Mater 2024, 7, 11518. [PubMed: 41531830]
[220]. Kansara V, Patel M, Talanta 2025, 283, 127185. [PubMed: 39532051]
[221]. Zhao W, Yang S, Zhang D, Zhou T, Huang J, Gao M, Zhang X, Liu Y, Yang J, J. Colloid Interface Sci 2023, 646, 872. [PubMed: 37235933]
[222]. Ghopry SA, Alamri MA, Goul R, Sakidja R, Wu JZ, Adv. Opt. Mater 2019, 7, 1801249.
[223]. Li Q, Zheng Q, Shi J, Yan Y, Guo X, Yang H, Anal. Chim. Acta 2025, 1336, 343466. [PubMed: 39788651]
[224]. Liang O, Wang P, Xia M, Augello C, Yang F, Niu G, Liu H, Xie Y-H, Biosens. Bioelectron 2018, 118, 108. [PubMed: 30059864]
[225]. Wu H, Duan Y, Jiang L, Cao X, Xie Z, Quan Y, Ren MX, Wu S, Zhang N, Yang Z, Zhao L, Jiang Z, Zhao G, Ren W, Niu G, ACS Appl. Nano Mater 2024, 7, 9167.
[226]. Zhang J, Lu S, Shi G, Xie W, Geng Y, Wang Z, J. Mater. Res. Technol 2023, 22, 1558.
[227]. Zhang J, Wu J, Wang B, Geng Y, Wang Z, Sens. Actuators B Chem 2024, 410, 135711.
[228]. Miao Y, Yang K, Zong S, Wang Z, Cui Y, ACS Appl. Nano Mater 2021, 4, 6844.

Author Manuscript Author Manuscript Author Manuscript Author Manuscript

[229]. Chen Y, Liu H, Li X, Tang S, Gu C, Wei G, Jiang T, Zhou X, Sens. Actuators B Chem 2021, 339, 129856.

[230]. Ghopry SA, Sadeghi SM, Farhat Y, Berrie CL, Alamri M, Wu JZ, ACS Appl. Nano Mater 2021, 4, 2941.

[231]. Bian J, Liu M, Liu X, Bian X, Gu C, Ma J, Jiang T, Microchem. J 2025, 210, 113021.

[232]. Liu Y, Dang A, Liu X, Wang X, Zada A, Chen J, Fan X, Zhao T, Li J, Li T, Sens. Actuators B Chem 2025, 422, 136685.

[233]. Hossain MI, Nanda SS, Cho S, Lee B, Kim BJ, Choi J-Y, Yi DK, Biosensors 2023, 13, 962. [PubMed: 37998137]

[234]. Geng Z-Q, Xu D, Song Y, Wang W-P, Li Y-P, Han C-Q, Yang G-H, Qu L-L, Ajayan PM, Sens. Actuators B Chem 2021, 334, 129634.

[235]. Fang X, Song Y, Huang Y, Yang G, Han C, Li H, Qu L, Analyst 2020, 145, 7421. [PubMed: 32945309]

[236]. Wu Z, Zhao D, Han X, Liu J, Sun Y, Li Y, Duan Y, J. Nanobiotechnol 2023, 21, 17.

[237]. Lv Q, Tan J, Wang Z, Gu P, Liu H, Yu L, Wei Y, Gan L, Liu B, Li J, Kang F, Cheng H-M, Xiong Q, Lv R, Nat. Commun 2023, 14, 2717. [PubMed: 37169769]

[238]. Wang S, Jiang H, Feng J, Jin Y, An F, Zhu L, Xiao A, Appl. Surf. Sci 2024, 646, 158926.

[239]. Sun T, Wu Y, Ma H, Zhang C, Li C, Man B, Yang C, Li Z, Nano Lett. 2024, 24, 15324. [PubMed: 39566895]

[240]. Luo W, Xiong W, Han Y, Yan X, Mai L, Phys. Chem. Chem. Phys 2022, 24, 26398. [PubMed: 36314502]

[241]. Yoon J, Lim J, Shin M, Lee S-N, Choi J-W, Materials 2021, 14, 518. [PubMed: 33494525]

[242]. Wei Y, Wang S, Zhang Z, Zang Z, Liang L, Huang S, Qian Q, J. Phys. Chem. C 2025, 129, 6332.

[243]. Chen L, Merino JP, Torrent-Sucarrat M, Hou H, Prato M, Adv. Mater. Interfaces 2024, 11, 2400272.

[244]. Briggs N, Bersch B, Wang Y, Jiang J, Koch RJ, Nayir N, Wang K, Kolmer M, Ko W, De La Fuente Duran A, Subramanian S, Dong C, Shallenberger J, Fu M, Zou Q, Chuang Y-W, Gai Z, Li A-P, Bostwick A, Jozwiak C, Chang C-Z, Rotenberg E, Zhu J, van Duin ACT, Crespi V, Robinson JA, Nat. Mater 2020, 19, 637. [PubMed: 32157191]

[245]. Zhang N, Zhang K, Zou M, Maniyara RA, Bowen TA, Schrecengost JR, Jain A, Zhou D, Dong C, Yu Z, Liu H, Giebink NC, Robinson JA, Hu W, Huang S, Terrones M, ACS Nano 2024, 18, 8876. [PubMed: 38497598]

[246]. Chen L, Hou H-L, Prato M, Chem. Mater 2023, 35, 5032.

[247]. Cao Y, Rodan-Legrain D, Rubies-Bigorda O, Park JM, Watanabe K, Taniguchi T, Jarillo-Herrero P, Nature 2020, 583, 215. [PubMed: 32499644]

[248]. Cai Q, Gan W, Falin A, Watanabe K, Taniguchi T, Zhuang J, Hao W, Huang S, Tao T, Chen Y, Li LH, ACS Appl. Mater. Interfaces 2020, 12, 21985. [PubMed: 32319287]

[249]. Jiang Y, Wang X, Zhao G, Shi Y, Wu Y, Yang H, Zhao F, Water Res. 2024, 255, 121444. [PubMed: 38492312]

[250]. Zhang Z, Mei L, Niu Y, Deng W, Shao Y, Mater. Lett 2024, 375, 137224.

[251]. Liu L, Shangguan C, Guo J, Ma K, Jiao S, Yao Y, Wang J, Adv. Opt. Mater 2020, 8, 2001214.

[252]. Ishtiak KM, Imam S-A, Khosru QDM, IEEE Access 2023, 11, 130601.

[253]. Rifat AA, Mahdiraji GA, Ahmed R, Chow DM, Sua YM, Shee YG, Mahamd Adikan FR, IEEE Photon. J 2016, 8, 1.

[254]. Stebunov YV, Yakubovsky DI, Fedyanin D. Y.u., Arsenin AV, Volkov VS, Langmuir 2018, 34, 4681. [PubMed: 29578717]

[255]. Pillai AM, Nair N, Das MK, Ram SK, Next Mater. 2025, 7, 100377.

[256]. Hwang R-B, Sci. Rep 2021, 11, 1999. [PubMed: 33479396]

[257]. Kumar A, Yadav AK, Kushwaha AS, Srivastava SK, Sens. Actuators Rep 2020, 2, 100015.

[258]. Akib TBA, Rana MM, Mehedi IM, Biosens. Bioelectron. X 2024, 16, 100434.

Author Manuscript Author Manuscript Author Manuscript Author Manuscript

[259]. Singh MK, Pal S, Verma A, Mishra V, Prajapati YK, Superlattices Microstruct. 2021, 156, 106969.
[260]. Kumar R, Pal S, Verma A, Prajapati YK, Saini JP, Superlattices Microstruct. 2020, 145, 106591.
[261]. Kumar R, Mayank PK, Rajiv A, Raish M, Pal A, Microchem. J 2025, 213, 113869.
[262]. Hossain M.d.M., Talukder MA, Opt. Commun 2021, 493, 126994.
[263]. Chung K, Lee JS, Kim E, Lee K, Kim K, Lee J, Kim D, Kim SO, Jeon S, Park H, Kim D, Kim DH, Adv. Mater. Interfaces 2018, 5, 1800433.
[264]. Panda A, Pukhrambam PD, Keiser G, Appl. Phys. A 2020, 126, 153.
[265]. Sharma AK, Dominic A, IEEE Photonics Technol. Lett 2018, 30, 95.
[266]. Jena R, Dhar P, Panda A, Wu F, Daher MG, Microchim. Acta 2025, 192, 351.
[267]. Alaaudeen KM, Manoharadas S, Dhasarathan V, Rajeshkannan S, Plasmonics 2024, 20, 709.
[268]. Barrios CA, Plasmonics 2022, 17, 745.
[269]. Ouyang Q, Zeng S, Jiang L, Hong L, Xu G, Dinh X-Q, Qian J, He S, Qu J, Coquet P, Yong K-T, Sci. Rep 2016, 6, 28190. [PubMed: 27305974]
[270]. Daher MG, Taya SA, Faragallah OS, Patel SK, Prajapati YK, Armghan A, Plasmonics 2024, 20, 3853.
[271]. Kumar V, Kumar R, Pal S, Prajapati YK, Optik 2024, 313, 171975.
[272]. Kumar V, Pal S, Singh V, Kumar Parajapati Y, Saini JP, Phys. B Condens. Matter 2024, 686, 416072.
[273]. Dey B, Rahman MT, in: 2025 4th International Conference on Robotics, Electrical and Signal Processing Technfques (ICREST), IEEE, Piscataway, NJ 2025, pp. 167–171.
[274]. Wu L, You Q, Shan Y, Gan S, Zhao Y, Dai X, Xiang Y, Sens Actuators B Chem 2018, 277, 210.
[275]. Verma VK, Kumar R, Pal S, Prajapati YK, Opt Mater (Amst) 2022, 133, 112977.
[276]. Kumar R, Agarwal S, Pal S, Verma A, Prajapati YK, Measurement 2024, 224, 113682.
[277]. Kumar R, Pal S, Prajapati YK, Kumar S, Saini JP, IEEE Sens. J 2022, 22, 6536.
[278]. Shivangani AS, Kumar D, Verma S, Chauhan SS, Tiwari RK, Kumar S, Plasmonics 2025.
[279]. Bouandas H, Kumar R, Benhaliliba M, Singh S, Garia L, Microchim. Acta 2025, 192, 114.
[280]. Daher MG, Taya SA, Faragallah OS, Armghan A, Plasmonics 2024, 20, 3887.
[281]. Karki B, Pal A, Singh Y, Sharma S, Opt. Commun 2022, 508, 127616.
[282]. Yuan Y, Yu X, Ouyang Q, Shao Y, Song J, Qu J, Yong K-T, 2D Mater. 2018, 5, 025015.
[283]. Akib TBA, Mostufa S, Rana M.d.M., Hossain M.d.B., Islam M.d.R., Opt. Quantum Electron 2023, 55, 448. [PubMed: 37008732]
[284]. Zeng S, Hu S, Xia J, Anderson T, Dinh X-Q, Meng X-M, Coquet P, Yong K-T, Sens. Actuators B Chem 2015, 207, 801.
[285]. Aksimsek S, Jussila H, Sun Z, Opt. Commun 2018, 428, 233.
[286]. Rouf HK, Haque T, Plasmonics 2021, 16, 1945.
[287]. Haque T, Rouf HK, Appl. Phys. A 2021, 127, 759.
[288]. Kumar A, Kumar A, Srivastava SK, Optik 2022, 258, 168885.
[289]. Pandey AK, Appl. Phys. A 2021, 127, 78.
[290]. Raikwar S, Srivastava DK, Saini JP, Prajapati YK, Appl. Phys. A 2021, 127, 92.
[291]. Kumar R, Pal S, Pal N, Mishra V, Prajapati YK, Appl. Phys. A 2021, 127, 259.
[292]. Wang Z, Yu M, Li K, Mao H, Liu K, Li H, Opt. Mater 2022, 133, 112966.
[293]. Chowdhury AS, Islam M.d.A., Islam M.d.S., Dey B, Park J, ACS Appl. Opt. Mater 2024, 2, 1046.
[294]. Srinivasan K, Raja MR, Balamurugan AM, Singh S, Plasmonics 2025.
[295]. Ghodrati M, Mir A, Farmani A, Diam. Relat. Mater 2023, 132, 109633.
[296]. Rahman MS, Anower MS, Rahman M.d.K., Hasan M.d.R., Hossain M.d.B., Haque M.d.I., Optik 2017, 140, 989.
[297]. Rahman MS, anower M.d.S., Abdulrazak LF, Photonics Nanostruct. 2019, 35, 100711.
[298]. Ma J, Wang R, Li D, Xu K, Microchem. J 2025, 213, 113753.

Author Manuscript Author Manuscript Author Manuscript Author Manuscript

[299]. Li H, Huang T, Yuan H, Lu L, Cao Z, Zhang L, Yang Y, Yu B, Wang H, Anal. Chem 2023, 95, 5142. [PubMed: 36892255]

[300]. Li G, Singh R, Guo J, Zhang B, Kumar S, Appl. Phys. Lett 2023, 122, 083701.

[301]. Singh R, Zhang W, Liu X, Zhang B, Kumar S, Biosensor WF, Opt. Laser Technol 2024, 171, 110357.

[302]. Zhang Y, Ding L, Xiao B, Wang S, Meng W, Gao L, Che T, Zheng X, Biosens. Bioelectron 2025, 273, 117146. [PubMed: 39832404]

[303]. Liu X, Dang A, Li T, Sun Y, Deng W, Lee T-C, Yang Y, Zada A, Wang B, Liu Y, Wu S, Zhao T, Sens. Actuators B Chem 2023, 390, 133888.

[304]. Bolognesi M, Prosa M, Toerker M, Sanchez LL, Wieczorek M, Giacomelli C, Benvenuti E, Pellacani P, Elferink A, Morschhauser A, Sola L, Damin F, Chiari M, Whatton M, Haenni E, Kallweit D, Marabelli F, Peters J, Toffanin S, Adv. Mater 2023, 35, 2208719.

[305]. Niu Z, Du H, Ma L, Zhou J, Yuan Z, Sun R, Liu G, Zhang F, Zeng Y, Molecules 2024, 29, 2811. [PubMed: 38930876]

[306]. Chuang C-S, Wu C-Y, Juan P-H, Hou N-C, Fan Y-J, Wei P-K, Sheen H-J, Analyst 2020, 145, 52.

[307]. Nasr N, Shafi M, Zhao T, Ali R, Ahmad I, Khan M, Deifalla A, Ragab AE, Ansari MZ, Spectrochim. Acta A Mol. Biomol. Spectrosc 2024, 304, 123331. [PubMed: 37688887]

[308]. Kim G, Kim J, Kim SM, Kato T, Yoon J, Noh S, Park EY, Park C, Lee T, Choi J-W, Sens. Actuators B Chem 2022, 352, 131060. [PubMed: 34785863]

[309]. Singh N, Kaushik A, Ghori I, Rai P, Dong L, Sharma A, Malhotra BD, John R, ACS Appl. Mater. Interfaces 2024, 16, 32794. [PubMed: 38860871]

[310]. Jordan MI, Mitchell TM, Science 2015, 349, 255. [PubMed: 26185243]

[311]. Lin LL, Alvarez-Puebla R, Liz-Marzán LM, Trau M, Wang J, Fabris L, Wang X, Liu G, Xu S, Han XX, Yang L, Shen A, Yang S, Xu Y, Li C, Huang J, Liu S-C, Huang J-A, Srivastava I, Li M, Tian L, Nguyen LBT, Bi X, Cialla-May D, Matousek P, Stone N, Carney RP, Ji W, Song W, Chen Z, et al., ACS Appl. Mater. Interfaces 2025, 17, 16287. [PubMed: 39991932]

[312]. Sebek M, Thanh NTK, Su X, Teng J, ACS Omega 2023, 8, 20792. [PubMed: 37323412]

[313]. Palai D, Tahara H, Chikami S, Latag GV, Maeda S, Komura C, Kurioka H, Hayashi T, ACS Biomater. Sci. Eng 2022, 8, 3765. [PubMed: 35905395]

[314]. Chang Y-F, Chen S-Y, Lee C-C, Chen J, Lai C-S, Anal. Chem 2022, 94, 10427. [PubMed: 35837692]

[315]. Malinick AS, Stuart DD, Lambert AS, Cheng Q, Biosens. Bioelectron. X 2022, 10, 100127.

Author Manuscript Author Manuscript Author Manuscript Author Manuscript

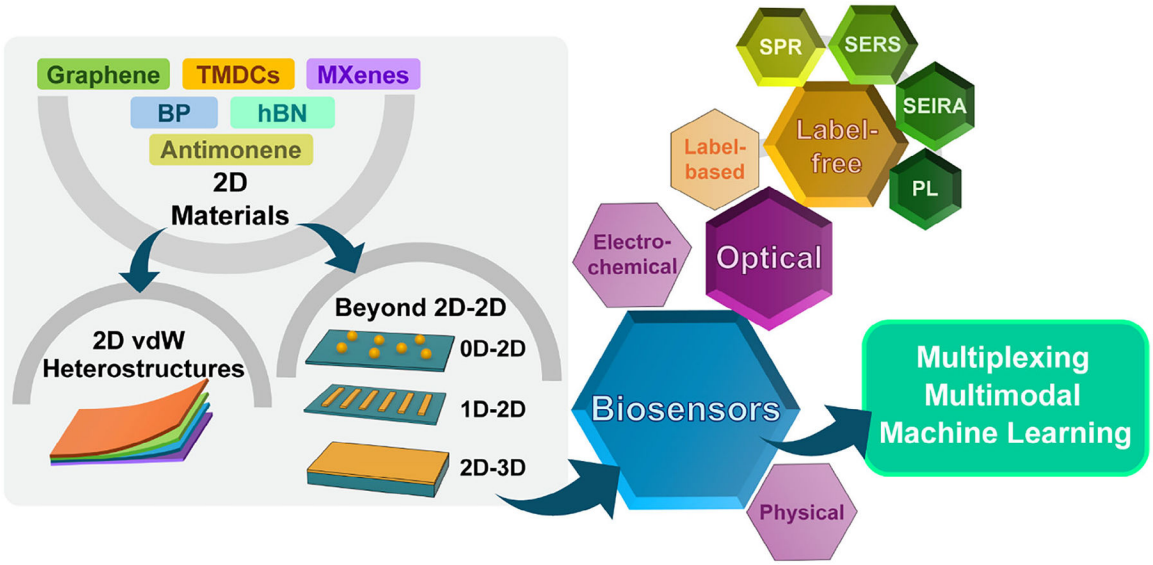


**Figure 1.**

2DMs and their mixed-dimensional hybrid nanostructures for label-free optical biosensing applications.

Author Manuscript

Author Manuscript

Author Manuscript

Author Manuscript

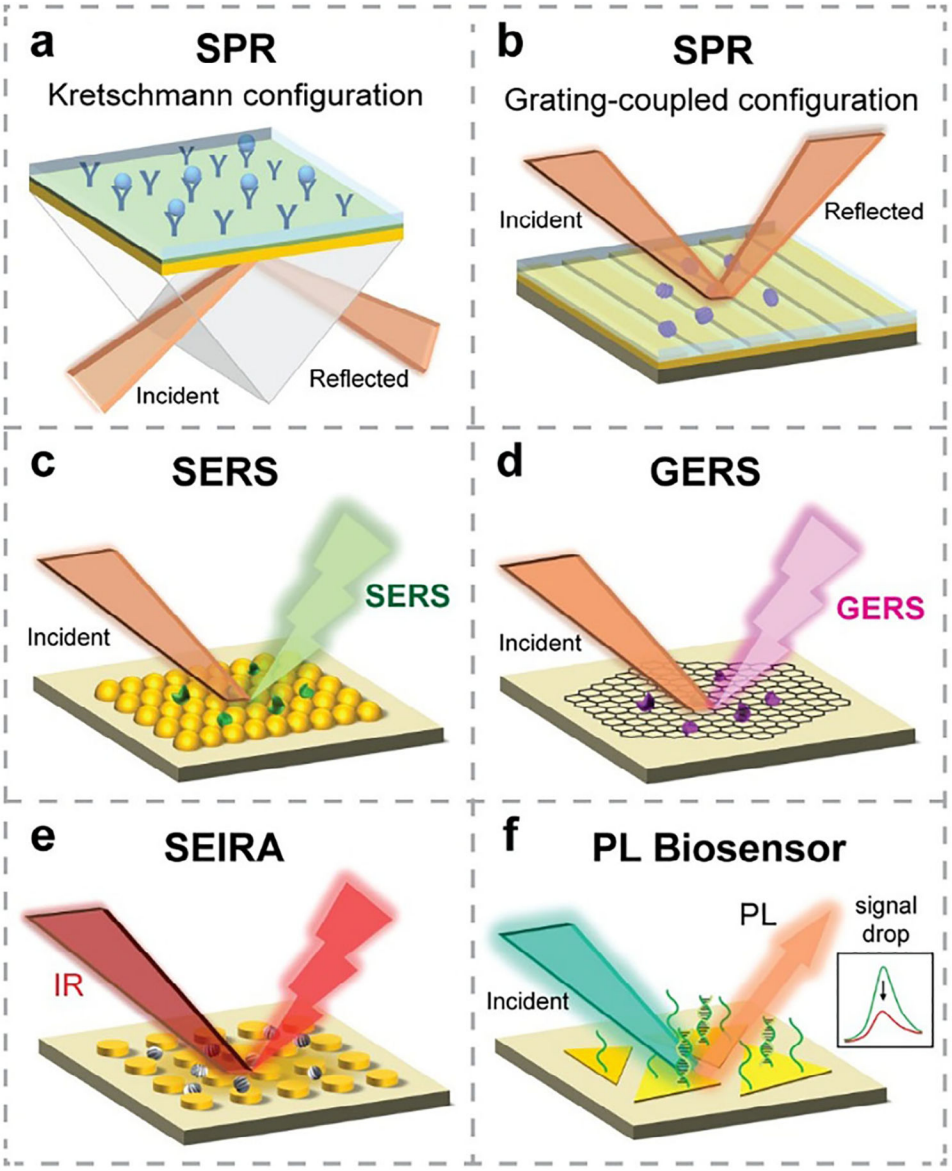


**Figure 2.**

Representative label-free optical biosensing techniques. a) SPR with Kretschmann configuration. b) SPR with grating-coupled configuration. c) SERS. d) GERS. e) SEIRA. f) PL biosensor.

Author Manuscript Author Manuscript Author Manuscript Author Manuscript

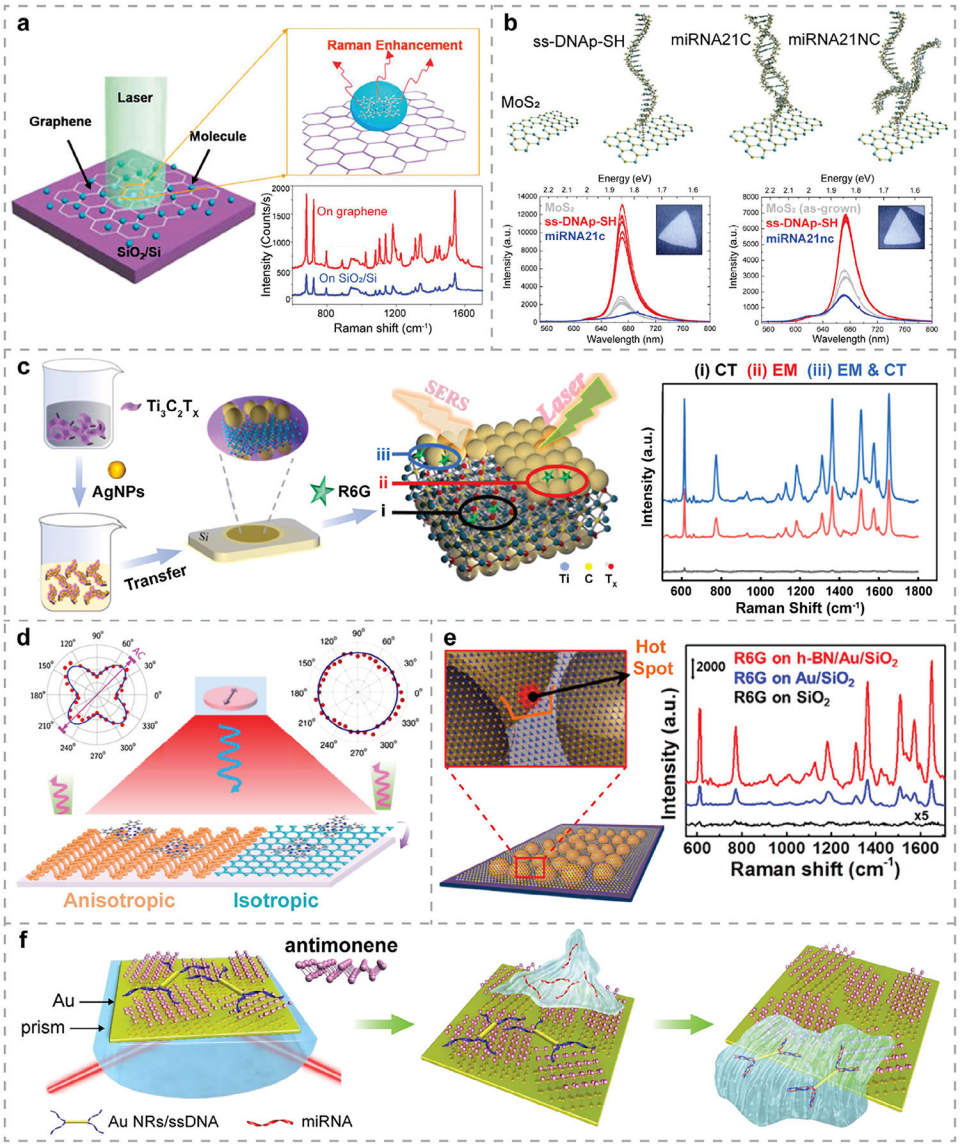


**Figure 3.**

Typical 2DMs and their applications in label-free optical biosensing. a) Graphene used as a substrate for Raman enhancement. Reproduced with permission.[97] Copyright 2010, American Chemical Society. b) Detection of breast cancer biomarkers via the PL of epitaxial monolayer $MoS_2$ flakes. Reproduced with permission.[72] Copyright 2020, Springer Nature. c) Synergistic CM and EM enhancements in a $Ti_3C_2T_x$/Ag NP-based SERS substrate for ultrasensitive detection. Reproduced with permission.[100] Copyright 2024, Elsevier. d) Observed anisotropic Raman enhancement with angular dependence on few-layer BP for detecting CuPc molecules. Reproduced with permission.[81] Copyright 2015, American Chemical Society. e) Designed hBN/Au NPs substrate for manipulating surface plasmons and enhancing SERS performance. Reproduced with permission.[87] Copyright 2016, American Chemical Society. f) Ultrasensitive detection of miRNA enabled by an antimonene-based SPR biosensor. Reproduced with permission.[88] Copyright 2019, Springer Nature.

Author Manuscript Author Manuscript Author Manuscript Author Manuscript

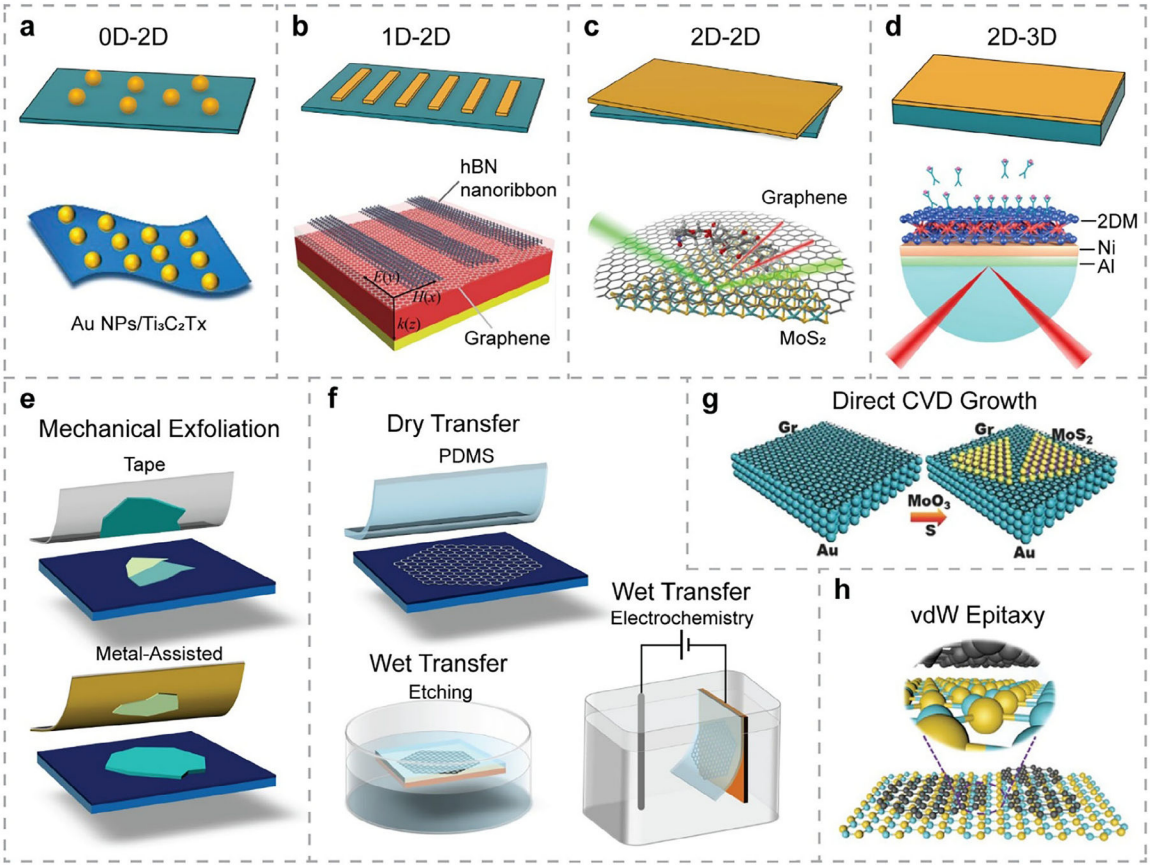


**Figure 4.**

Mixed-dimensional hybrid nanostructures and typical fabrication techniques of 2D vdWHs. a) Schematic of a 0D-2D hybrid structure and example of Au NPs/MXene used as SERS substrate for bacterial detection. Reproduced with permission.[153] Copyright 2021, Elsevier. b) Schematic of a 1D-2D hybrid structure and example of theoretically proposed hBN nanoribbons/graphene hybrids for SPR biosensing. Reproduced with permission.[154] Copyright 2020, IOP Publishing. c) Schematic of a 2D vdWH and example of graphene/$MoS_2$ heterostructure for label-free optical biosensing. Reproduced with permission.[63] Copyright 2022, American Chemical Society. d) Schematic of a 2D-3D hybrid structure and example of integrated 2DMs for enhanced SPR performance. Reproduced with permission.[155] Copyright 2023, MDPI. e) Mechanical exfoliation. f) Dry and wet transfer techniques. g) Direct CVD growth of $MoS_2$ on graphene. Reproduced with permission.[156] Copyright 2015, Wiley. h) Schematic of vdW epitaxy. Reproduced with permission.[157] Copyright 2022, Wiley.

Author Manuscript Author Manuscript Author Manuscript Author Manuscript

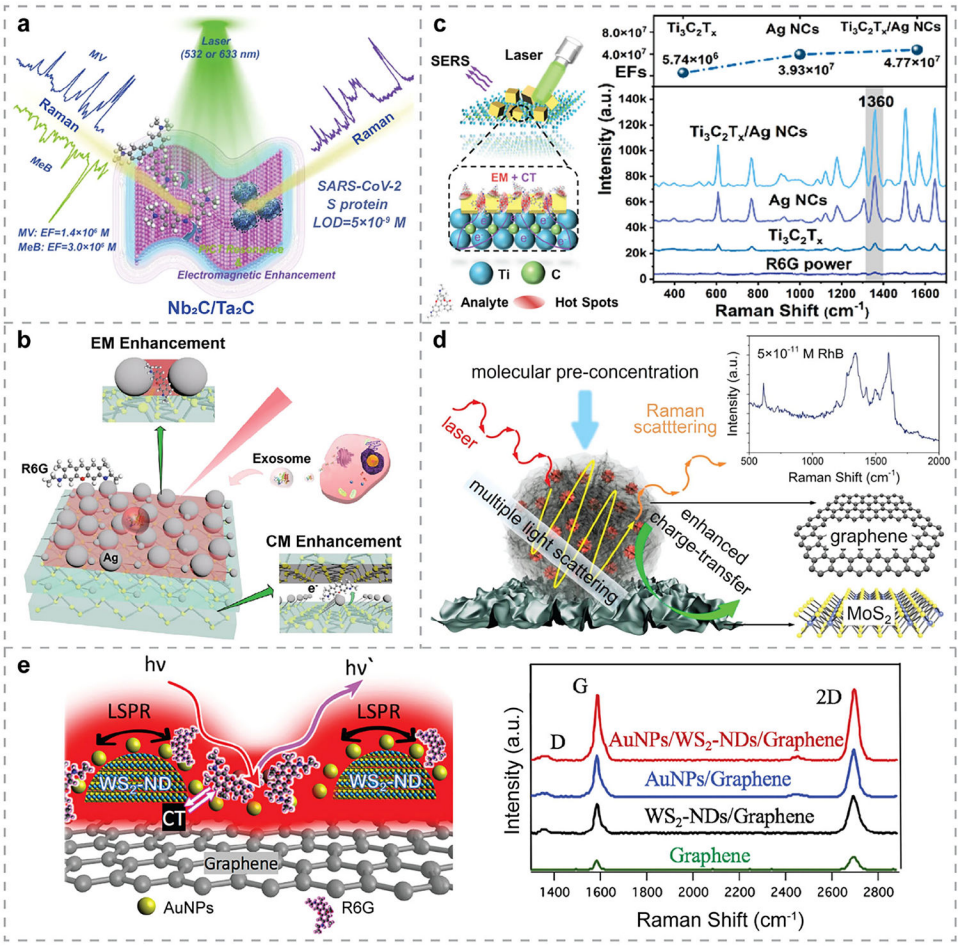


**Figure 5.**

Recent advances in using 2DMs and 0D-2D hybrid nanostructures for SERS biosensing. a) MXene-based SERS platform for highly sensitive SARS-CoV-2 S protein detection enabled by the synergistic effects of charge-transfer resonance and EM enhancement. Reproduced with permission.[187] Copyright 2021, Springer Nature. b) Single-molecule SERS detection using Ag NPs/BP hybrid nanosheets. Reproduced with permission.[135] Copyright 2022, Springer Nature. c) Ag NCs/$Ti_3C_2T_x$ SERS substrate for therapeutic drug monitoring facilitated by the synergistic CM and EM effects. Reproduced with permission.[189] Copyright 2023, Elsevier. d) Hybrid nanostructures of Gr MFs/wrinkled $MoS_2$ used as SERS substrate for ultrasensitive molecular sensing. Reproduced with permission.[190] Copyright 2020, Elsevier. e) Au NPs/$WS_2$ NDs/graphene hybrid nanostructures with enhanced SERS performance. Reproduced with permission.[191] Copyright 2020, American Chemical Society.

Author Manuscript Author Manuscript Author Manuscript Author Manuscript

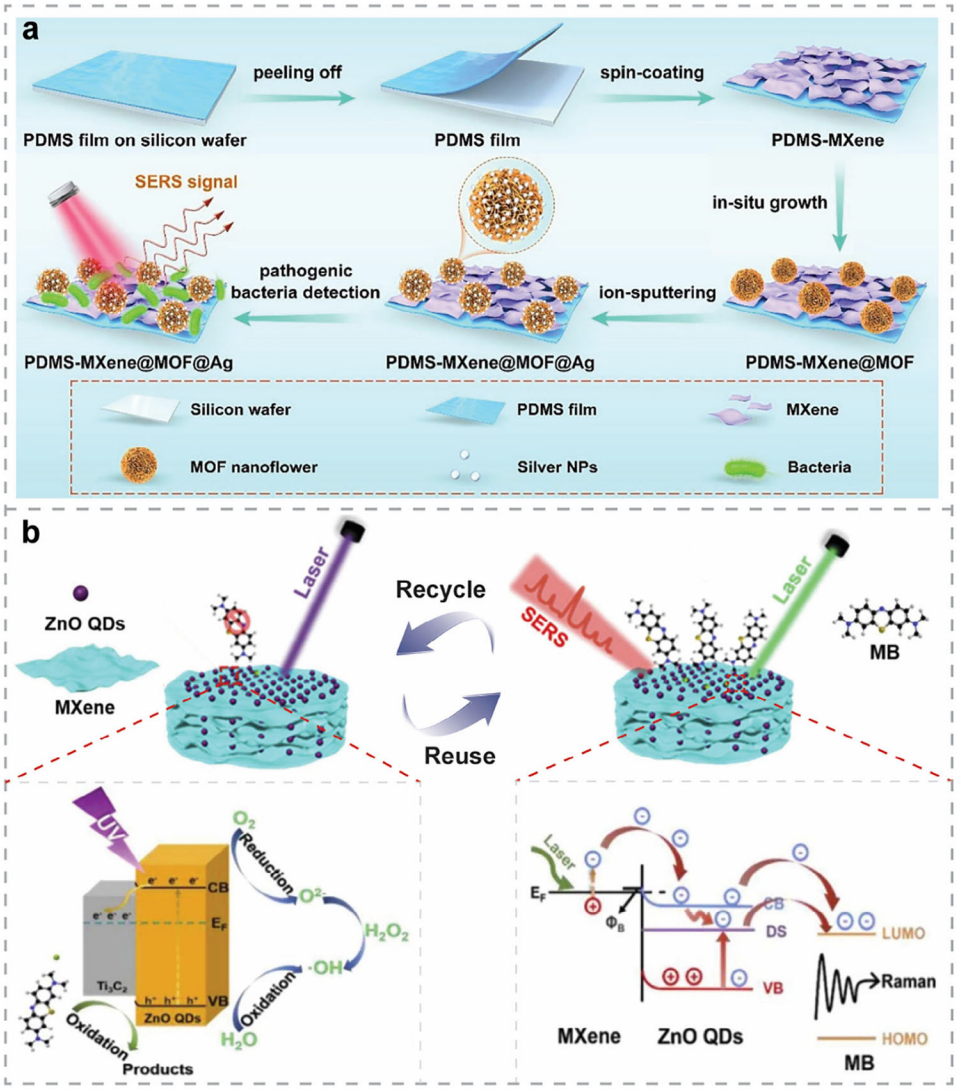


**Figure 6.**

Recent advances in using novel 0D-2D hybrid nanostructures for SERS biosensing. a) Fabricated flexible MOF@Ag/MXene hybrids on PDMS for sensitive SERS detection of pathogenic bacteria. Reproduced with permission.[231] Copyright 2025, Elsevier. b) Recyclable SERS substrate based on ZnO QDs/MXene hybrid structures. Reproduced with permission.[232] Copyright 2024, Elsevier.

Author Manuscript Author Manuscript Author Manuscript Author Manuscript

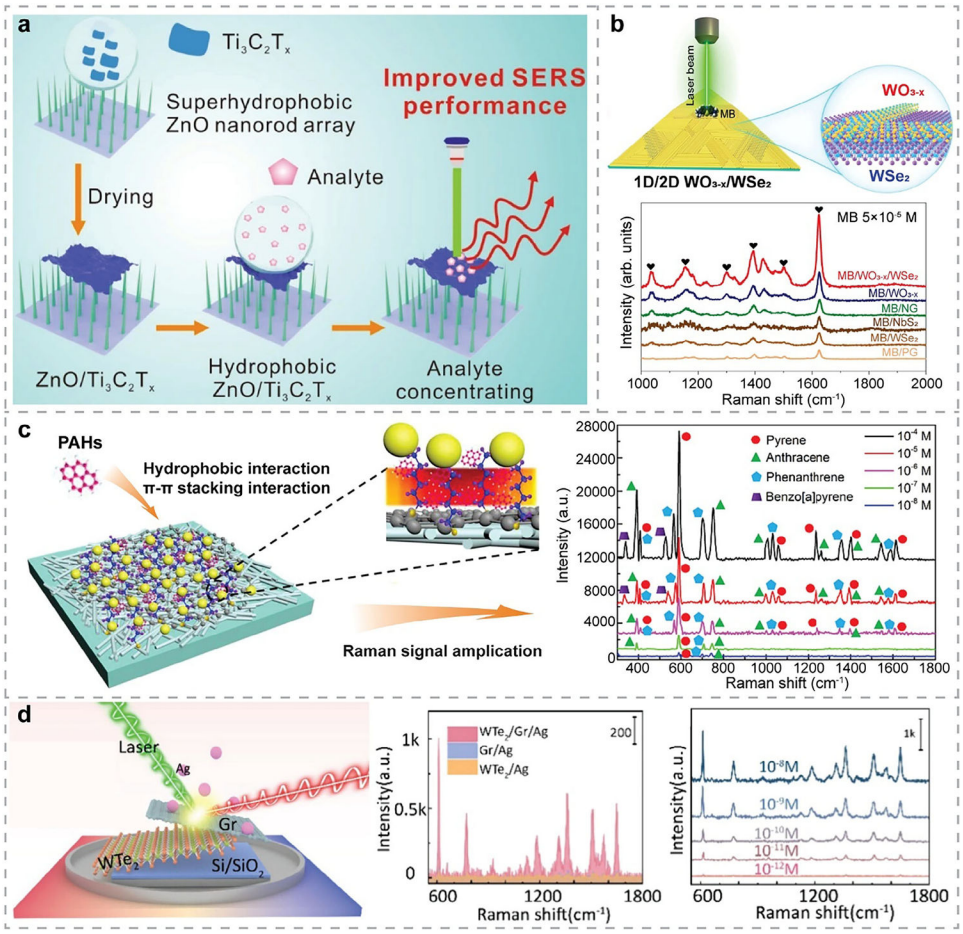


**Figure 7.**

Recent advances in using 1D-2D and multicomponent hybrid nanostructures for SERS biosensing. a) Deposition of hydrophilic $Ti_3C_2T_x$ on ZnO NRs for improved SERS performance. Reproduced with permission.[236] Copyright 2023, Springer Nature. b) Fabricated 1D-2D $WO_{3-x}$ NW/$WSe_2$ heterostructures used as SERS substrate for attomolar-level molecular sensing. Reproduced with permission.[237] Copyright 2023, Springer Nature. c) Developed metal–dielectric–metal hybrid nanostructures composed of Ag NPs/GO/Ag NWs as SERS sensors for PAH detection. Reproduced with permission.[238] Copyright 2023, Elsevier. (d) Designed Ag NPs/graphene/$WTe_2$ hybrid nanostructures with enhanced CM effect for SERS applications. Reproduced with permission.[239] Copyright 2024, American Chemical Society.

Author Manuscript Author Manuscript Author Manuscript Author Manuscript

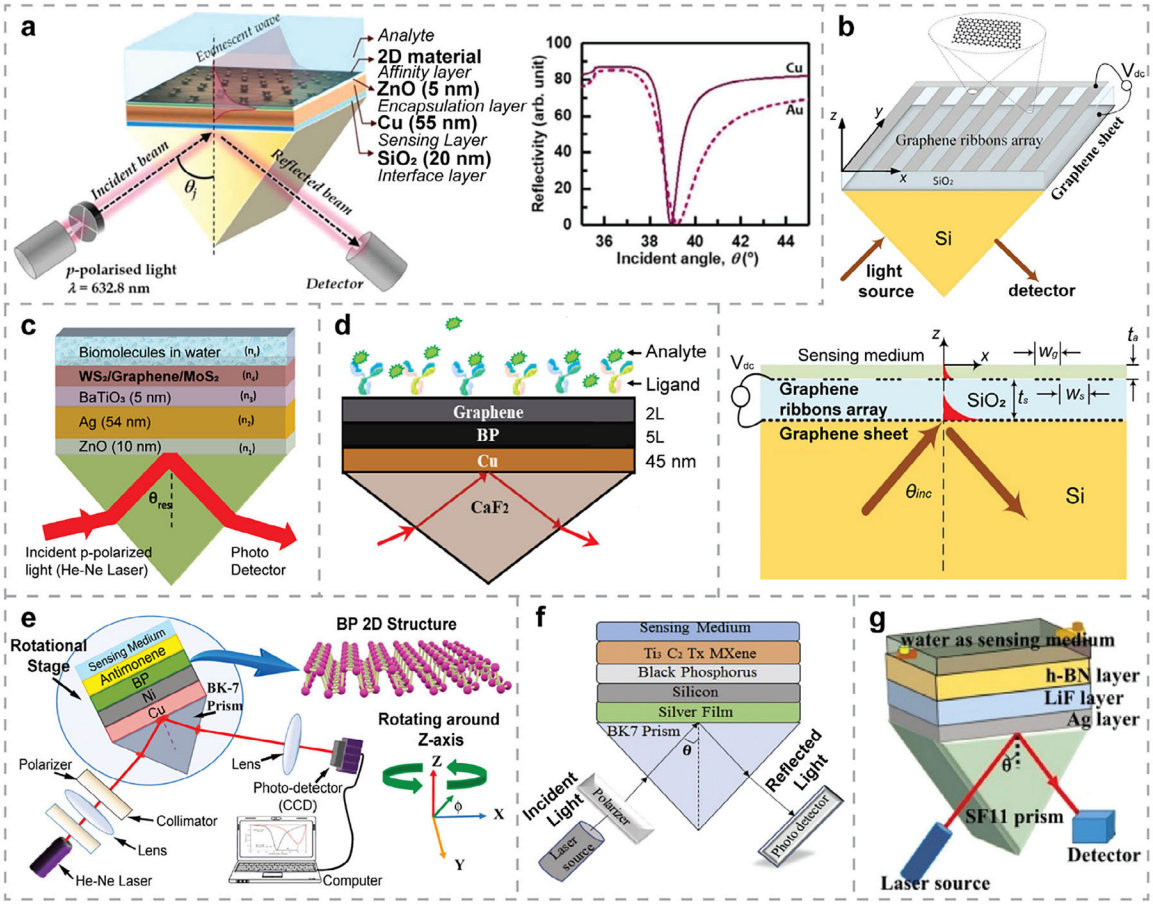


**Figure 8.**

Recent advances in using hybrid nanostructures for SPR biosensing with Kretschmann configuration. a) Strategies to enhance performance and commercial feasibility of copper-based SPR sensors through multilayer structural design. Reproduced with permission.[255] Copyright 2024, Elsevier. b) Proposed evanescent-wave SPR biosensor based on gate-controlled graphene nanoribbons array. Reproduced with permission.[256] Copyright 2021, Springer Nature. c) Comparative performance study of multilayer SPR biosensors integrating different 2DMs ($WS_2$, $MoS_2$, and graphene). Reproduced with permission.[257] Copyright 2020, Elsevier. d) Graphene/BP-integrated SPR biosensor proposed for in situ monitoring of SARS-CoV-2 Omicron. Reproduced with permission.[258] Copyright 2023, Elsevier. e) Integration of antimonene/BP heterostructure with Ni/Cu-based SPR biosensor for enhanced sensitivity. Reproduced with permission.[259] Copyright 2021, Elsevier. f) Proposed SPR biosensor composed of $Ti_3C_2T_x$ MXene/BP/Si/Ag/BK7 prism with improved sensitivity. Reproduced with permission.[260] Copyright 2020, Elsevier. g) Ultrasensitive Fano-resonance SPR sensor based on hBN/LiF/Ag/SF11 multilayer structure. Reproduced with permission.[261] Copyright 2025, Elsevier.

Author Manuscript Author Manuscript Author Manuscript Author Manuscript

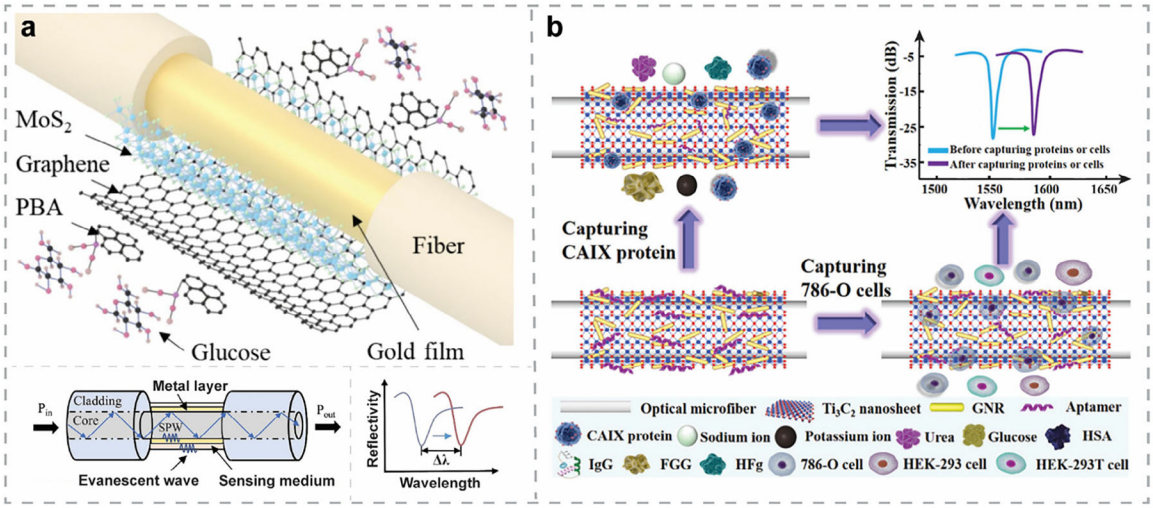


**Figure 9.**

Recent advances in using hybrid nanostructures for optical fiber-based SPR biosensing. a) Designed and fabricated fiber-optic SPR biosensor utilizing graphene/$MoS_2$ heterostructure for highly sensitive glucose detection. Reproduced with permission.[298] Copyright 2025, Elsevier. b) Functionalized optical fiber SPR biosensor based on $Ti_3C_2$ MXene/Au NRs for ultrasensitive detection of renal cancer proteins and cells. Reproduced with permission.[299] Copyright 2023, American Chemical Society.

Author Manuscript Author Manuscript Author Manuscript Author Manuscript

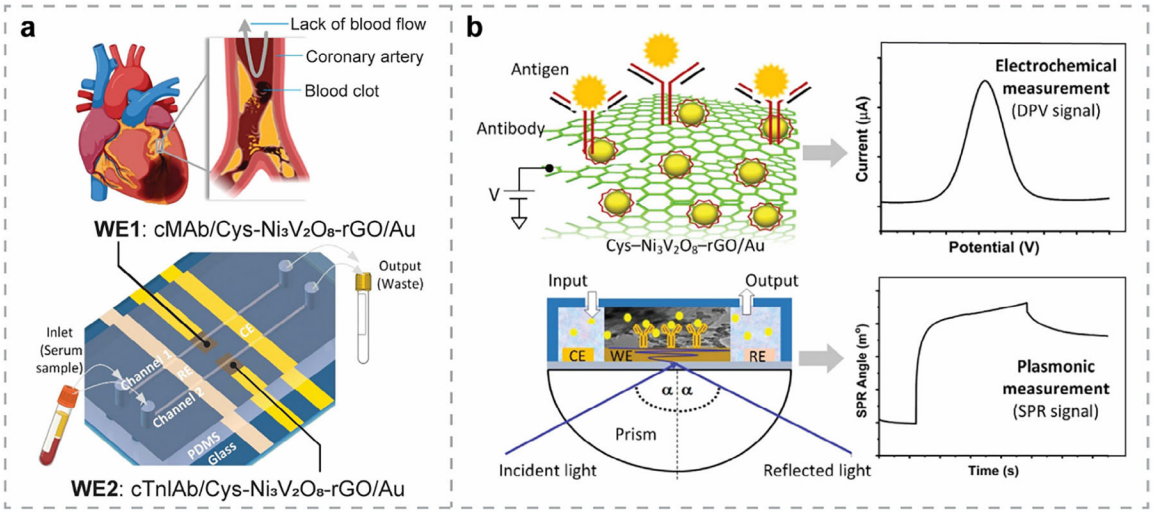


**Figure 10.**

Electrochemical and SPR detection of myocardial infarction using microfluidic biochip based on hybrid nanostructures. a) Schematics of myocardial infarction (heart attack) (upper panel) and the designed microfluidic device (lower panel). b) Dual-modal detection capability of the developed biosensing platform. Reproduced with permission.[309] Copyright 2024, American Chemical Society.

Author Manuscript Author Manuscript Author Manuscript Author Manuscript



*Adv Funct Mater*. Author manuscript; available in PMC 2026 April 08.

**Table 1.**

Overview of different 2DMs and their applications in label-free optical biosensing.

| 2DMs | Properties/advantages | Synthesis methods | Applications in label-free optical biosensing | | Disadvantages | Refs. |
|---|---|---|---|---|---|---|
| Graphene | Zero-bandgap semi-metal, very high electrical conductivity; high tensile strength; excellent thermal conductivity; high optical transparency; excellent biocompatibility; easy surface functionalization | Mechanical exfoliation; CVD; epitaxial growth | SPR | Charge transfer at the graphene-metal thin film interface; modifies the local RI and enhances the electric field intensity | Low intrinsic optical absorption (~2.3% per layer) limits its effectiveness in SPR and SERS; graphene supports plasmons in MIR and terahertz ranges, making it less compatible with biosensing platforms based on visible light | [51, 69, 70, 71] |
| | | | SERS/ GERS | Charge transfer (strong $\pi$-$\pi$ interaction) | | |
| | | | SEIRA | Enhances IR absorption | | |
| TMDCs | Semiconducting nature; tunable bandgap; layer-dependent PL properties, light absorption in the visible-NIR regime; strong fluorescence quenching capability | Mechanical exfoliation; CVD; MOCVD | SPR | Higher light absorption efficiency (than graphene); strong charge transfer | Degradation and oxidation upon exposure to air; photoinduced oxidation; many TMDCs are hydrophobic, making them less efficient in biomolecule adsorption | [72, 71, 73, 74, 75] |
| | | | SERS | Charge transfer; EF increases as the number of layers decreases | | |
| | | | PL biosensors | PL signals are modulated upon interaction with bound target analytes | | |
| Mxenes | High electrical conductivity; plasmonic behavior in the NIR-MIR regime; surface termination groups can be modified to tune the electrical, optical, and chemical properties; fluorescence quenching capability; hydrophilic | Selective chemical etching of *MAX* phases; liquid-phase exfoliation | SPR | Tunable plasmonic behavior; charge transfer between MXenes and metal thin films; Effective analyte recognition layer | Lack of controllable synthesis methods; challenges in mass production; prone to oxidation and structural degradation, limiting long-term use | [76, 77, 78, 79, 80] |
| | | | SERS | Strong affinity capability; strong charge transfer; EF increases as the number of layers increases | | |
| BP | High in-plane anisotropy; high carrier mobility; layer-dependent direct bandgap; broadband optical absorption in the visible-NIR regime; strong fluorescence quenching capability | Exfoliation | SPR | Increases carrier mobility; enhances the electric field intensity at the interface when combined with other 2DMs; charge transfer | Instability in air and water; relatively low EF when used as SERS substrates | [81, 82, 83, 84, 85, 86] |
| | | | SERS | Charge transfer; EF increases as the number of layers decreases; polarization-dependent enhancement; minimal spectral interference with NIR excitation, highly desirable for biological samples | | |
| hBN | Large bandgap, electrical insulator; optically transparent (UV-NIR); excellent thermal stability; chemical inertness; smooth surface | Mechanical exfoliation; CVD | SPR | Protective layer or dielectric spacer | Limited sensing capabilities as direct transducer material due to its electrical | [20, 25, 87, 75] |

Author Manuscript Author Manuscript Author Manuscript Author Manuscript



| 2DMs | Properties/advantages | Synthesis methods | Applications in label-free optical biosensing | | Disadvantages | Refs. |
|---|---|---|---|---|---|---|
| | | | SERS | Dipole-dipole interactions; no dependence on number of layers; Protective layer | insulating nature; relatively low EF when used as SERS substrates | |
| Antimonene | High carrier mobility; semiconductor; tunable bandgap; larger work function than graphene and other 2DMs; strong spin-orbit coupling; high stability; hydrophilic | Liquid-phase exfoliation; epitaxial growth | SPR | High binding energy enables strong adsorption of analytes | Challenges in scalable synthesis; limited surface functionalization strategies | [88, 71, 89, 90, 91, 92] |

*Adv Funct Mater*. Author manuscript; available in PMC 2026 April 08.

Author Manuscript Author Manuscript Author Manuscript Author Manuscript



**Table 2.**

Overview of recently reported 2DMs used as SERS substrates.

| Materials | Target analyte | LOD | EF | Other features/functions | Refs. |
|---|---|---|---|---|---|
| Metallic 2H-$TaS_2$ nanosheets | R6G | $3.01 \times 10^{-18}$M | $1.3 \times 10^{14}$ | – | [176] |
| | NBA | $4.05 \times 10^{-21}$M | – | | |
| 2D $HfTe_2$ nanosheets | R6G | $10^{-9}$M | $2.32 \times 10^{6}$ | – | [177] |
| | Uric acid | 0.1 mmol $L^{-1}$ | – | | |
| CVD-grown few-layer 1T′-$MoTe_2$ | $\beta$-sitosterol | $10^{-9}$M | – | Reusability | [178] |
| CVD-grown | 2H-$MoTe_2$ MB | $10^{-8}$M | $5.4 \times 10^{8}$ | – | [179] |
| | 1T'-$MoTe_2$ | | $1.8 \times 10^{7}$ | | |
| Mono- and bi-layer 1T-MoSSe | R6G | $10^{-12}$M | $6.0 \times 10^{6}$ | – | [180] |
| $Ti_3C_2$ MXene | MB | $10^{-7}$M | $2.9 \times 10^{6}$ | – | [163] |
| | Methyl violet (MV) | $10^{-6}$M | $2.84 \times 10^{5}$ | | |
| Highly crystalline monolayer $Ti_3C_2$ nanosheets | Typical environmental pollutants (azo dyes, trichlorophenol, and bisphenol A) | $10^{-11}$M | $3.82 \times 10^{8}$ | | [194] |
| $Ti_3C_2T_x$ nanosheets (with varying thickness) | MB | – | ~$1.3 \times 10^{5}$ (2 μm-thick) | – | [78] |
| MXenes ($Nb_2C$, $Mo_2C$, $Ti_2C$, $V_2C$, $Ti_3C_2$, $Mo_2TiC_2$, and $Ti_3CN$) | R6G | $10^{-7}$M | – | – | [184] |
| $V_4C_3$ | R6G | $10^{-7}$M | $1.32 \times 10^{5}$ | Flexible; rapid molecular enrichment | [185] |
| $V_2C$ | | | $0.76 \times 10^{5}$ | | |
| Few-layered TiVC nanosheets | R6G | $10^{-15}$M | $3.27 \times 10^{12}$ | – | [186] |
| $Ta_4C_3$ | R6G | $10^{-7}$M | $1.51 \times 10^{5}$ | – | [188] |
| | CV | $10^{-6}$M (0.24 mg $kg^{-1}$) | – | | |
| $Nb_4C_3$ | R6G | $5 \times 10^{-7}$M | $0.52 \times 10^{5}$ | | |
| $Nb_2C$ nanosheets | MB | $10^{-8}$M | $3 \times 10^{6}$ | – | [187] |
| | MV | $10^{-6}$M | $1.5 \times 10^{5}$ | | |
| $Ta_2C$ nanosheets | MB | $10^{-6}$M | $3.8 \times 10^{5}$ | | |
| | MV | $10^{-7}$M | $1.4 \times 10^{6}$ | | |
| | SARS-CoV-2 S protein | $5 \times 10^{-9}$M | – | | |
| Few-layer hBN film | MB | – | $1.4 \times 10^{4}$ | Highly stable hBN (> 7 months) | [192] |
| | MG | | $6.4 \times 10^{3}$ | | |

Author Manuscript Author Manuscript Author Manuscript Author Manuscript

| Materials | Target analyte | LOD | EF | Other features/functions | Refs. |
|---|---|---|---|---|---|
| | R6G | | $1.5 \times 10^4$ | | |

Author Manuscript Author Manuscript Author Manuscript Author Manuscript



**Table 3.**

Overview of recently reported metal NPs/2DM hybrids used as SERS substrates.

| Materials | Target analyte | LOD | EF | Other features/functions | Refs. |
|---|---|---|---|---|---|
| Au NPs/CVD hBN film | MB | – | $1.6 \times 10^{6}$ | Highly stable hBN (> 7 months) | [192] |
| Ag NPs/BP-nanosheets | R6G | $10^{-20}$M | $1.01 \times 10^{11}$ | Polarization-mapping strategy; combined with ML | [135] |
| Ag NPs/BP flakes | Sepsis biomarkers: interleukin-3 (IL-3); procalcitonin (PCT) | 1000 fM; 100 fM | ~$1 \times 10^{14}$ | – | [197] |
| Au NPs-Ag NPs/BP nanosheet | 4-MBA | $4.5 \times 10^{-10}$M | $2.5 \times 10^{7}$ | Photocatalytic property (self-cleaning, recyclable); molecular enrichment; flexible | [198] |
| | Thiram | $2.6 \times 10^{-6}$ mg mL$^{-1}$ | – | | |
| Ag NPs/$Ti_3C_2T_x$ | R6G | $10^{-14}$M | $3.8 \times 10^{8}$ | – | [100] |
| | Adenosine triphosphate (ATP) | $4.27 \times 10^{-9}$M | – | | |
| | Folate acid (FA) | $7.26 \times 10^{-13}$M | – | | |
| Au NPs/$Ti_3C_2T_x$ | 4-MBA | $10^{-9}$M | – | Antibacterial and photothermal sterilization effects | [153] |
| | *E. coli* | $10^{6}$ CFU mL$^{-1}$ | | | |
| | *B. subtilis* | $3 \times 10^{5}$ CFU mL$^{-1}$ | | | |
| Ag NPs/$Ti_3C_2T_x$ | 4-MBA | $10^{-8}$M | $3.15 \times 10^{6}$ | Long-term stability (1 month) | [162] |
| | Adenine | $10^{-8}$M | – | | |
| | Dopamine | $5 \times 10^{-8}$M | – | | |
| Au NPs/$Mo_2C$ nanosheets | MB | $10^{-8}$M | $2.2 \times 10^{4}$ | Long-term stability (~1 month) | [171] |
| Ag NPs/$Ti_3C_2T_x$ | R6G | $10^{-9}$M | $7.08 \times 10^{5}$ | Long-term stability (1 month) | [172] |
| | Furfural | 0.5 mg L$^{-1}$ | – | | |
| Ag NPs/$Ta_4C_3$ | R6G | $10^{-8}$M | $1.53 \times 10^{6}$ | – | [202] |
| | Pesticide ziram | $10^{-6}$M | $1.35 \times 10^{4}$ | | |
| Au NPs/TiVC MXene | R6G | $10^{-15}$M | $8.08 \times 10^{10}$ | Flexible; wearable; target enrichment | [201] |
| | Nicotine | 10 nM | – | | |
| | Methotrexate | $10^{-8}$M | | | |
| | Nikethamide | | | | |
| | 6-acetylmorphine | | | | |
| Ag NPs/$Ti_3C_2T_x$/PMMA | MB | $4.37 \times 10^{-10}$M | $7.14 \times 10^{6}$ | Flexible; self-rectification capability | [200] |
| | SARS-CoV-2 N-protein | $3.24 \times 10^{-9}$ mg mL$^{-1}$ | – | | |
| Au nanostars/$Ta_4C_3$ | PATP | $10^{-9}$M | – | Flexible; in situ analysis (paper-based SERS) | [204] |

Author Manuscript Author Manuscript Author Manuscript Author Manuscript



| Materials | Target analyte | LOD | EF | Other features/functions | Refs. |
|---|---|---|---|---|---|
| | Thiram | $10^{-7}$M | | | |
| Au NPs/TiC | Chlorpromazine (CPZ) | $3.92 \times 10^{-11}$M | $10^{9}$ | – | [199] |
| Au-Ag nanoshuttles/$Ti_2C$ MXene | Carbendazim (CBZ) | 0.01 μM | – | Electrochemical and SERS; combined with ML | [203] |
| Ag NCs/$Ti_3C_2T_x$ | R6G | $6.9 \times 10^{-11}$M | $4.77 \times 10^{7}$ | – | [189] |
| | Ritonavir | $5.62 \times 10^{-7}$ mg mL$^{-1}$ | – | | |
| | Ibrutinib | $1.17 \times 10^{-6}$ mg mL$^{-1}$ | – | | |
| Au NPs/$MoS_2$ nanosheets | TNT | $2 \times 10^{-7}$M | – | – | [205] |
| Ag NPs/mesh-like $MoS_2$ | R6G | $10^{-8}$M | $3.14 \times 10^{3}$ | Rapid detection capability in flowing water | [206] |
| | MG | $10^{-8}$M | $2.77 \times 10^{2}$ | | |
| Au NPs/$ReSe_2$ | R6G | $10^{-10}$M | $3.8 \times 10^{5}$ | – | [207] |
| Au NPs/$MoS_2$ | | $10^{-10}$M | $3.5 \times 10^{5}$ | | |
| Au NPs/$PdSe_2$ | | $10^{-12}$M | $4.5 \times 10^{5}$ | | |
| Au NPs/CVD graphene/polyester film | R6G | $10^{-8}$M | $10^{9}$ | Flexible; transparent | [208] |
| | L-tyrosine | $10^{-8}$M | $7.5 \times 10^{9}$ | | |
| Ag NPs/graphene | R6G | $10^{-13}$M | $3.03 \times 10^{11}$ | – | [210] |
| Ag NPs/laser-induced graphene | R6G | $10^{-8}$M | $3.19 \times 10^{5}$ | – | [211] |
| | CV | $10^{-7}$M | – | | |
| | MG | $10^{-7}$M | – | | |
| Au NPs/GO | RhB | $10^{-2}$ mM | $> 7.8 \times 10^{2}$ | Combined with ML | [212] |
| | *Aβ* 1–42 | 0.0232 ng mL$^{-1}$ (monomer) | – | | |
| | 0 | .0192 ng mL$^{-1}$ (fibrils) | | | |
| Au NPs/GO | R6G | $10^{-10}$M | $3.5 \times 10^{6}$ | Flexible | [213] |
| | Direct Blue 200 | $10^{-10}$M | – | | |
| | Adenine | $< 10^{-10}$M | – | | |
| Ag NPs/rGO | R6G | $10^{-7}$M | $3.03 \times 10^{5}$ | In situ enrichment effect; excellent catalytic property | [214] |
| Au nanostars/rGO | BaP | 0.0028 μg L$^{-1}$ | – | – | [215] |
| Au@Ag NPs-Au nanostars/GO | 4-MBA | – | $1.2 \times 10^{8}$ | Enrichment capability | [221] |
| | BR | $10^{-11}$M | – | | |



*Adv Funct Mater*. Author manuscript; available in PMC 2026 April 08.

Author Manuscript Author Manuscript Author Manuscript Author Manuscript



| Materials | Target analyte | | LOD | EF | Other features/functions | Refs. |
|---|---|---|---|---|---|---|
| Ag NCs/graphene | | R6G | $10^{-12}$M | ~$1.5 \times 10^{9}$ | – | [216] |
| | POPs | Dichlorodiphenyltrichloroethane (DDT) | ~$4.13 \times 10^{-9}$M | | | |
| | | Fluorene | ~$4.47 \times 10^{-9}$M | – | | |
| | | Naphthalene | ~$1.7 \times 10^{-8}$M | – | | |
| Triangular Ag nanoplates/GO | | Adenine | $10^{-8}$M | $1.09 \times 10^{8}$ | Flexible | [217] |
| | | *Staphylococcus aureus* (*S. aureus*) | $10^{2}$ CFU mL$^{-1}$ | – | | |
| Au NPs/GO | | 5,5′-dithiobis(2-nitrobenzoic acid) (DTNB) | $10^{-14}$M | $1.01 \times 10^{5}$ | Molecular enrichment; multiplex capability | [218] |
| | Pesticides | Fenthion | 38.01 ng mL$^{-1}$ | – | | |
| | | Phoxim | 8.13 ng mL$^{-1}$ | – | | |
| | | Isocarbophos | 48.97 ng mL$^{-1}$ | – | | |
| | | Thiram | 8.74 ng mL$^{-1}$ | – | | |
| Au@Ag nanostars/GO | | Thiophenol (TP) | 0.05 nM | $3.2 \times 10^{8}$ | Multiplex capability | [219] |
| | Pesticides | Ziram | 10 pM | – | | |
| | | Phorate | 50 pM | – | | |
| | | Triazophos | 100 pM | – | | |
| | | Azinphos-methyl | 100 pM | – | | |

*Adv Funct Mater*. Author manuscript; available in PMC 2026 April 08.

Author Manuscript Author Manuscript Author Manuscript Author Manuscript



**Table 4.**

Overview of 0D-2D hybrids featuring complex or specially engineered architectures for SERS sensing.

| Materials | Target analyte | LOD | EF | Other features/functions | Refs. |
|---|---|---|---|---|---|
| Gr MFs/wrinkled $MoS_2$ | RhB | $5 \times 10^{-11}$M | $2.96 \times 10^7$ | Molecular enrichment; long-term stability (>50 days) | [190] |
| $MoS_2$@Ag NFs/rGO | MB | $5.2 \times 10^{-11}$M | $8.6 \times 10^6$ | Photocatalytic capability (in situ degradation; recyclable); molecular enrichment; multiplex capability | [229] |
| | Melamine | $4.72 \times 10^{-9}$ M | – | | |
| | Vanillin (VA) | $5.58 \times 10^{-9}$ M | | | |
| | BPA | $7.71 \times 10^{-8}$ M | | | |
| TMD ($MoS_2$ and $WS_2$) NDs/graphene vdW | R6G | $5 \times 10^{-11}$–$5 \times 10^{-12}$M | – | – | [222] |
| Au NPs/$WS_2$ NDs/graphene | R6G | $10^{-12}$M | – | – | [191] |
| $WS_2$ nanodisks-$MoS_2$ nanodisks/graphene | R6G | ~$5 \times 10^{-13}$M | – | – | [230] |
| Au@$Cu_2O$ nanotriangles/$Ti_3C_2T_x$ ultrathin nanosheets | MB | $10^{-12}$M | $2.4 \times 10^9$ | Structure-adjustable; photocatalytic potential | [164] |
| MOF@Ag NFs/$Ti_3C_2T_x$ ultrathin nanosheets | MB | $6.99 \times 10^{-8}$M | – | Flexible; molecular enrichment | [231] |
| | *E. coli* | $< 9 \times 10^2$ CFU mL$^{-1}$ | – | | |
| ZnO QDs/$Ti_3C_2$ MXene | 4-MPY | $10^{-7}$M | $4.6 \times 10^4$ | Flexible; photocatalytic capability (self-cleaning, recyclable); in situ detection; long-term stability (60 days) | [232] |
| $Fe_3O_4$@Au NPs/GO | PAHs BaP | 3.8 μg L$^{-1}$ | – | Photocatalytic capability (in situ degradation); long-term stability (> 130 days) | [223] |
| | Phenanthrene | 10 μg L$^{-1}$ | – | | |
| | Anthracene | 10 μg L$^{-1}$ | – | | |
| | Pyrene | 1 μg L$^{-1}$ | – | | |
| | Fluoranthene | 1 μg L$^{-1}$ | – | | |
| Graphene/Au nanopyramids | R6G | $10^{-13}$M | $1.5 \times 10^{10}$ | Wafer-scale; multiplex capability; PCA | [225] |
| | Tau & phospho-Tau (P-Tau) proteins | $10^{-15}$M | – | | |
| | A$\beta$42 polypeptide | $10^{-14}$M | $2 \times 10^8$ | | |
| Au NPs/graphene/Cu cone cavities | MG | $10^{-9}$ mol L$^{-1}$ | – | Long-term stability | [226] |
| | Paraquat | $10^{-7}$ mol L$^{-1}$ | – | | |
| Graphene/Au NPs/rectangular pyramid PMMA hybrids | Paraquat | $10^{-8}$M | – | Flexible; in situ detection; long-term stability (30 days) | [227] |
| | 2,4-d | $10^{-6}$M | – | | |
| $Ti_3C_2$ nanosheets/Au-Ag bimetallic nanocuboids | CV; MG; MB | $10^{-12}$M | – | Multiplex capability | [228] |

*Adv Funct Mater*. Author manuscript; available in PMC 2026 April 08.

Author Manuscript Author Manuscript Author Manuscript Author Manuscript



**Table 5.**

Overview of recently reported 1D–2D hybrid nanostructures used as SERS substrates.

| Materials | Target analyte | LOD | EF | Other features/functions | Refs. |
|---|---|---|---|---|---|
| Monolayer hBN/Ag NRs | R6G | $7.9 \times 10^{-10}$M | $1.26 \times 10^{8}$ | Recyclable; long-term stability | [234] |
| | BR | $2.5 \times 10^{-8}$M | – | | |
| $Ti_3C_2$ MXene/Ag NRs | CV | $2.48 \times 10^{-11}$M | – | Multiplex capability; long-term stability | [235] |
| | PCB-77 | $2.43 \times 10^{-10}$M | – | | |
| | PCB-3 | $2.14 \times 10^{-9}$M | – | | |
| $Ti_3C_2T_x$/ZnO NRs | R6G | $10^{-11}$M | $1.49 \times 10^{7}$ | – | [236] |
| | miRNA | $10^{-6}$M | – | | |
| $WO_{3-x}$ NWs/$WSe_2$ | MB | $5 \times 10^{-18}$M | $5.0 \times 10^{11}$ | – | [237] |

*Adv Funct Mater*. Author manuscript; available in PMC 2026 April 08.

Author Manuscript Author Manuscript Author Manuscript Author Manuscript



**Table 6.**

Overview of recently reported multicomponent nanohybrids with mixed dimensions for SERS sensing.

| Materials | Target analyte | | LOD | EF | Other features/functions | Refs. |
|---|---|---|---|---|---|---|
| hBN/graphene/Ag NPs | R6G | | $10^{-6}$M | $3.65 \times 10^{5}$ | Reusable | [248] |
| GO/Ag/PS nanospheres | 2-Naphthalenethiol (2-NAT) | | $2.8 \times 10^{-8}$M | $2.27 \times 10^{6}$ | Multiplex capability; molecular enrichment | [174] |
| | Melamine | | $2.81 \times 10^{-10}$M | – | | |
| | Dicyandiamide | | $6.03 \times 10^{-9}$M | – | | |
| Ag nanostars-MWCNT/GO | 4-MPY | | $10^{-8}$M | – | Analyte enrichment | [249] |
| | PS (50–500 nm) | | $5 \times 10^{-5}$ mg mL$^{-1}$ | | | |
| | PMMA nanoplastics (50 nm) | | $5 \times 10^{-4}$ mg mL$^{-1}$ | | | |
| Au NPs/GO/Ag NWs | PAHs | Pyrene | $10^{-8}$M | $1.48 \times 10^{5}$ | Multiplex capability | [238] |
| | | Anthracene | $10^{-8}$M | – | | |
| | | Phenanthrene | $10^{-8}$M | – | | |
| | | BaP | $10^{-7}$M | – | | |
| Au/graphene/Ag/ZnO | R6G | | $10^{-13}$M | $5.68 \times 10^{7}$ | Molecular enrichment; photocatalytic degradation capability (reusable) | [173] |
| Ag NPs/graphene/Cu | R6G | | $10^{-14}$M | $8.86 \times 10^{8}$ | Flexible | [250] |
| Ag NPs/graphene/$WTe_2$ | R6G | | $10^{-13}$M | $1.34 \times 10^{12}$ | – | [239] |
| | CV | | $10^{-10}$M | $4.76 \times 10^{10}$ | | |
| | MB | | $10^{-8}$M | $4.53 \times 10^{8}$ | | |
| | MG | | $10^{-7}$M | $5.19 \times 10^{7}$ | | |
| Au NPs/$MoS_2$/ $Ti_3C_2$ MXene | miRNA-182 | | 6.61 aM | $4.8 \times 10^{8}$ | Self-internal standards (synergistic calibrated strategy) | [251] |

*Adv Funct Mater*. Author manuscript; available in PMC 2026 April 08.

Author Manuscript Author Manuscript Author Manuscript Author Manuscript



**Table 7.**

Summary of recent Kretschmann SPR biosensors with 2DMs and their hybrid nanostructures.

| Materials | Analyte | | Sensitivity [deg $RIU^{-1}$] | Quality factor [$RIU^{-1}$] | Refs. |
|---|---|---|---|---|---|
| Graphene/Au/N-FK51A prism | Glucose (25–175 $mgdL^{-1}$) | | 275.15 | 76.2 | [264] |
| | Gas (RI: 1.0000–1.0007) | | 92.1 | 230.2 | |
| Graphene/AlN/Ag/$TiO_2$/BK7 prism | Infected plasma | | 138.46 | – | [266] |
| | Infected platelet | | 163.63 | | |
| | Infected hemoglobin | | 182.85 | | |
| Thiol-tethered ssDNA/graphene/$BaTiO_3$/Ag/$TiO_2$/$CaF_2$ prism | SARS-CoV-2 virus | | 433.63 | 136.79 | [267] |
| Graphene nanoribbons/$SiO_2$/graphene/Si | RI | 1.33 | 36 401.1 mV $RIU^{-1}$ | 21.84 | [256] |
| | | 1.34 | 40 676.5 mV $RIU^{-1}$ | 24 | |
| | | 1.35 | 40 918.2 mV $RIU^{-1}$ | 23.74 | |
| | | 1.36 | 41 160 mV $RIU^{-1}$ | 23.69 | |
| Au NRs/Antimonene/Au/prism | RI | | 171 | – | [88] |
| | miRNA-21 and miRNA-155 | | 10 aM | | |
| Antimonene/Au/BK7 prism | RI | | 181.9 | 26.400 | [142] |
| Graphene/Au/BK7 prism | | | 147.95 | 30.370 | |
| Au/BK7 prism | | | 144.45 | 33.671 | |
| Antimonene/$BaTiO_3$/Ag/$BaF_2$ prism | RI | | 303.83 | 50.39 | [147] |
| | Hemoglobin concentration | | 0.045 deg/$gL^{-1}$ (concentration sensitivity) | – | |
| Antimonene/ZnO/Ag/SF11 prism | RI | | 105.72 | 14.89 | [146] |
| $WS_2$/$BaTiO_3$/Ag/ZnO/BK7 prism | RI | | 180 (1L); 235.00 (2L) | 63.51 | [257] |
| $MoS_2$/$BaTiO_3$/Ag/ZnO/BK7 prism | | | 174 (1L); 202.00 (2L) | 34.17 | |
| Graphene/$BaTiO_3$/Ag/ZnO/BK7 prism | | | 157 (1L); 162.50 (2L) | 70.96 | |
| $WSe_2$/Si/Ag/prism | Urea in blood (1 g $dL^{-1}$) | | 373.49 | – | [270] |
| $WS_2$/GaSe/Cu/BK7 prism | RI (dengue virus) | | 303.28 | 97.51 | [271] |
| $WSe_2$/Al/Ag/$CaF_2$ prism | RI | | 210 | 225.80 | [273] |
| $Ti_3C_2T_2$ (T=O, OH, F) MXene/Au/Cr/BK7 prism | RI | | 150.131 ($Ti_3C_2F_2$) | – | [80] |
| $Ti_3C_2T_x$/Ag/$CaF_2$ prism | RI | | 350.87 | 42.10 | [276] |

*Adv Funct Mater*. Author manuscript; available in PMC 2026 April 08.

Author Manuscript Author Manuscript Author Manuscript Author Manuscript



| Materials | Analyte | Sensitivity [deg $RIU^{-1}$] | Quality factor [$RIU^{-1}$] | Refs. |
|---|---|---|---|---|
| $Ti_3C_2T_x$/Au/Ag/MgO/FK51A prism | RI | 236 | ~63 | [79] |
| $Ti_2C$ MXene/Au/prism | RI | 3579.6 nm $RIU^{-1}$ | 26.168 | [128] |
| | $Pb^{2+}$ | 79.2 ng $L^{-1}$ (LOD) | – | |
| | $Cr^{2+}$ | 56.5 ng $L^{-1}$ (LOD) | | |
| | $Hg^{2+}$ | 92.8 ng $L^{-1}$ (LOD) | | |
| BP/Ni/$SiO_2$/Cu/BK7 prism | RI | 479.10 | 102.19 | [279] |
| BP/Ag/$BaTiO_3$/Ag/BK7 prism | RI | 360 | 72.6 | [281] |
| BP/Au/$BaTiO_3$/Au/BK7 prism | | 299 | 39.6 | |
| BP/Cu/$BaTiO_3$/Cu/BK7 prism | | 378 | 145.1 | |
| Graphene/BP/Ag/$TiO_2$/$CaF_2$ prism | RI (SARS-CoV-2) | 390 | 92.86 | [283] |
| Graphene/BP/Cu/$CaF_2$ prism | RI (SARS-CoV-2 Omicron) | 410 | 94.25 | [258] |
| Antimonene/borophene/Au/BK7 prism | RI; biomolecules (DNA/RNA) | 206.26 | – | [144] |
| Antimonene/BP/Si/Al/SF10 prism | RI | 202.37 | 28.86 | [143] |
| | DNA hybridization | 2.8 pM | 0.037 $nM^{-1}$ | |
| Antimonene/BP/Ni/Cu/BK7 prism | RI | 446.90 | 93.10 | [259] |
| Graphene/$MoSe_2$/Ag/Ti/BK7 prism | RI | 215.5 | – | [286] |
| Graphene/Ag/Ti/BK7 prism | CEA in PBS | 133.33 | 107.52 | [288] |
| Graphene/MXene/Ag/Ti/BK7 prism | | 140.27 | 62.62 | |
| Graphene/$MoS_2$/Ag/Ti/BK7 prism | | 144.72 | 62.38 | |
| $Ti_3C_2T_x$/graphene/Ag/glass prism | RI (1.33–1.36) | 214.20 | – | [289] |
| Antimonene/$Ti_3C_2T_x$/Au/TiO2/BK7 prism | RI | 224.26 | 19.06 | [290] |
| $Ti_3C_2T_x$/BP/Ni/Cu/BK7 prism | RI | 304.47 | 57.85 | [291] |
| $Ti_3C_2T_x$/BP/Si/Ag/BK7 prism | RI | 264 | 41.25 | [260] |
| hBN/LiF/Ag/SF11 prism | RI | 1000 | 225 | [261] |
| $Ti_3C_2T_x$/$MoS_2$/optical waveguide layer/coupling dielectric layer/S-BSL7M prism | RI | 86.13 | 281.74 | [292] |
| Blue phosphorus-$MoS_2$/Au/$PtSe_2$/$CaF_2$ prism | RI (1.33–1.36) | 240.54 | 29.23 | [293] |
| $WS_2$/$HfSe_2$/BP/Ag/BAK1 prism | RI: 1.33–1.39 (volatile organic compounds (VOCs)) | 227.14 | – | [294] |
| $Ti_3C_2T_x$/$MoO_3$/$MoS_2$/Ag/BK7 prism | RI (glucose solution) | 227.08 | 35.09 | [295] |

Author Manuscript Author Manuscript Author Manuscript Author Manuscript



**Table 8.**

Recent fiber-optic SPR biosensors with 2DM hybrid nanostructures.

| 2DM hybrid nanostructures | Analyte | Sensitivity | LOD | Quality factor [$RIU^{-1}$] | Refs. |
|---|---|---|---|---|---|
| Graphene/BP/Ag | RI | 4050 nm $RIU^{-1}$ | – | 39.70 | [297] |
| $MoS_2$/BP/Ag | | 3950 nm $RIU^{-1}$ | | 40.25 | |
| $WS_2$/BP/Ag | | 3975 nm $RIU^{-1}$ | | 47.89 | |
| $MoSe_2$/BP/Ag | | 3975 nm $RIU^{-1}$ | | 41.40 | |
| $WSe_2$/BP/Ag | | 4000 nm $RIU^{-1}$ | | 47.62 | |
| Antimonene/graphene/Au RI (cancerous cells) | Skin | 7.3465 μm $RIU^{-1}$ | 7.2 × $10^{-5}$ RIU | 131.1525 | [145] |
| | Cervical | 10.9250 μm $RIU^{-1}$ | | | |
| | Blood | 11.8914 μm $RIU^{-1}$ | | | |
| | Adrenal | 15.2414 μm $RIU^{-1}$ | | | |
| Graphene/$MoS_2$/Au/Cr | RI | 8631.54 nm $RIU^{-1}$ | – | – | [298] |
| | Glucose (0–500 mg $dL^{-1}$) | 12 593.06 nm $RIU^{-1}$ | | | |
| $Nb_2CT_x$/Au NPs (S-tapered) | Tyramine | 34 pm $\mu M^{-1}$ | 0.35 μM | – | [300] |
| $Nb_2CT_x$/Au NPs (W-shaped) | Tyramine | 0.0385 nm $\mu M^{-1}$ | 6.96 μM | – | [301] |
| $Ti_3C_2$ Mxene/Au NRs | Carbonic anhydrase IX (CAIX) protein | Pure buffer 1.46 nm/$\log_{10}$M | 13.8 zM | – | [299] |
| | | 30% serum solution 0.986 nm/$\log_{10}$M | 0.19 aM | | |
| $Ti_3C_2$ Mxene/Au NRs | Acetylcholine | 0.04521 nm $\mu M^{-1}$ | 4.42 μM | – | [302] |



*Adv Funct Mater*. Author manuscript; available in PMC 2026 April 08.